Signal Design and Processing Techniques for WSR-88D Ambiguity Resolution

Staggered PRT and updates to the SZ-2 Algorithm

National Severe Storms Laboratory Report

prepared by: **Sebastian Torres, Svetlana Bachmann, and Dusan Zrnic**

**Part 11
December 2007**
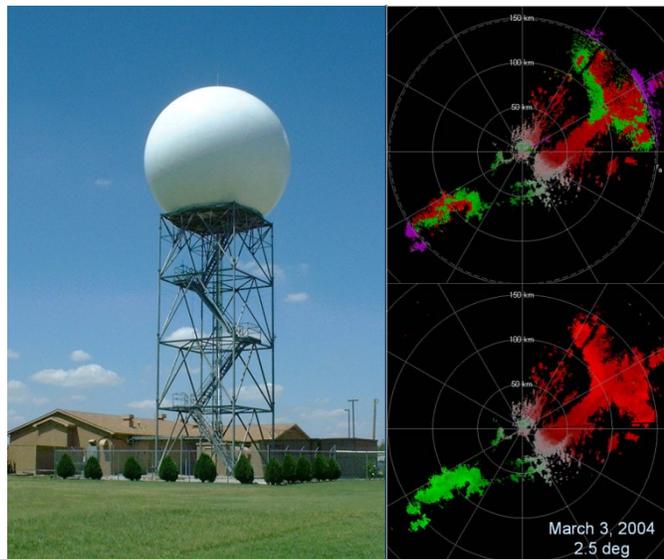
March 3, 2004
2.5 deg

SIGNAL DESIGN AND PROCESSING TECHNIQUES FOR WSR-88D AMBIGUITY RESOLUTION

Part 11: Staggered PRT and updates to the SZ-2 Algorithm

National Severe Storms Laboratory Report
prepared by: Sebastián Torres, Svetlana Bachmann, and Dusan Zrnić

December 2007

SIGNAL DESIGN AND PROCESSING TECHNIQUES FOR WSR-88D AMBIGUITY RESOLUTION

Part 11: Staggered PRT and updates to the SZ-2 Algorithm

Contents

SIGNAL DESIGN AND PROCESSING TECHNIQUES FOR WSR-88D AMBIGUITY RESOLUTION

Part 11: Staggered PRT and updates to the SZ-2 Algorithm

1. Introduction

The Radar Operations Center (ROC) of the National Weather Service (NWS) has funded the National Severe Storms Laboratory (NSSL) to address the mitigation of range and velocity ambiguities in the WSR-88D. This is the eleventh report in the series that deals with range and velocity ambiguity resolution in the WSR-88D (other relevant reports are listed at the end). It documents NSSL accomplishments in FY07.

We start in section 2 with a brief description of three data sets that were collected during this year. These sets augment our large collection of data sets from previous years. Some of these cases are listed on our website (*http://cimms.ou.edu/rvamb/home.htm*); only few have been thoroughly analyzed.

Section 3 documents our accomplishments with staggered PRT. In particular, we analyzed the performance of the spectral clutter filter under a wide variety of conditions and provided tools and guidelines to design operational VCPs that employ staggered PRT.

During FY07, we continued supporting the testing and evolution of the SZ-2 algorithm. Section 4 documents this significant effort that resulted in resolving several issues that

were reported after the operational implementation of the algorithm in Build 9 of the ORDA.

This report also includes three appendices. Appendix A contains an updated and corrected algorithm description for the staggered PRT ground clutter filter. Appendix B is the latest SZ-2 algorithm description which is an update to the last document delivered to the ROC on April 13, 2007. Appendix C explores generalized systematic phase codes with some interesting properties.

Once again, the work performed in FY07 exceeded considerably the allocated budget; hence, a part of it had to be done on other NOAA funds. Further, considerable amount of this fiscal year (FY08) effort including new results went into the report (these efforts cover about 50% of allocated funding).

2. Data Collection

Due to the numerous data cases collected in previous years and other projects competing for radar time, data collection during FY07 was limited to just few cases.

Two new volume coverage patterns (VCP) were created: TEMP-ST-64331.vcp (Table.2.1.1) and TEMP-ST-64333.vcp (Table 2.1.2). The VCP summarized in Table 2.1.1 was developed to compare ground clutter filtering (GCF) in *batch mode* and *split cut* with the staggered PRT (SPRT) GCF. The entire VCP was formed at lowest elevation 0.5° to enforce maximum ground clutter contamination for different scanning strategies. The dwell times of the SPRT scans were matched to the dwell times of the *split cut* and *batch mode* of the VCP-11. The range coverage for different strategies does not match due to the limited choice of PRT values that the system had at the time. A data set was collected in clear air on February 22, 2007 at 21:12 UTC. The VCP summarized in Table 2.1.2 was created to replicate the range coverage and dwell times of VCP-11 with the staggered PRT scans. The choice of PRTs was based on preliminary analyses presented by Dr. Torres, NSSL during Spring 2007 NCAR/ROC/NSSL technical interchange meeting on "Data quality and range/velocity ambiguity mitigation." New PRTs were created in the system to accommodate the proposed design. Two data sets were collected in clear air on June 08, 2007 at 15:58 UTC, and in precipitation on Jun 14, 2007 at 21:05 UTC in dual polarization.

Table 2.1.1.

Set	Cut	El.	Waveform type	Prf #1 #2	T_1(ms)	Pulses (pairs)	Rotation rate	Dwell time
VCP: TEMP-ST-64331.vcp								
Split cut and SPRT	1	0.5	CS	1	3.10667	17	18.675	52.33
	2	0.5	CD	5	0.98667	52	19.224	51.31
	3	0.5	STAG	23 24	1.6 (2.4)	52 (26)	9.6	104
Batch mode and SPRT	4	0.5	B	1	3.10667	6	16.166	18.64
				5	0.98667	41	16.166	40.83
	5	0.5	STAG	23 24	1.6 (2.4)	30 (15)	16.9	60
Batch mode &SPRT	6	0.5	B	02	2.24067	6	17.893	13.44
				05	0.98667	41	17.893	40.45
	7	0.5	STAG	23 24	1.6 (2.4)	26 (13)	18.5	54
Contiguous Doppler & SPRT	8	0.5	CDX	5	5	43	25.168	39.27
	9	0.5	STAG	23 24	1.6 (2.4)	20 (10)	25.6	40

Collected data:
Feb.22 2007 21:12 UTC –clear-air

Table 2.1.2.

Cut	El.	Waveform	Prf #1 #2	T_1(ms)	Number of pairs	Rotation Rate	Dwell time
VCP: TEMP-ST-64333.vcp							
1	0.5	STAG	09 10	1.97	21	9.669	104.12
2	1.45	STAG	09 10	1.97	20	10.15	101.02
3	2.4	STAG	09 10	1.97	12	16.92	59.09
4	3.3	STAG	11 12	1.65	13	18.64	53.89
5	4.3	STAG	13 14	1.38	16	18.12	53.89
6	5.2	STAG	15 16	1.18	19	17.84	55.99
7	6.2	STAG	17 18	1.03	22	17.66	55.99
8	7.5	STAG	19 20	0.87	18	25.54	39.27
9	8.7	STAG	21 22	0.77	20	25.97	39.27
10	10.	STAG	21 22	0.77	20	25.97	38.95
11	12.0	STAG	21 22	0.77	20	25.97	38.95
12	14.0	STAG	21 22	0.77	20	25.97	38.95
13	16.7	STAG	21 22	0.77	20	25.97	38.95
14	19.5	STAG	21 22	0.77	20	25.97	38.95

Collected data:
Jun 08 2007 15:58:46 (raw_001_070608_155846.dat –14cuts) – clear-air
Jun 14 2007 21:05:45 (raw_002_070614_210545.dat –14cuts) – weather

3. Staggered PRT

3.1. Clutter filtering

3.1.1. *SPRT short review*

Staggered pulse repetition time (SPRT) data acquisition scheme was developed during the last decade to mitigate range/velocity ambiguity in weather radar (Sachidananda et. 1999, Sachidananda and Zrnić 2000). One of the proposed and comprehensively studied SPRT schemes uses pairs of two different PRTs, (T_1 and T_2) such that $3T_1 = 2T_2$ (Sachidananda et. al 1999, Sachidananda and Zrnić 2000, Torres et al. 2005, Sachidananda and Zrnić 2006). The SPRT technique has shown to successfully mitigate the range/velocity ambiguities in the WSR-88D, but it was not used at low elevations due to challenges in ground clutter filtering caused by the non-uniform sampling (Sachidananda et. al 1999, Sachidananda and Zrnić 2000, Torres et al. 2005, Sachidananda and Zrnić 2006, Torres 2003). The non-uniform-sampled data can be zero padded to create an artificial uniform-sampled sequence. However, a spectrum of the zero padded SPRT sequence (obtained using PRTs such that $3T_1 = 2T_2$) contains five replicas of weather and clutter compared to the spectrum of equivalent uniform PRT time series. Fig. 3.1.1 illustrates this concept. The uniform PRT spectrum (blue dotted line) contains two peaks. The ground clutter peak is at zero Doppler velocity, and the weather peak is at 11 m s^{-1}. The SPRT spectrum (red solid line) contains five clutter and weather replicas. The main clutter replica is the largest of the five clutter replicas; its location is known *a priori*. The main weather replica is also the largest of the five weather replicas, but due to noise and overlaid clutter replicas, the location of the main weather replica might be

obscured. Recently, an involved spectral procedure was developed to filter the ground clutter contributions from all replicas of the SPRT spectrum (Torres et al. 2005, Sachidananda and Zrnić 2006). The procedure removes all five clutter components and uses the remaining spectral coefficients to reconstruct the spectrum of weather signal. The filtering is based on the fact that the ground clutter replicas have deterministic locations in the spectrum. The vital parameter for successful filtering is the clutter width parameter corresponding to the inherent spectral spread of the ground clutter signature in the spectrum. This parameter was tabulated as a function of clutter to noise ratio CNR and presented in NSSL report #9 (Torres et al. 2005). After thorough spectral evaluation, we recommend replacing the tabulated clutter width with the GMAP-based assessment of the inherent clutter width. Section 3.1.3b provides the methodology for the SPRT-GMAP clutter filtering. The updates and changes to the existing algorithm are discussed in Section 3.1.5 and the functional description is in Appendix A.
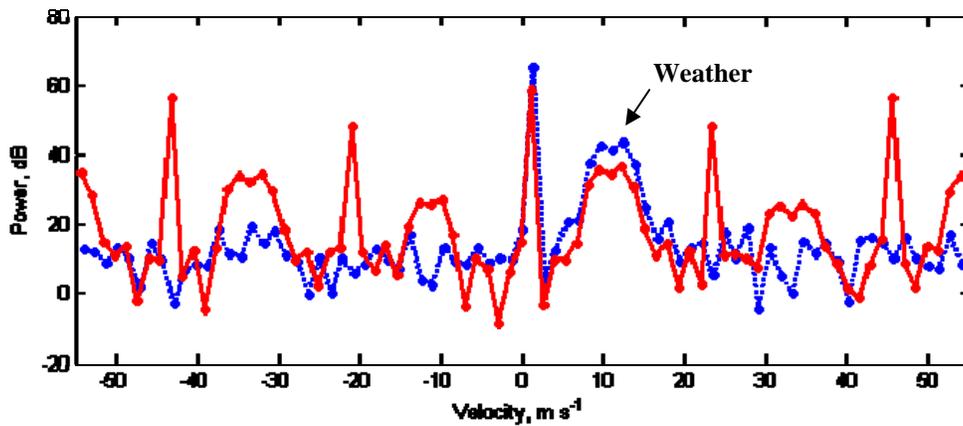
Fig. 3.1.1: Spectrum of a uniform PRT time series (blue dotted line) vs. spectrum of the equivalent zero padded staggered PRT ($3T_1 = 2T_2$) time series (red solid line).

To distinguish Sachidananda's involvement in developing the SPRT scheme and to shorten notation, we proposed acronym SACHI - Spectral Algorithm for Clutter Harmonics Identification and removal in staggered PRT data. SACHI is a procedure in which a spectral filter is one component. We use notation SACHI-TABL to specify that the SPRT GCF procedure is used with the tabulated values of clutter width parameter, and SACHI-GMAP to indicate that elements of GMAP are used in the procedure for adaptive clutter identification.

3.1.2. *Comparing GCF for uniform and staggered PRT in clear air.*

To compare the GCF techniques in *split cut* and *batch mode* with SACHI, we created a test VCP that is summarized in Table 2.1.1. The VCP contains 9 cuts that constitute 4 testing sets:

> *split cut* and SPRT scans,
>
> *batch mode* and SPRT scans,
>
> another *batch mode* and SPRT set for shorter dwell time, and
>
> *contiguous Doppler* and SPRT scans.

The second set of *batch mode* and SPRT with a shorter dwell time, and a set of *contiguous Doppler* followed by SPRT scans are not presented here. We realize that the unnecessary large range coverage produced by the SPRT with $T_1 = 1.6$ ms compared to the corresponding range coverage of these scans are not a good choice for fair evaluation. The lowest elevation 0.5° for all cuts is chosen to maximize ground clutter contamination for testing. The choice of PRT for staggering scheme was preliminary, resulting in exceeding range coverage. Time series were collected in clear air conditions. At elevation

7

0.5°, the ground clutter pattern of KOUN radar is mostly contained within 30 km range. Therefore, we consider only powers within 30 km range of the radar for analyses and examples.

Split cut, containing 17 samples of surveillance (CS) and 52 samples of Doppler (CD) scans is followed by 26 pairs of the SPRT scan (Fig. 3.1.2). The unfiltered power of CS scan, shown in Fig. 3.1.2a, portrays the distinctive ground clutter pattern of KOUN. Figs. 3.1.2b-c show power filtered using GMAP on 17 samples of CS scan and 52 samples of CD scan respectively. The strong residual clutter power (i.e., a line of stronger than background echoes about 2 km west of the radar that stretches to about 20 km north) is from traffic on the interstate road I-35. The weak residual clutter power is from the spectral noise floor that is elevated in regions with strong clutter due to contamination through the spectral window and/or transmitter spectral impurities. These residuals are generally removed by an adaptive dB-per-dB threshold (see subsection 3.1.4b.i for a brief description of the threshold). The SPRT scan filtered using SACHI-GMAP and *dc* removal are shown in Figs. 3.1.2d-e. Visually, the performance of SACHI-GMAP is comparable to the performance of the uniform PRT scans filtered with GMAP. The similarity in shapes of clutter residuals shown in Figs. 3.1.2b-d provides supplementary evidence that *split cut* can be replaced by the SPRT scan.

Batch mode, containing 6 samples of long PRT and 41 samples of short PRT, is followed by 15 pairs of SPRT scan (Fig. 3.1.3). Unfiltered power is shown in Fig. 3.1.3a. Long PRT of *batch mode* is filtered using *dc* removal (Fig. 3.1.3b). The power is only partially suppressed, and the ground clutter pattern is still decipherable. Short PRT of *batch mode* is filtered using GMAP (Fig. 3.1.3c). Most of the clutter power is suppressed similar to

split cut; the clutter residuals and echoes from traffic are exposed. SPRT contains 15 pairs and is filtered using SACHI-GMAP (Fig. 3.1.3d) and *dc* removal (Fig. 3.1.3e). The clutter residuals pattern is different after SACHI-GMAP, with more suppression at ranges beyond 10 km and less suppression close to the radar. Later, after error analyses, we discovered that relatively long PRT and odd number of pairs result in degradation of SACHI performance. We anticipate that increase in the number of staggered pairs by 1 (16 pairs instead of 15, even instead of odd) for the same scan would improve the results of SACHI-GMAP suppression. After the *dc* removal the clutter powers are slightly suppressed, but the clutter pattern is still in place. Figs.3.1.2-3.1.3 illustrate that *dc* removal provides only partial suppression of ground clutter for both uniform and staggered PRT.
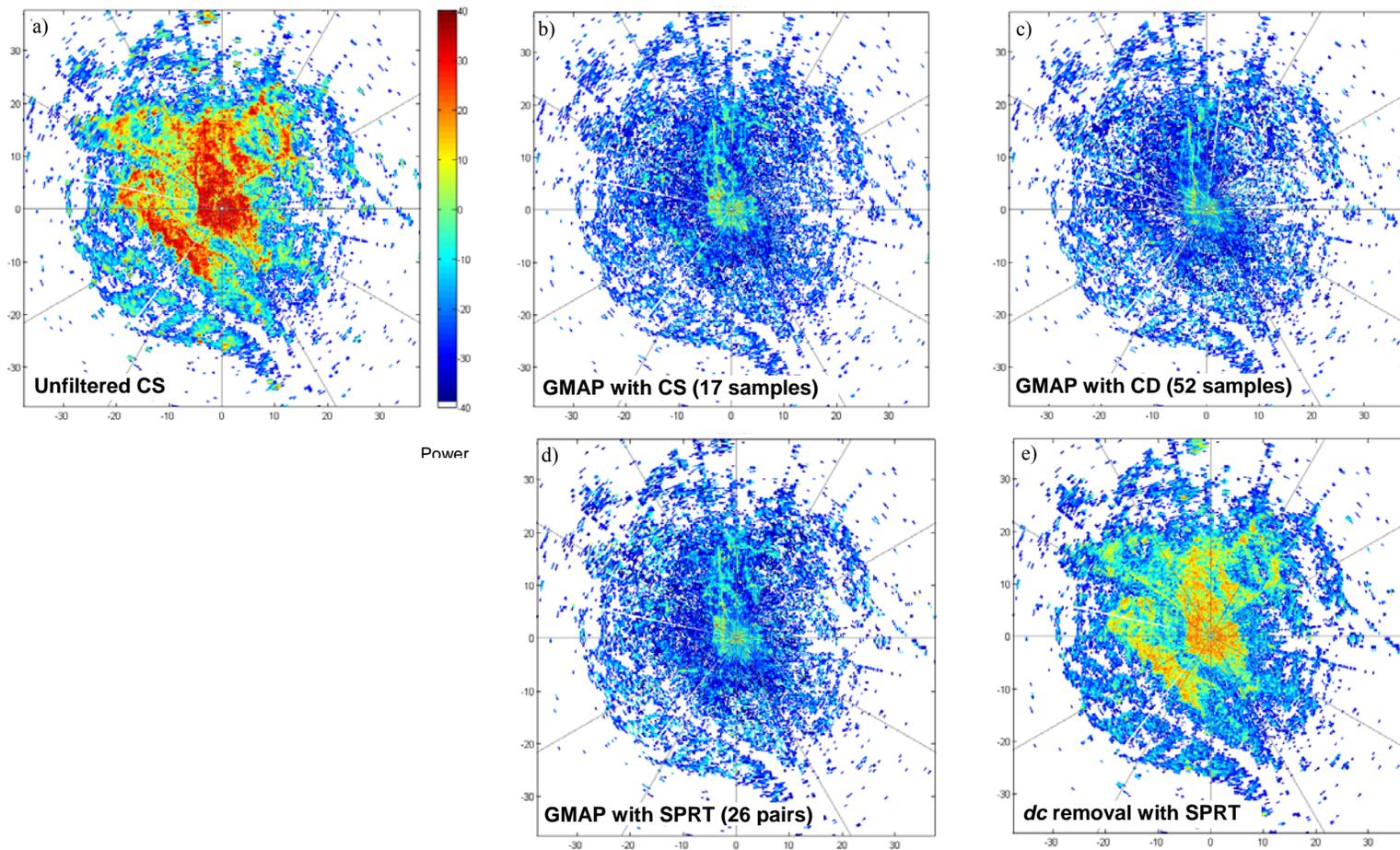
Fig. 3.1.2: *Split cut* and SPRT scans: a) unfiltered CS of the *split cut*, b) CS filtered using GMAP, c) CD filtered using GMAP, d) SPRT scan filtered using GMAP, and e) SPRT scan filtered using *dc* removal. Data are from clear air on Feb 22 2007, elevation 0.5°.
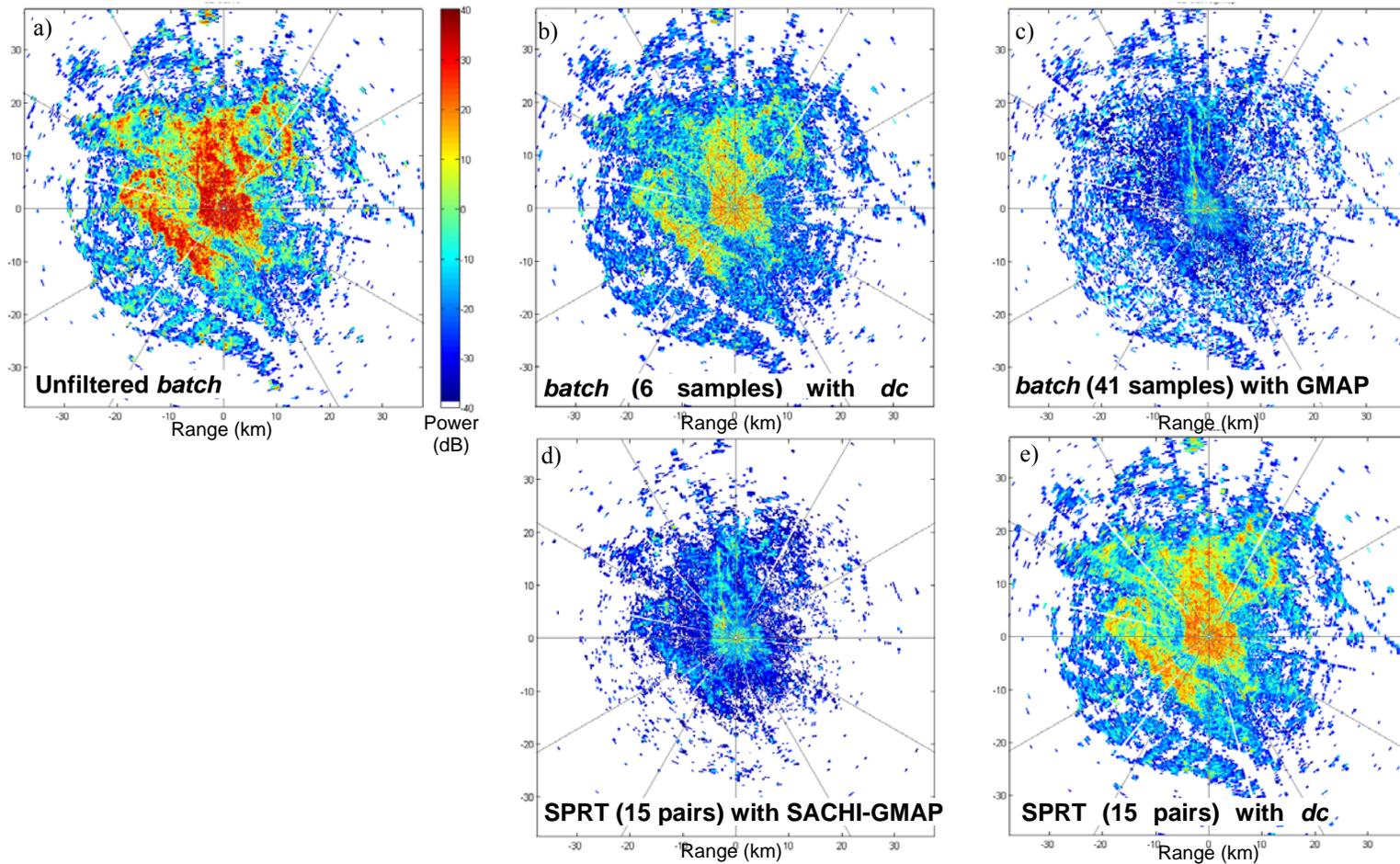
Fig. 3.1.3: *Batch mode* and SPRT scans: a) unfiltered long PRT cut of *batch mode*, b) long PRT cut after *dc* removal, c) short PRT cut after GMAP, d) SPRT scan after SACHI-GMAP, e) SPRT scan after *dc* removal. Data are from clear air on Feb 22 2007, el. 0.5°.

Clutter filtering attained in *split cut* and SPRT scans are illustrated in Fig. 3.1.2. To examine the clutter suppression levels achieved with different GCF we generate scatter plots of filtered and unfiltered powers (Fig. 3.1.4). The occurrences are color coded to note the areas of large values. Fig. 3.1.4a shows scatter-histogram of the filtered/unfiltered power for surveillance scan of *split cut* filtered using GMAP. Fig. 3.1.4b shows scatter-histogram of the filtered/unfiltered power for Doppler scan of *split cut* filtered using GMAP. Sometimes, due to the Gaussian fit that GMAP performs on spectral coefficients identified as clutter, additional power can be infused into the filtered spectrum. This detail is visible in the scatter plots. In some occasions power after filtering exceeds the unfiltered power. Figs. 3.1.4c-d show scatter-histograms for SACHI-GMAP and SPRT with *dc* removal respectively.

The achieved clutter suppression levels are

> CS of *split cut* with GMAP provides about 40 dB suppression,
> CD of *split cut* with GMAP provides up to 50 dB suppression,
> SPRT with *dc* removal provides about 10 dB suppression, and
> SPRT with SACHI-GMAP provides about 45 dB suppression.

The number of samples causes the diversity of suppression levels. Considering that GMAP processes a spectrum with 17 coefficients for CS of *split cut*, 52 coefficients for CD of *split cut*, and 26 coefficients for SPRT data, we expect the following performance ranking – CD, SPRT, and CS. This is in agreement with the scatter-histogram results and explains why staggered SACHI-GMAP outperforms uniform CS-GMAP.
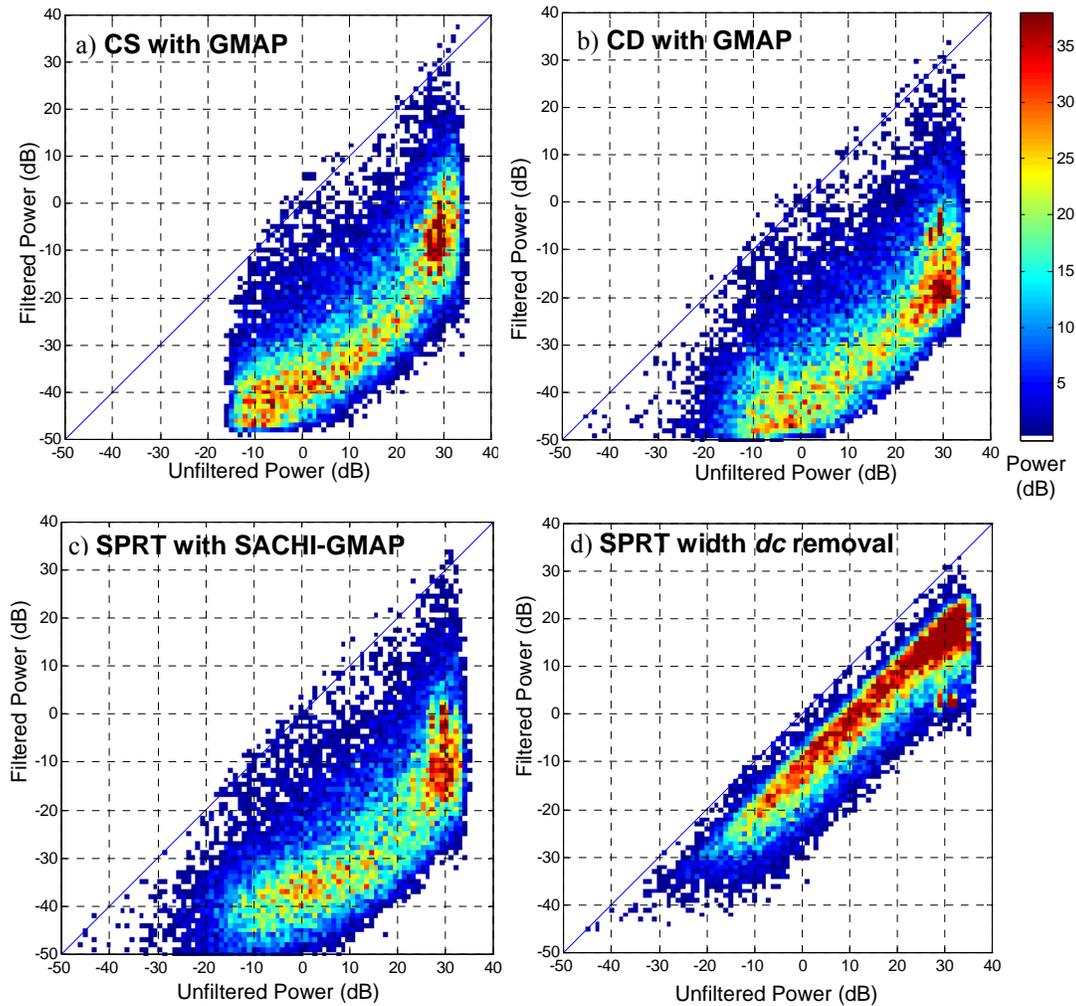
Fig. 3.1.4: Scatter-histograms comparing filtered and unfiltered power in *split cut* and SPRT scans. Unfiltered/filtered power from a) CS with GMAP, b) CD with GMAP, d) SPRT with SACHI-GMAP, e) SPRT with *dc*

The amount of power removed by the GCF in of *split cut* and SPRT scans is compared in Fig. 3.1.5. The scatter-histogram in Fig. 3.1.5a shows the amounts of power removed from CS by GMAP and from SPRT by SACHI-GMAP. The amounts are equivalent but SACHI removes slightly more power at larger suppression levels. Fig. 3.1.5b shows that the amounts of power removed from CD and SPRT scans are comparable. The red colors in scatter-histogram indicate that powers removed from CD-GMAP exceed those from

SACHI-GMAP by about 5 dB. Figs. 3.1.5c-d show how the amounts of power removed from SPRT with *dc* removal compare to those from CS with GMAP, and from CD with GMAP, respectively. Obviously, *dc* removal is not as efficient as GMAP and provides only limited suppression levels. GMAP offers good suppression levels that are comparable for both uniform PRT and staggered PRT time series.
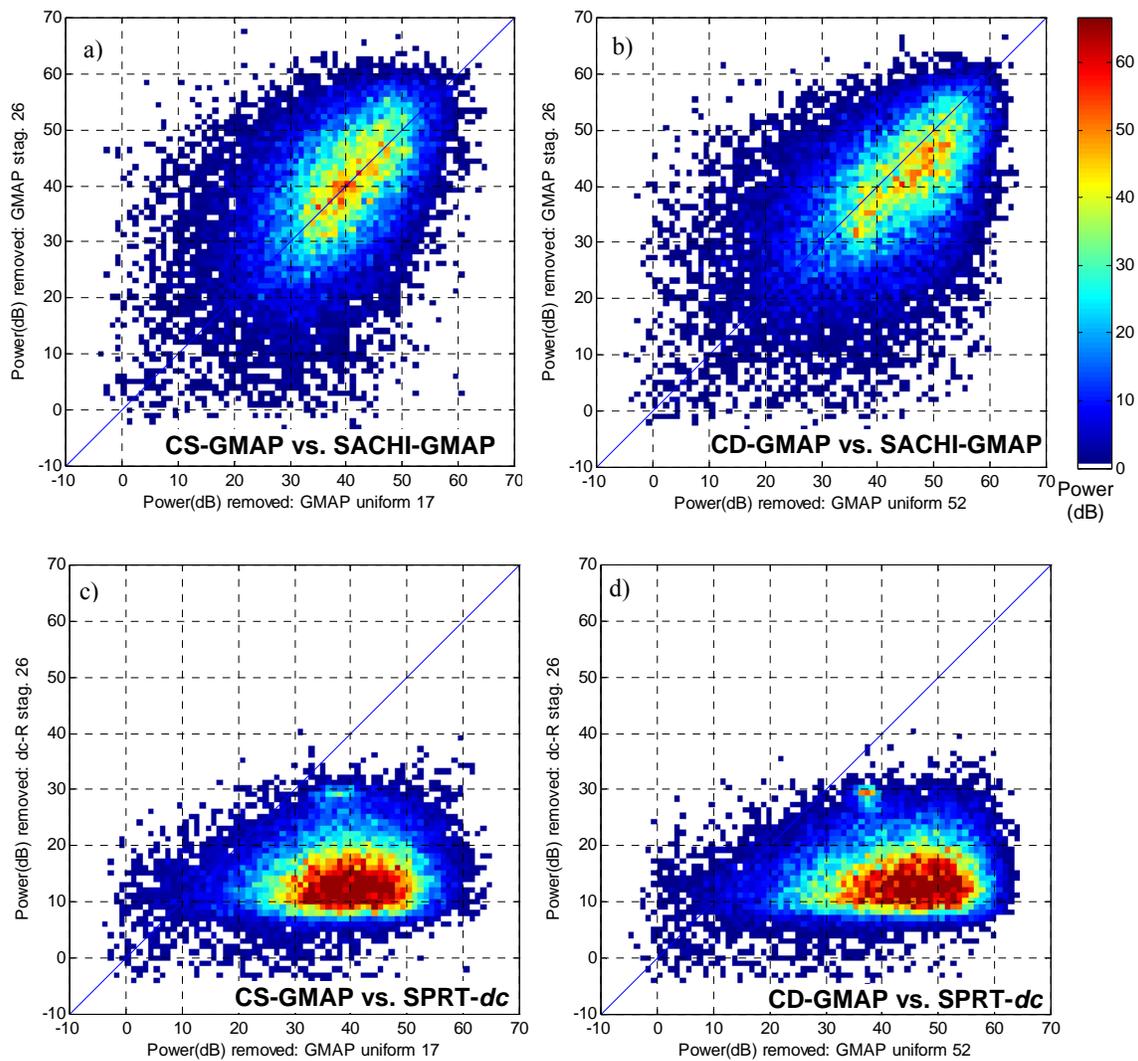
Fig. 3.1.5: Scatter-histograms comparing power removed by GCF in *split cut* and SPRT scans: a) CS with GMAP vs. SACHI-GMAP, b) CD with GMAP vs. SACHI-GMAP, c) CS with GMAP vs. SPRT with *dc* removal, d) CD with GMAP vs. SPRT with *dc* removal.

Similar to *split cut* and SPRT, we analyze powers in the *batch mode* and SPRT (Fig. 3.1.3) by generating color coded scatter plots. *Batch mode* (6 samples of long PRT and 41 samples of short PRT) and SPRT (15 pairs) scatter-histograms of powers unfiltered vs. powers filtered using indicated GCF schemes (dc removal, GMAP, and SACHI-GMAP) are shown in Fig. 3.1.6. The clutter suppression levels are:
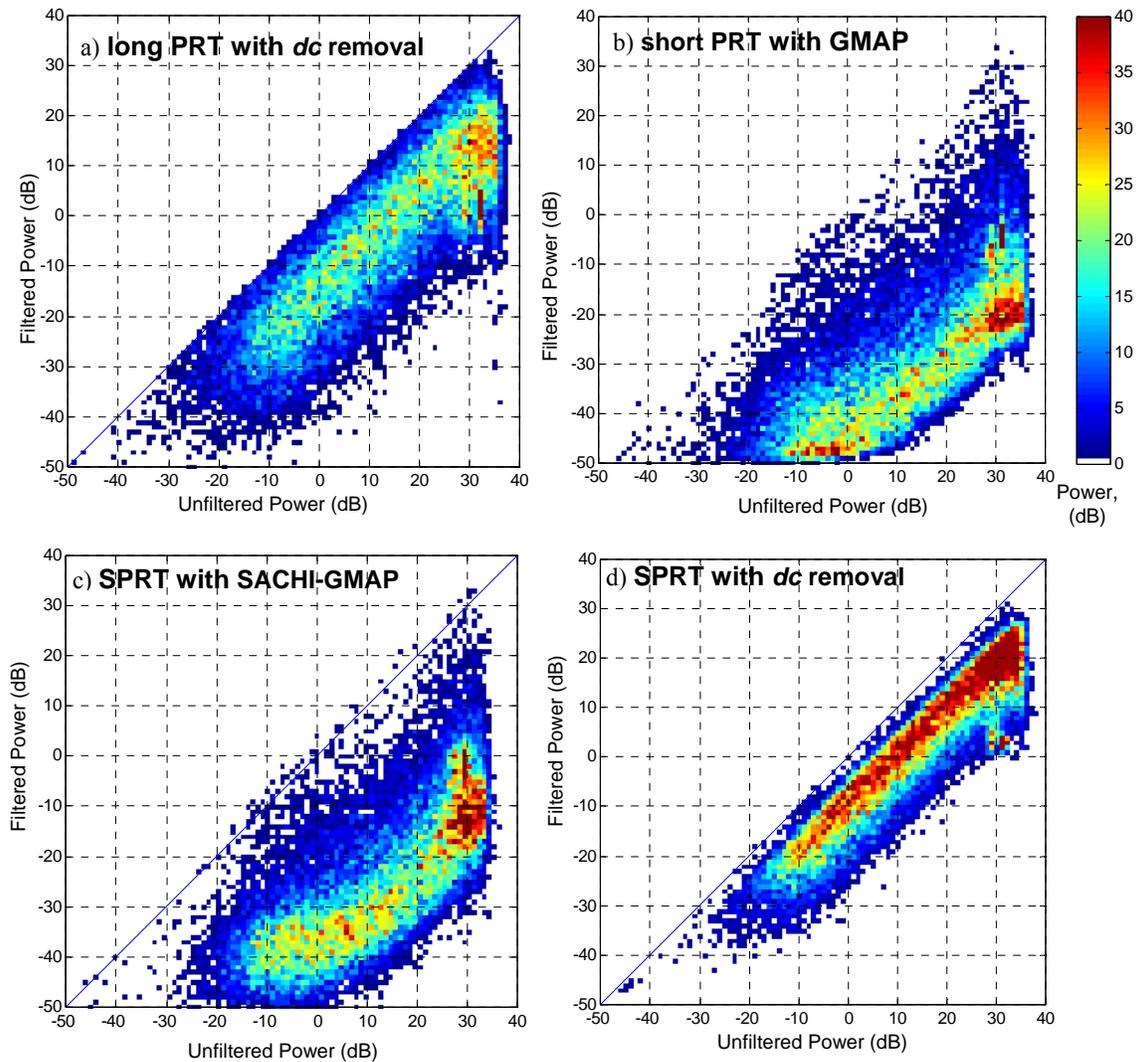
Fig. 3.1.6: Scatter-histograms comparing filtered and unfiltered power in *batch mode* and SPRT scans. Unfiltered/filtered power from: a) long PRT with *dc* removal, b) short PRT scan with GMAP, d) SPRT with SACHI-GMAP, e) SPRT with *dc* removal.

Short PRT of *batch mode* with *dc* removal offers about 10 dB suppression,

Long PRT of *batch mode* with GMAP provides up to 50 dB suppression,

SPRT with *dc* removal gives about 10 dB suppression, and

SPRT with SACHI-GMAP provides about 40 dB suppression.

The scatter-histograms in Fig. 3.1.7 compare the amounts of power removed with different GCF scenarios for *batch mode* and SPRT scans. Fig. 3.1.7a depicts the power removed from short PRT of *batch mode* scan by GMAP in comparison to power removed from SPRT scan by SACHI-GMAP. There is about 5 dB more power removed by GMAP from the 41 samples of uniform PRT compared to 15 pairs of staggered PRT. Fig. 3.1.7b shows scatter-histogram for *dc* removal from both long PRT and SPRT. The asymmetric shape of the scattergram indicates that slightly more power is removed from the SPRT data. Fig. 3.1.7c shows short PRT of *batch mode* scan with GMAP compared to SPRT scan with *dc* removal. Fig. 3.1.7d shows short PRT of *batch mode* scan with *dc* removal compared to SPRT scan with SACHI-GMAP, demonstrating limited suppression of the *dc* removal. The scatter-histograms confirmed our findings that GMAP performs well with both uniform and staggered sequences.

The SPRT data in clear air was processed with SACHI-GMAP and reprocessed with SACHI-TABL (not shown). Recall, TABL is the tabulated values for clutter width parameter from NSSL report #9 (Torres et al. 2005). The suppression levels did not match. The question arose, "Does SACHI-TABL outperform SACHI-GMAP?" The amounts of power removed by GCF from SPRT data using SACHI-GMAP and SACHI-TABL are compared in Fig. 3.1.8. The SPRT with 26 pairs (Fig. 3.1.8a) shows a different trend then SPRT with 15 pairs (Fig. 3.1.8b). SACHI-GMAP removes less power from

SPRT with 26 pairs and more power from SPRT with 15 pairs compared to SACHI-TABL. The number of stagger pairs is the trigger for the differences between SACHI-GMAP cases. The choice of PRTs is the cause of differences between SACHI-GMAP and SACHI-TABL. We anticipate the least difference between performances of SACHI-TABL and SACHI-GMAP for data acquired with 32 staggered pairs of PRTs $T_1 = 1$ ms and $T_2 = 1.5$ ms. In subsection 3.1.4 we provide a detailed explanation that clarifies how and why GMAP and TABL disagree. It suffices to state that SACHI-GMAP execution is superior in both cases.
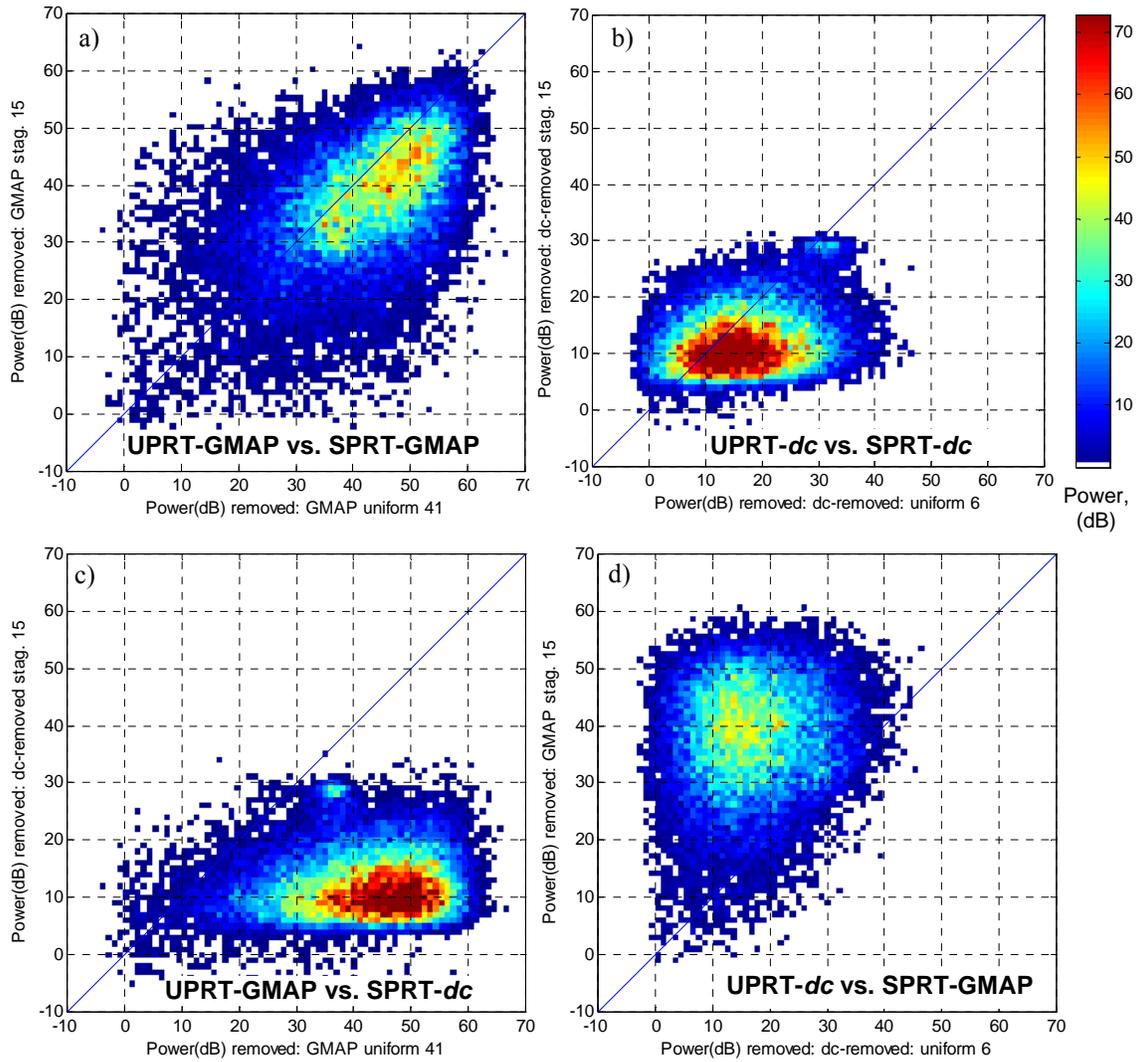
Fig. 3.1.7: Scatter-histograms comparing power removed by GCF in *batch mode* and SPRT scans: a) short PRT with GMAP vs. SACHI-GMAP, b) long PRT with *dc* removal vs. SPRT with *dc* removal, c) short PRT with GMAP vs. SPRT with *dc* removal, d) long PRT with *dc* removal vs. SACHI-GMAP.
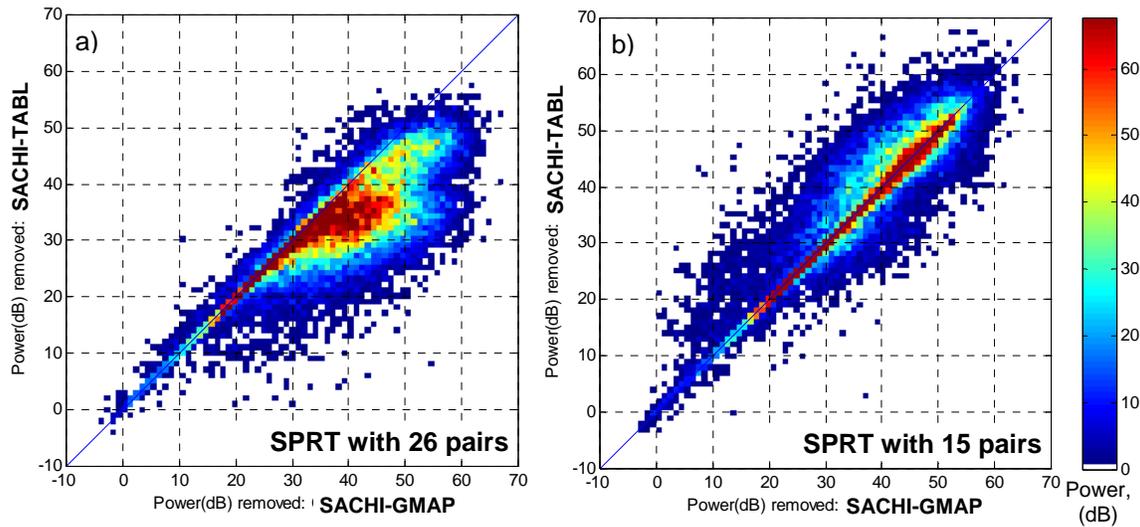
Fig. 3.1.8: Comparing power removed by GCF from SPRT data using SACHI-GMAP and SACHI-TABL: a) SPRT with 26 pairs; b) SPRT with 15 pairs.

3.1.3. *Issues with the clutter width parameter q of SACHI-TABL*

a)   Shortcomings of tabulated *q*

The parameter *q* was introduced in NSSL's Report #9 (Torres et al. 2005, page 103, item 5). To recollect, *q* (an integer) is the clutter width parameter used in the SPRT procedure for clutter filtering. The value of *q* specifies the number of spectral coefficients to be considered as the ground clutter contribution (one sided including *dc*). Report #9 provides a look-up table for estimation of *q* depending on the approximate clutter to noise ratio (CNR) that is estimated from three spectral coefficients near *dc*. We refer to this table as TABL. The TABL provides excellent performance for the signal parameters similar to the ones specified in report #9 (PRT $T_1 = 1$ ms and 32 stagger pairs). If PRTs or the number of pairs change, the TABL performance degrades. This is expected, as clutter

will occupy different number of spectral coefficients for a different set of PRTs or/and pairs. Therefore, the choice of q based on the CNR will overestimate/underestimate the number of spectral coefficients that need to be considered as clutter. Accurate q estimation is imperative especially in the situations when clutter and weather replicas overlap. If q is increased by one, ten extra spectral coefficients are filtered! Filtering "too much" might alter the residuals of the main weather replica such, that it is no longer the largest, and a wrong weather replica would be chosen. Filtering "too little" might leave clutter residuals, and the main clutter replica would be chosen as the one contributing the most power. For examples of spectra reconstructed after "too much" filtering refer to subsection 3.1.4a.i.

b)   SPRT spectrum handling for GMAP

Gaussian model adaptive processing (GMAP) is an adaptive ground clutter filter that performs iterative fit of the Gaussian curve to the spectral coefficients to be replaced as ground clutter (Siggia and Passareli 2004). The filter has shown to successfully remove ground clutter from the uniform PRT sequences if the latter have a sufficient number of samples (Ice et. Al 2007). GMAP is currently used by the National Weather Service to filter ground clutter from weather radar data (ROC 2007, *WSR-88D Specs, #* 2810000G). The elements of GMAP can be used to determine the clutter width parameter for the main replica of ground clutter. We refer to the clutter width parameter estimated using the elements of GMAP as qGMAP.

Example shown in Fig. 3.1.9 illustrates how to use GMAP with the SPRT spectrum. The main replica of ground clutter, located at zero Doppler velocity in the spectrum, can be

treated as a separate spectrum for the GMAP processing. The main clutter replica is indicated with a blue solid line in Fig.3.1.9a and is shown separately in Fig. 3.1.9b. In the presented example, the main replica contains 16 spectral coefficients. These coefficients are passed to GMAP. A minor modification to the GMAP routine is required. The number of spectral coefficients k that GMAP replaces by a Gaussian fit must be made available. This number is used to compute the clutter width parameter $q=(k+1)/2$. The interpolation that GMAP performs to fill in the gap from removed spectral coefficients can be ignored. In Fig. 3.1.9b the spectral coefficients that were not modified by GMAP are indicated with a bold black line. The Gaussian interpolation is not shown for clarity. The five spectral coefficients that were identified as clutter provide the estimate of $q=3$ (one sided including dc), indicated with circles.
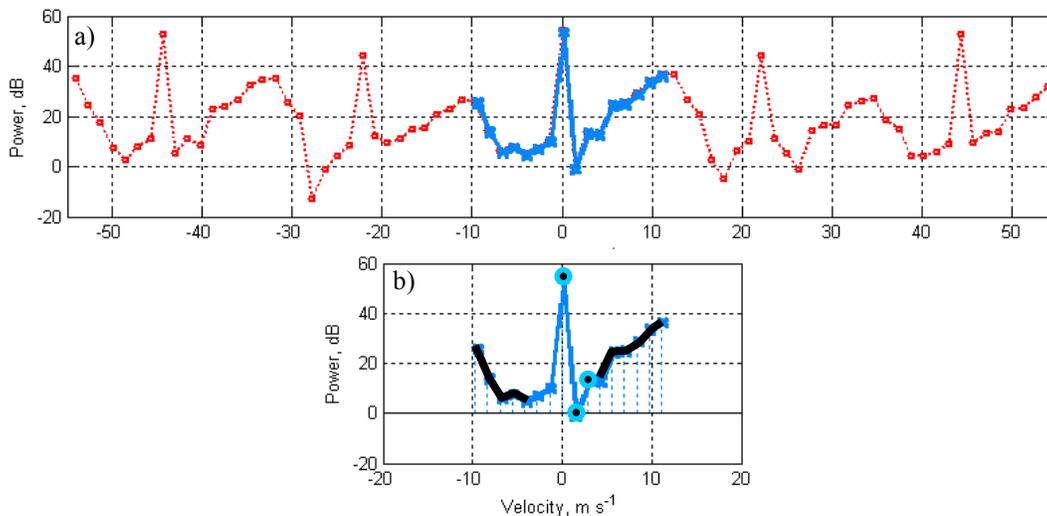
Fig. 3.1.9. SPRT spectrum handling for GMAP clutter identification: a) 5 replicas of the SPRT spectrum and highlighted main clutter replica (blue solid line); b) main clutter replica with GMAP-identified weather (black bold line) and q (circles).

c) Evaluation of q3D using GMAP and different parameters (T_1, v_a, CNR).

A look-up table is faster and simpler than an iterative fit performed by GMAP. A look-up table for a clutter width parameter can be generated using GMAP on the simulated data. As a matter of fact, such table outperforms SACHI-GMAP in speed, and mimics its performance error wise if the weather signal is identical to the parameters that were used to generate such table (i.e., SNR and spectral width). However, if these parameters (SNR and spectral width) change, the table performance degrades. Therefore, we recommend GMAP for the adaptive estimation of the clutter filter width parameter for each resolution volume contaminated by ground clutter. Nonetheless, we describe how to generate a GMAP driven table and indicate possible artifacts and dependences.

We choose three dimensional parameter space (CNR, unambiguous velocity v_a, and number of pair M_p) to generate a new table of clutter width parameter q3D. Our expectation is that such table can accommodate different scanning strategies and a variety of echo strengths. A table q3D is estimated using GMAP on simulated SPRT time series weighted with a Blackman window. We simulate 100 realizations of signal consisting of weather and ground clutter. The simulated signal is passed to GMAP for the clutter width parameter determination. The average of 100 clutter width parameters is recorded.

The table can be generated with different resolutions: coarse (i.e., with steps of 5 dB in CNR, 5 pairs in M_p, and 5 m s^{-1} in v_a) or fine (i.e., with steps of 1 dB in CNR, 1 pair in M_p, and 1 m s^{-1} in v_a). The step changes of q in such table will affect the performance of GCF, but this is not a big issue. The three items that introduce significant changes to the values of q3D and dramatically affect the performance of GCF are velocity and spectral

width of the simulated weather signal, and the choice of the weighting window. There are five Doppler velocity regions collocated with the SPRT clutter replicas. If a q3D table is generated using weather with velocity in a non-clutter-replica region, than it has values lower compared to a table generated using velocity in the clutter-replica region. Moreover, for the time-series weighted with a Blackman window these five regions are wider compared to the time-series weighted with a rectangular window. Simulated weather with varying spectral widths also lead to varying q estimates – narrower width prompts higher q values.

The error requirements (ROC 2007, *WSR-88D Specs, # 2810000G*) are specified for 4 m s^{-1} weather and the Blackman window, therefore we provide a table generated for these parameters. The dimension of the generated q3D is 30x50x10 (Fig. 3.1.10a)

    for a 2dB step of CNR between 2 dB and 60 dB,

    for a 1 pair step in M_p between 11 and 50 pairs, and

    for a 5 m s^{-1} step in v_a between 20 m s^{-1} and 65 m s^{-1}.

The rotations and tilts of the q3D are shown in Fig.3.1.10b to give a general idea of q distribution in the parameter space. Slices of q3D for different v_a, CNR, and M_p are shown in Fig.3.1.10c-e respectively. The q value increases with the increase of M_p and CNR, and decrease of the unambiguous velocity.
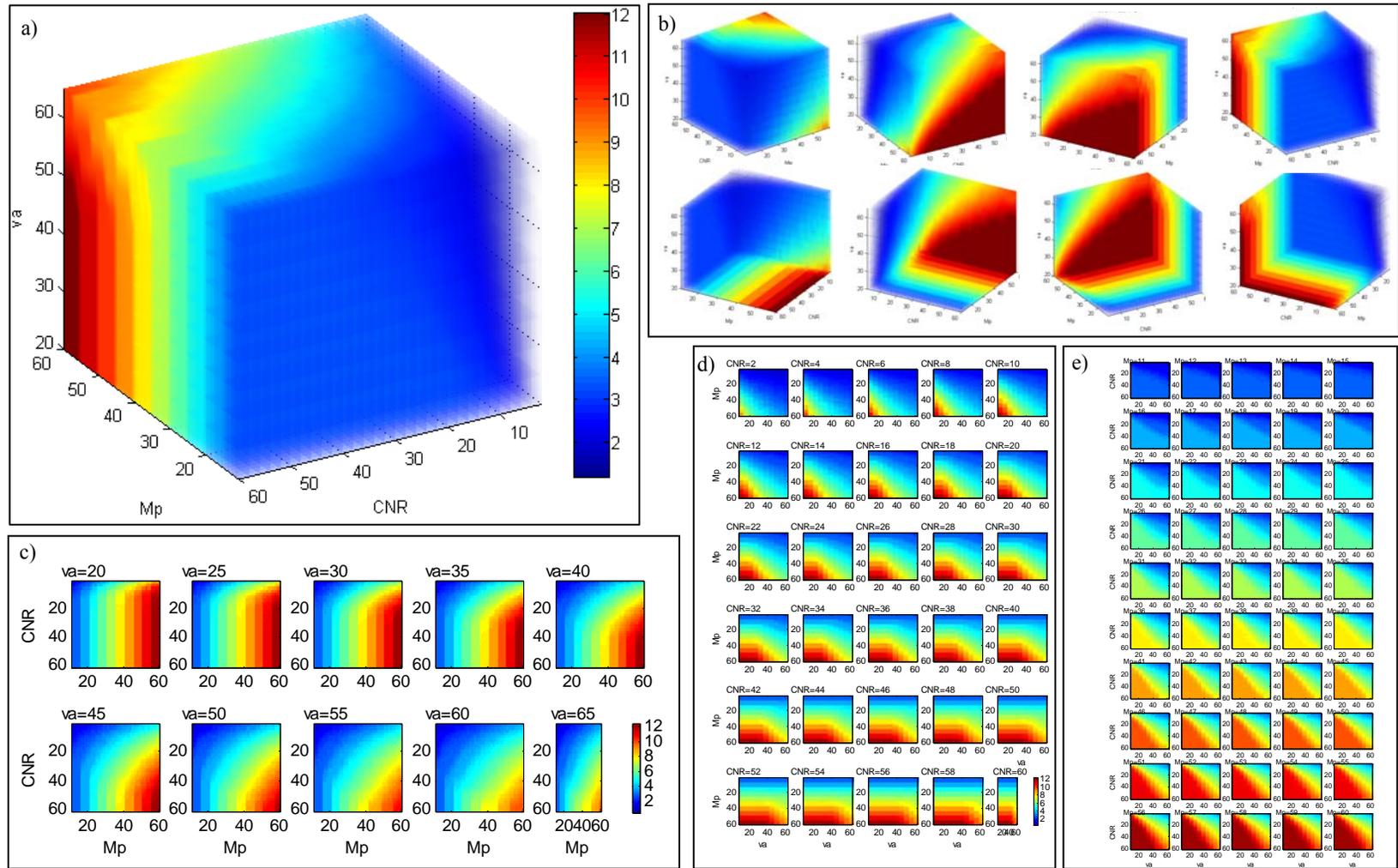
Figure 3.1.10. q3D: a) cube dimensions 30x50x10: CNR = 2:2:60 dB, M_p = 11:1:50 pairs, v_a = 20:5:65 m s^{-1}; b) rotations of q3D; c) CNR(M_p) slices of q3D for different v_a:, d) v_a (M_p) slices for different CNR, e) CNR(v_a) slices for different M_p.

24

3.1.4. *GCF performance evaluation with simulated data.*

a) Spectral analyses

i) *Analyses of SPRT spectra before and after clutter filtering with different filtering and data parameters*

SACHI-TABL provides a good reconstruction of clutter filtered spectrum for the SPRT data simulated with PRT T_1=1 ms and 32 pairs. For the same PRT and a smaller number of pairs (i.e., 12 pairs), SACHI-TABL reconstructs the correct spectrum if the weather and clutter replicas do not overlap, but fails if the weather and clutter replicas are collocated. Figs. 3.1.11 and 3.1.12 illustrate this trend depicting 100 realizations of simulated SPRT spectra for 11 m s^{-1} and 21 m s^{-1} respectively. In this case one of the clutter replicas is centered on 21 m s^{-1}. The figures are organized in the following manner. Spectra for different iterations with color coded power are displayed in the top rows (panels a-c); the same spectra overlaid for different interactions are displayed in the bottom row (panels d-f); the unfiltered SPRT spectra are shown in the left column (panels a and d); the spectra reconstructed using SACHI-TABL are shown in the right column (panels c and f); the middle column depicts spectral reconstruction achieved by SACHI-GMAP (panels b and d). Fig. 3.1.11 shows that both methods SACHI-GMAP and SACHI-TABL remove clutter, pinpoint the correct weather replica, and reconstruct the weather spectrum. In this example, SACHI-TABL clearly overestimates the clutter width parameter. Comparing reconstruction results presented in Fig.3.1.11b and 3.1.11c we note that SACHI-GMAP provides a more prominent and narrower ridge (peak) location and the gaps at clutter replica locations are narrower compared to those of SACHI-

TABL. Nonetheless both methods work well for the weather velocity in non-clutter-replica region.
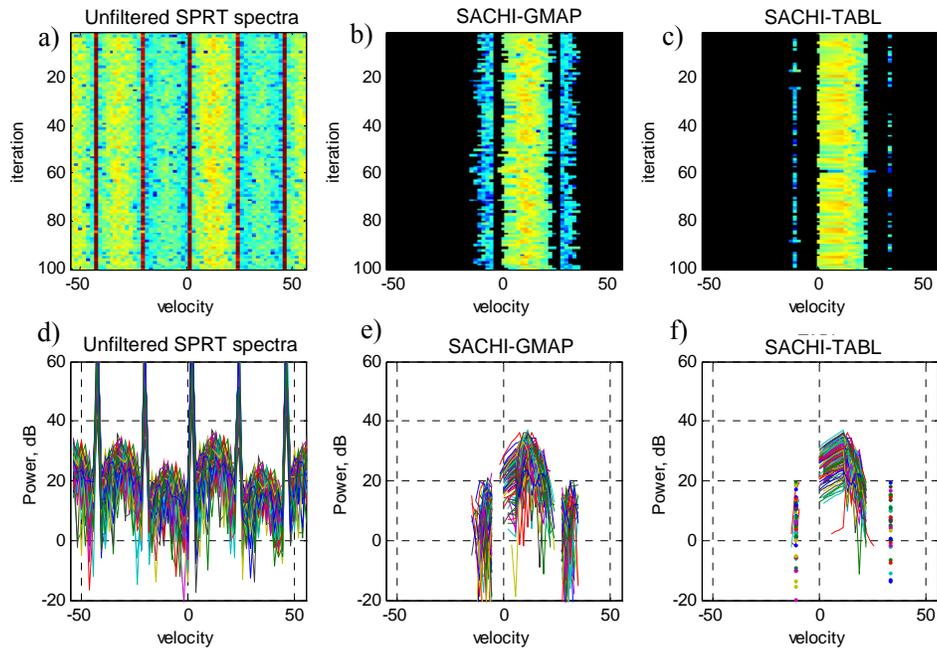
Fig. 3.1.11. SPRT spectra: a,d) unfiltered; b,e) GCF with SACHI-GMAP; c,f) GCF with SACHI-TABL. Simulation parameters are T_1=1ms, 12 pairs, SNR=20 dB, CNR=50 dB, weather velocity v=**11** m s^{-1}.
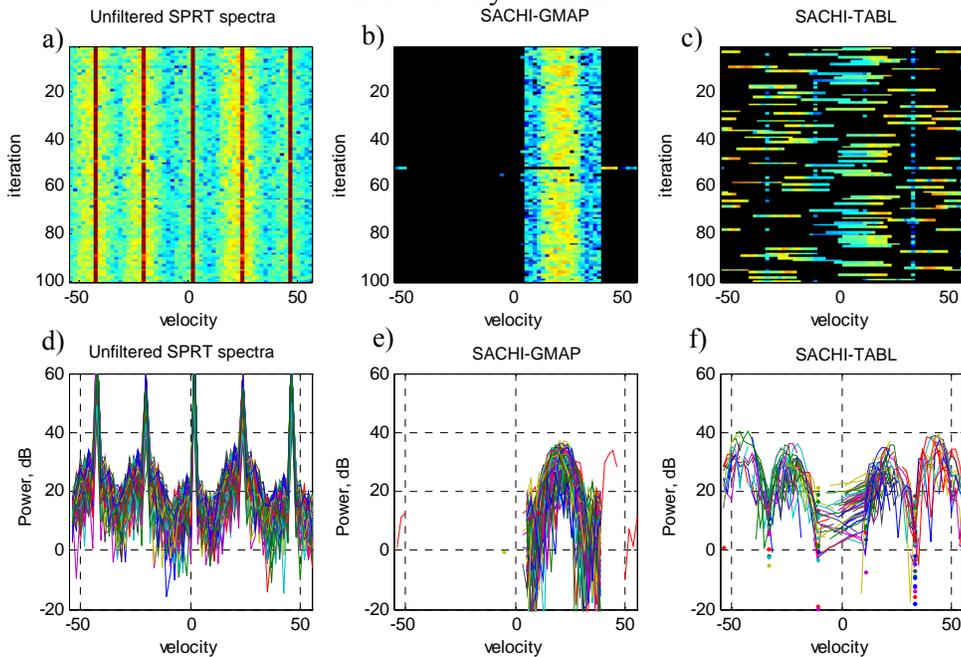
Fig. 3.1.12. SPRT spectra a,d) unfiltered, b,e) GCF with SACHI-GMAP; c,f) GCF with SACHI-TABL. Simulation parameters are T_1=1ms, 12 pairs, SNR=20 dB, CNR=50 dB, weather velocity v=**21** m s^{-1}.

The situation is different in Fig. 3.1.12, where the simulated weather velocity is in the clutter-replica region. Fig. 3.1.12c shows that on many occasions SACHI-TABL fails to locate the correct weather replica. This is the result of over filtering. The over filtering is caused by the wrong choice of clutter width parameter q. For optimal clutter filtering a sophisticated scheme that takes into account the inherent spectral width of clutter signature and provides an adaptive estimate of q is needed. SACHI-GMAP is the adaptive scheme that works. SACHI-GMAP provides an accurate estimate of clutter width that results in a choice of correct clutter replica in 199 out of 200 presented spectra (all except the iteration #51 in Fig. 3.1.12b). In general, SACHI procedure can leave gaps in the reconstructed spectrum at the locations of clutter replicas if these do not coincide with the reconstructed peak. Such gaps are visible on each side of the weather band (peak) in Figs. 3.1.11b, c, e, and f, and additional examples of SACHI-GMAP in Fig.3.1.11g. The width of gaps depends on the clutter width parameter and weighting window function. Figs. 3.1.12 show a complete failure of SACHI-TABL and a remarkable reconstruction of the spectra with SACHI-GMAP. We recommend GMAP for the adaptive estimate of clutter width. If GMAP is not available, a table q3D, estimated using GMAP on simulated SPRT time series for different parameters as described in subsection 3.1.3c, can be provided by NSSL.
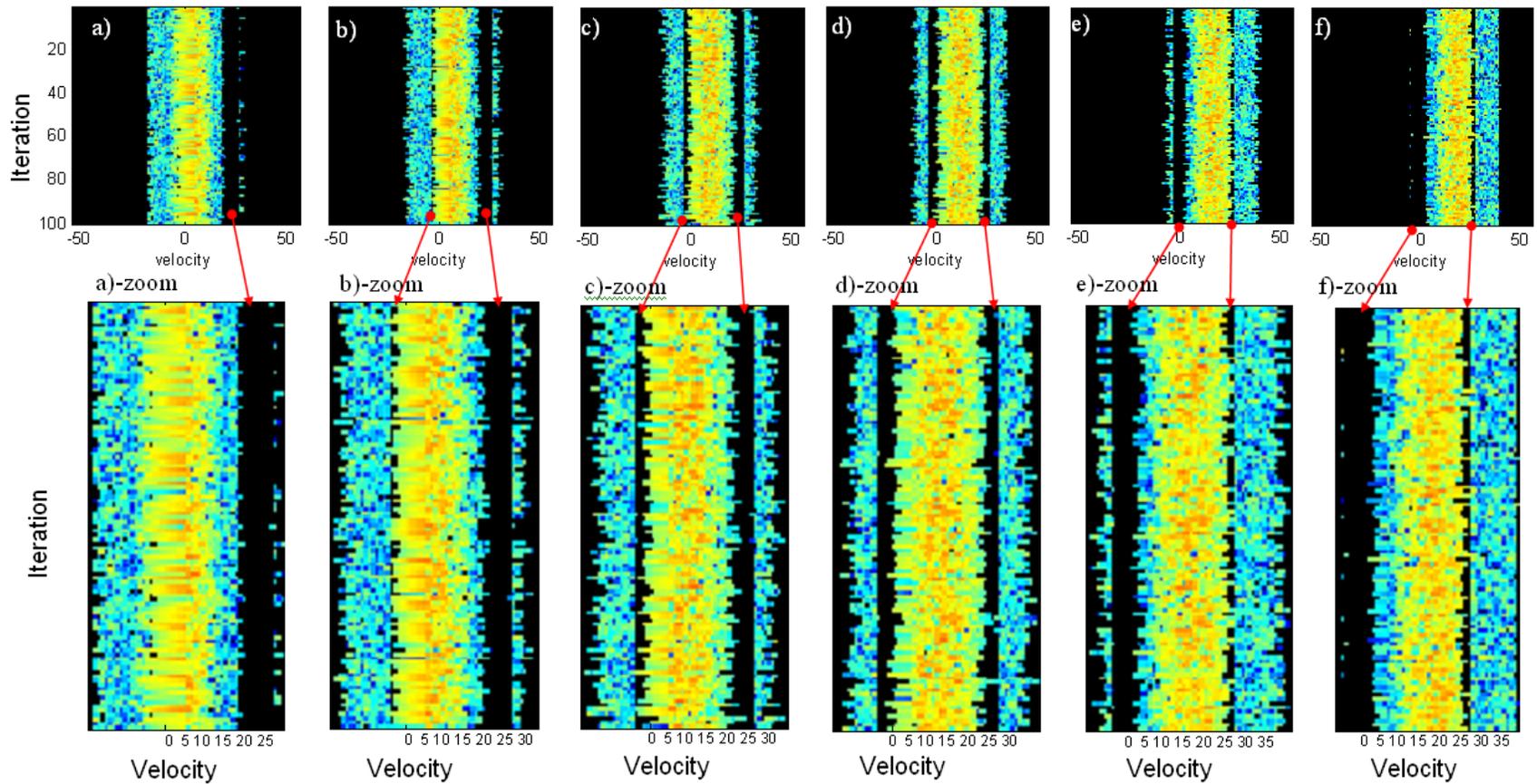
Fig. 3.1.11g: Gaps in the reconstructed by SACHI-GMAP spectra. Simulation parameters are T_1=1ms, 24 pairs, SNR=20 dB, CNR=50 dB, 100 realizations, weather velocity a) 3 m s^{-1}, b) 6 m s^{-1}, c) 9 m s^{-1}, d) 12 m s^{-1}, e) 16 m s^{-1} and f) 20 m s^{-1}.

ii)   *Analyses of filtered mean spectral fields*

Spectral analyses can reveal problems with spectral clutter filtering. Irregularities in spectral fields expose issues by disclosing unexpected features that protrude over the background textures in the parameter space. In the SPRT case spectral analyses led us to discover sources of large errors for certain parameters, artifacts, unexpected degradation of performance due to the window effect (Blackman window), and irregularities in performance between even and odd number of pairs. We also observed that an increase of CNR does not aggravate the performance of the filter significantly (i.e., when filter "breaks" it "breaks" for large and for small CNR equally). We present only several examples of averaged spectral fields to illustrate the type of analyses and to spotlight discovered issues.

The spectra were simulated for the constant dwell time, spectral width and SNR (60 ms, 4 m s^{-1}, and 20 dB). Note, that the dwell of 60 ms is the maximum time allowed in the simulation; true dwell times change for different PRTs. The varying parameters were PRT, CNR, and weather velocity. The PRTs T_1 were tested for values between 1 ms and 2 ms with a step of 0.1 ms. The CNR were tested for values between 0 dB and 60 dB with a step of 5 dB. The weather velocity was varied from 0 to the extended unambiguous velocity with a step of 1 m s^{-1}. The combination of PRT and dwell time dictates the number of pairs that can be staggered for each time series (Table 3.1.1).

Table 3.1.1

PRT T_1, ms	1.0	1.1	1.2	1.3	1.4	1.5	1.6	1.7	1.8	1.9	2.0
Number of stagger pairs	24	21	20	18	17	16	15	14	13	13	12

The images of spectra in Fig.3.1.13 are in 3 panels: uniform PRT spectra (top panel), unfiltered SPRT spectra (middle panel), and SPRT spectra reconstructed with SACH-GMAP (bottom panel). Both axes show velocity. The Doppler velocity axis is the velocity/frequency component in the Doppler spectrum. The velocity axis is the velocity of simulated weather echo. The spectra from uniform PRT simulation are displayed in Fig.3.1.13a. Every row in the image shows a spectrum with color coded power spectral density. This spectrum represents an average of hundred spectra formed for the hundred realizations of weather signal contaminated by ground clutter and simulated for a certain weather velocity. Each consecutive row shows the mean spectrum for weather with a larger velocity value. Therefore, the collection of mean spectra (for the uniform time series) forms a spectral field displaying a slanted band for the weather velocity and a vertical band for clutter. The uniform PRT time series are converted to SPRT time series by deleting samples in the pattern 10100. The spectrum is estimated for each realization; and the average of 100 spectra is displayed in each row in Fig.3.1.13b. The resulting spectral field contains five replicas of weather that appear as slanted bands of different intensity and five replicas of ground clutter that appear as equally spaced vertical lines. Note that the band corresponding to the main weather replica is the most prominent and is surrounded by the bands/replicas with lower color intensity/power. The symmetric location of the bands (in order not to bias moment estimates) and their different intensity levels (to locate the weather signal) are the foundation of the success of the SPRT technique.
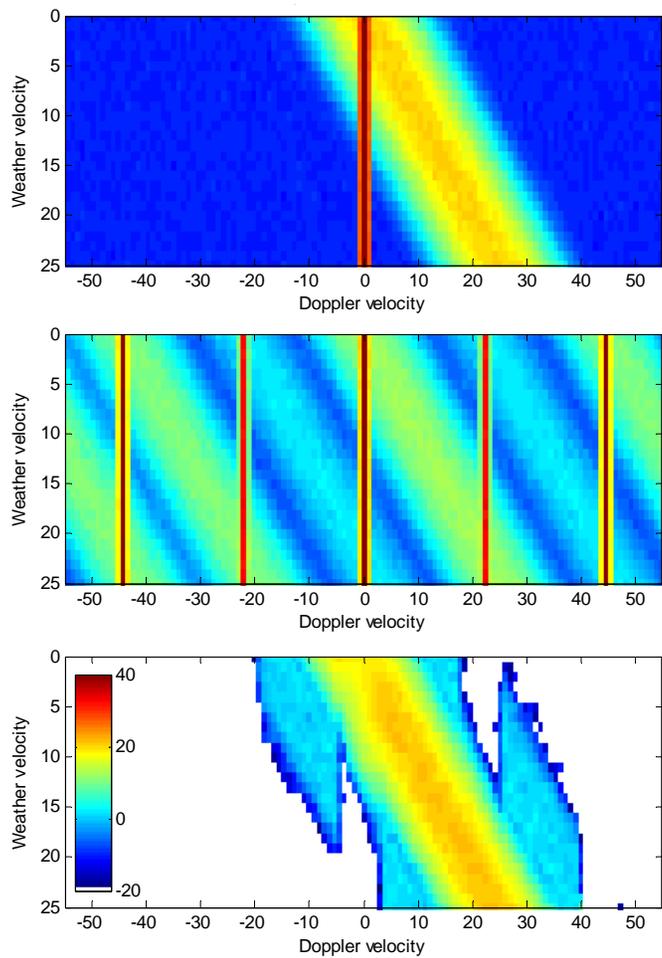
Fig. 3.1.13: Mean spectra for a) uniform PRT unfiltered, b)
SPRT unfiltered, c) SPRT filtered by SACH-GMAP.
Simulation parameters are SNR=20 dB, CNR=40 dB, 24 pairs,
T_1=1 ms, σ_v of weather 4 m s^{-1}, σ_v of clutter 0.28 m s^{-1}, 100
realizations.
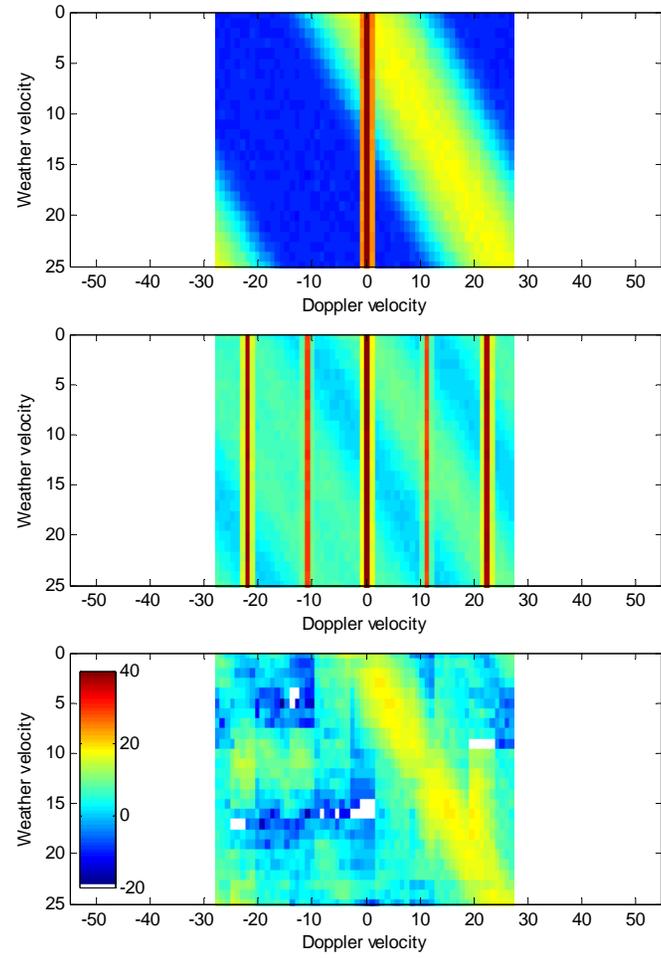
Fig. 3.1.14: Mean spectra for a) uniform PRT unfiltered, b)
SPRT unfiltered, c) SPRT filtered by SACHI-GMAP.
Simulation parameters are SNR=20 dB, CNR=40 dB, 12 pairs,
T_1=2 ms, σ_v of weather 4 m s^{-1}, σ_v of clutter 0.28 m s^{-1}, 100
realization.

31

Each of the 100 SPRT spectra are filtered and reconstructed using SACHI-GMAP, averaged, and the resulting averaged spectrum is plotted in the corresponding row in Fig.3.1.13c. Ideally, if all of 100 spectra were reconstructed correctly, the 3/5 of the corresponding row in panel c would be empty. If some of the 100 reconstructed spectra contained errors (i.e., a wrong replica was chosen), the spectral average would show a decrease in the area with empty space. We show only simulations for weather velocities from 0 to 25 m s^{-1}. After the image is formed the simulations are repeated for the different CNRs, and for the different PRTs.

Example of average spectral fields for T_1=1 ms, presented in Fig.3.1.13, illustrates excellent reconstruction of weather spectra. The empty spaces centered at velocities of zero and 22 m s^{-1} are from the gaps due to the clutter replicas. The example of average spectral fields for T_1=2 ms, presented in Fig.3.1.14, is alarming. The 3/5 of the expected empty space in each row in panel c is gone. The spectral field is filled with errors. On many occasions, a wrong weather replica was chosen by SACHI-GMAP. For the weather velocity between 15 and 19 m s^{-1} the correct weather replica is chosen in most of the cases. Decreasing CNR does not improve the situation and points to the inability of SACHI to handle the 12 stagger pairs of T_1=2 ms. More pairs, longer dwell times, and shorter PRT could improve the performance as will be shown in subsection 3.1.4b. The velocity regions collocated with clutter replicas are problematic for SACHI. The Blackman window expands these regions due to window characteristics (it brings down sidelobes, but increases the width of the main lobe). The rectangular window preserves the width of clutter and therefore can be used to decrease the areas of bad velocity region, especially in the situations with small number of stagger pairs. Fig.3.1.15 illustrates this

32

phenomenon for T_1=1.5 ms. The area of the average spectral field where SACHI is prone to mistakes is smaller in the case with the rectangular window.
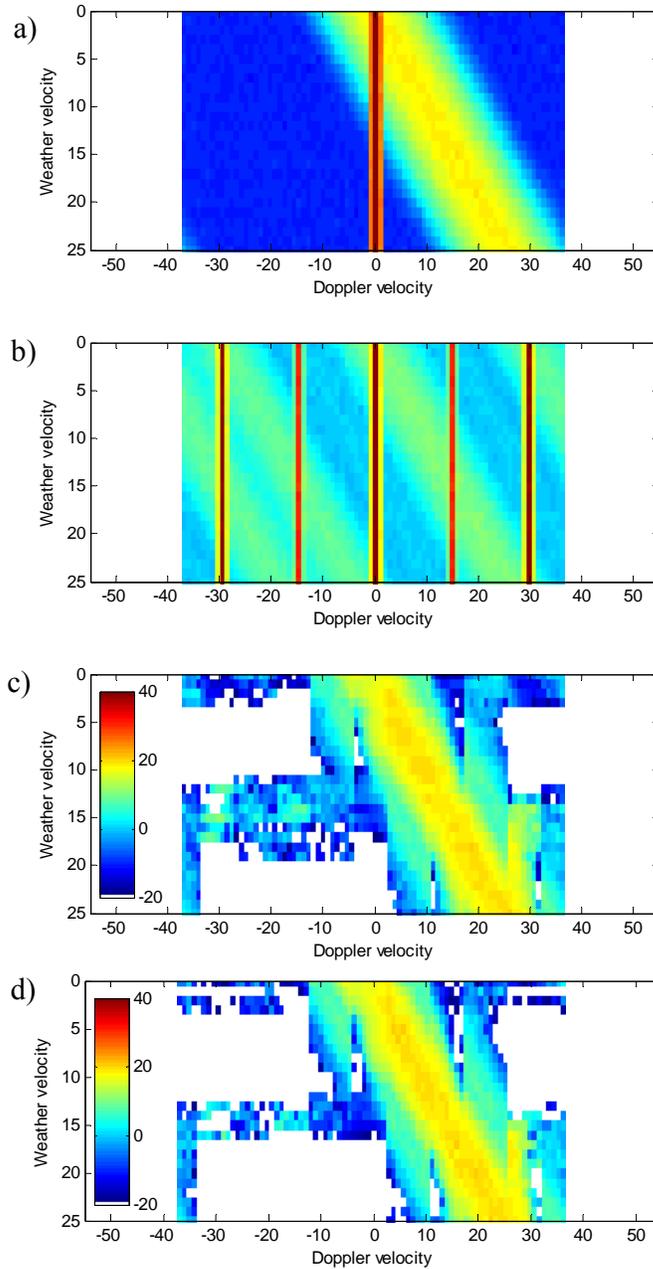
Fig. 3.1.15: Mean spectra for a) uniform PRT unfiltered, b) SPRT unfiltered, c,d) SPRT weighted by the Blackman window and filtered by SACHI-GMAP d) SPRT weighted by the rectangular window and filtered with SACHI-GMAP. Simulation parameters are SNR=20 dB, CNR=40 dB, 16 stagger pairs, T_1=1.5 ms, σ_v of weather 4 m s^{-1}, σ_v of clutter 0.28 m s^{-1}, 100 realizations.

b)   Performance Evaluation

i)   *Errors and biases*

The requirements for acceptable errors and biases are specified in document #2810000G (ROC 2007, *WSR-88D Specs*). In expectation of problems associated with spectral clutter filtering of the uniform PRT sequence, a relaxation on requirements, expressed in terms of *minimum usable velocity,* is defined. For example, for a clutter suppression level of 50 dB, the *minimum usable velocity* is 4 m s^{-1}. This defines a permissible region of bad Doppler velocities in the spectrum. In application to a staggered sequence such relaxation considers only the region containing the main clutter replica and ignores other four regions with clutter replicas. Therefore, the rules in document #2810000G (ROC 2007, *WSR-88D Specs*) are more stringent when dealing with staggered PRT data. A cumulative dB-per-dB threshold makes it difficult to specify a level of tolerable errors for power. For example, a base threshold (2 dB for CS) is specified for clutter suppression of 30 dB; the base is adjusted by adding 0.15 dB for each dB above 30 dB and below 50 dB of suppressed clutter; the result is further adjusted by adding 1 dB for each dB above 50 dB. Consequently, the threshold is 2 dB for 30 dB clutter suppression, 3.5 dB for 40 dB clutter suppression, 5 dB for 50 dB clutter suppression, and 15 dB for 60 dB clutter suppression (2 + 0.15(50-30) + 1(60-50) = 15). To summarize, errors and biases

> for velocity and spectral width below 2 m s^{-1} are considered tolerable, and
>
> for power below 2 dB for 30 dB suppression is within the requirements.

To determine if SACHI meets error requirements we established a parameter space; simulated SPRT data contaminated with ground clutter for the given set of parameters;

subjected these data to spectral filtering and reconstruction; estimated power, velocity and spectral width from the reconstructed spectra; and evaluated results against the simulation parameters. For each simulation, 100 realizations are obtained. A portion of the Matlab code is shown in Table 3.1.2 to indicate used estimators and methodology.

Table.3.1.2.

```
%Spectral_Coefficients are from the reconstructed by SACHI spectrum

%power estimation
Power = mean(abs(Spectral_Coefifients).^2); %power
Pi(i)=Power;

%velocity estimation
R1 = mean((abs(Spectral_Coefifients).^2).*exp(j*2*pi*(0:M-1)'));
velocity = va/pi * angle(R1);
vi(i)=velocity;

%spectra width estimation
width = sqrt(2)*va/pi* sqrt(abs(log(Power/abs(R1)))).*sign(log(Power/abs(R1)));
wi(i)=width;

%errors
SD_P = 10*log10(1+std(Pi)/Simulated_Power);
SD_v = std(vi);
SD_w = std(wi);

%biases
Bias_P = mean(Pi) – Simulated_Power;
Bias_v = mean(vi) – Simulated_velocity;
Bias_w = mean(wi) – Simulated_width;
```

Fig.3.1.16 shows an example of errors and biases obtained for simulations of SPRT sequence (T_1=1 ms, 60 ms dwell time resulting in 24 stagger pairs, Blackman weighting window, CNR of 40 dB, SNR of 20 dB, spectral width of weather 4 m s^{-1}) for weather velocities changing from 0 to v_a. The plots depict performance of SACHI-GMAP (top row), SACHI-TABL (middle row), and SACHI-q3D (bottom row). For this parameter set (24 pairs with T_1=1 ms), SACHI-GMAP and SACHI-q3D produce identical results, and errors within specifications. The plot with velocity errors SD(v) of SACHI-TABL (middle row 2nd column) shows that for weather velocities between 20 m s^{-1} and 30 m s^{-1}

the errors are unacceptable. Other than that the overall performance is good. The performance degrades if T_1 is changed from 1 ms to 2 ms and the remaining parameters are kept the same. The change of T_1 for the same dwell time results in decrease of the number of staggered pairs from 24 to 12. Example presented in Fig.3.1.17 shows that errors and biases of power and spectral width remain within the tolerance levels, but the error and bias of velocity grows out of proportion. These examples disclose the trends in errors and biases for the specific weather spectrum width of 4 m s^{-1}. Next, we reiterate these analyses for different spectral widths of weather from 0.5 m s^{-1} to 8 m s^{-1} (see Figs. 3.1.18-19) for T_1 of 1 ms and 2 ms respectively. In these examples small errors are indicated by blue colors (less than 2 m s^{-1}), and small biases are light green (near 0 m s^{-1})

The power bias in Fig.3.1.18 (4th column) shows several regions with different values. There is a tolerable positive bias through most of the parameter space. Larger but tolerable biases at the locations of clutter replicas for σ_v <1 m s^{-1} expose an artifact – negative and positive biases in adjacent locations of clutter replica regions. The large negative bias for weather velocities <1 m s^{-1} is not a problem due to its location below the *minimum usable velocity*. The positive bias at velocity of ~5 m s^{-1} is acceptable for σ_v <1 m s^{-1} as it must be less than 10 dB, and satisfactory for 1<σ_v <2 m s^{-1} as it must be <3.5 dB for 40 dB suppression.

The velocity bias in Fig.3.1.18 (5th column) shown with light green colors, indicates zero bias. Dark red and dark blue colors indicate areas with intolerable bias exceeding 2 m s^{-1} in the absolute value. The biases at the locations of clutter replicas for σ_v <1.5 m s^{-1} are

not acceptable. Biases at many of the locations for $\sigma_v > 7$ m s^{-1} could be considered not acceptable, but there is no specification for these widths of weather.

Width bias (Fig.3.1.18, 6th column) shown for SNR of 20 dB exposes a trend of ripples with positive bias. This trend decreases to zero bias for higher SNR (not shown). The biases at the locations of clutter replicas for $\sigma_v < 1.5$ m s^{-1} are not acceptable. The bias for weather velocities < 1 m s^{-1} is not a problem because it is in the region defined as non usable (i.e., below the *minimum usable velocity*).

The velocity errors in Fig.3.1.18 (2rd column) have a peculiar division with mainly two areas: blue color indicates small errors; dark red color indicates large errors. The regions at clutter replicas for $\sigma_v < 2$ m s^{-1} indicate large errors. The region for $\sigma_v > 6$ m s^{-1} shows oscillations between clutter replicas locations, indicating large errors. Nonetheless, all of the velocity errors are acceptable as the specifications consider only $\sigma_v = 4$ m s^{-1}. The regions of small velocity errors shrink in Fig.3.1.19 (second column) compared to Fig.3.1.18 (second column). In both examples T_1=1 ms and T_1=2 ms (Figs.3.1.18-19) the errors and biases are largest with SACHI-TABL. The power and spectrum width errors and biases for SACHI-GMAP are within specifications. The velocity errors and biases do not meet requirements for T_1=2 ms (at the dwell time of 60 ms, and weather spectrum width of 4 m s^{-1}).
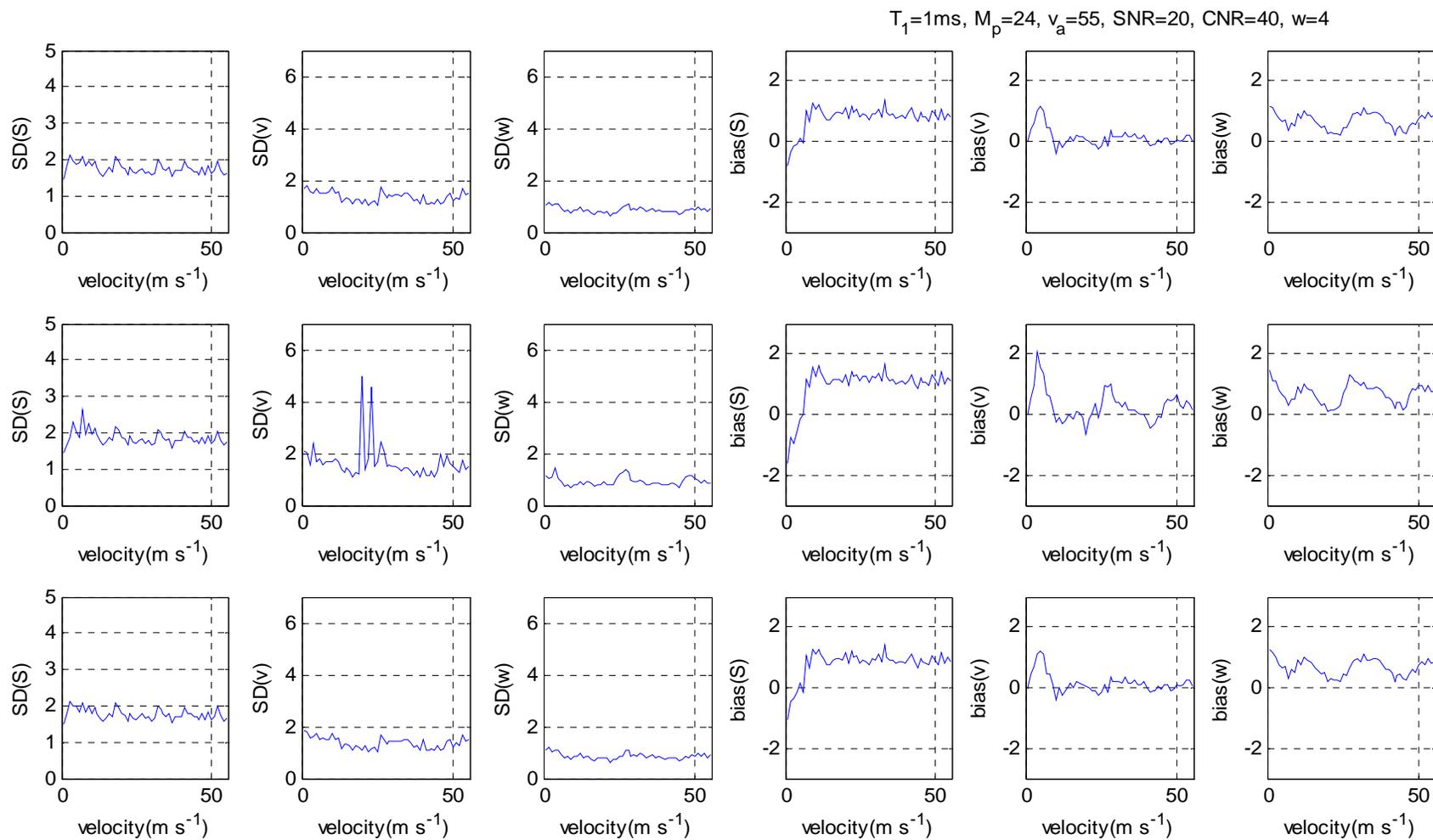
Fig.3.1.16. Standard deviations and biases of power, velocity, and widths computed for the SPRT sequence filtered using (top) SACHI-GMAP, (middle) SACHI-TABL, (bottom) SACHI-q3D. The simulation parameters are 100 realizations, Blackman window, T_1=1 ms, CNR=40 dB, M_p=24 (dwell 60 ms), SNR = 20 dB, σ_v of weather 4 m s^{-1}, σ_v of clutter 0.28 m s^{-1}.
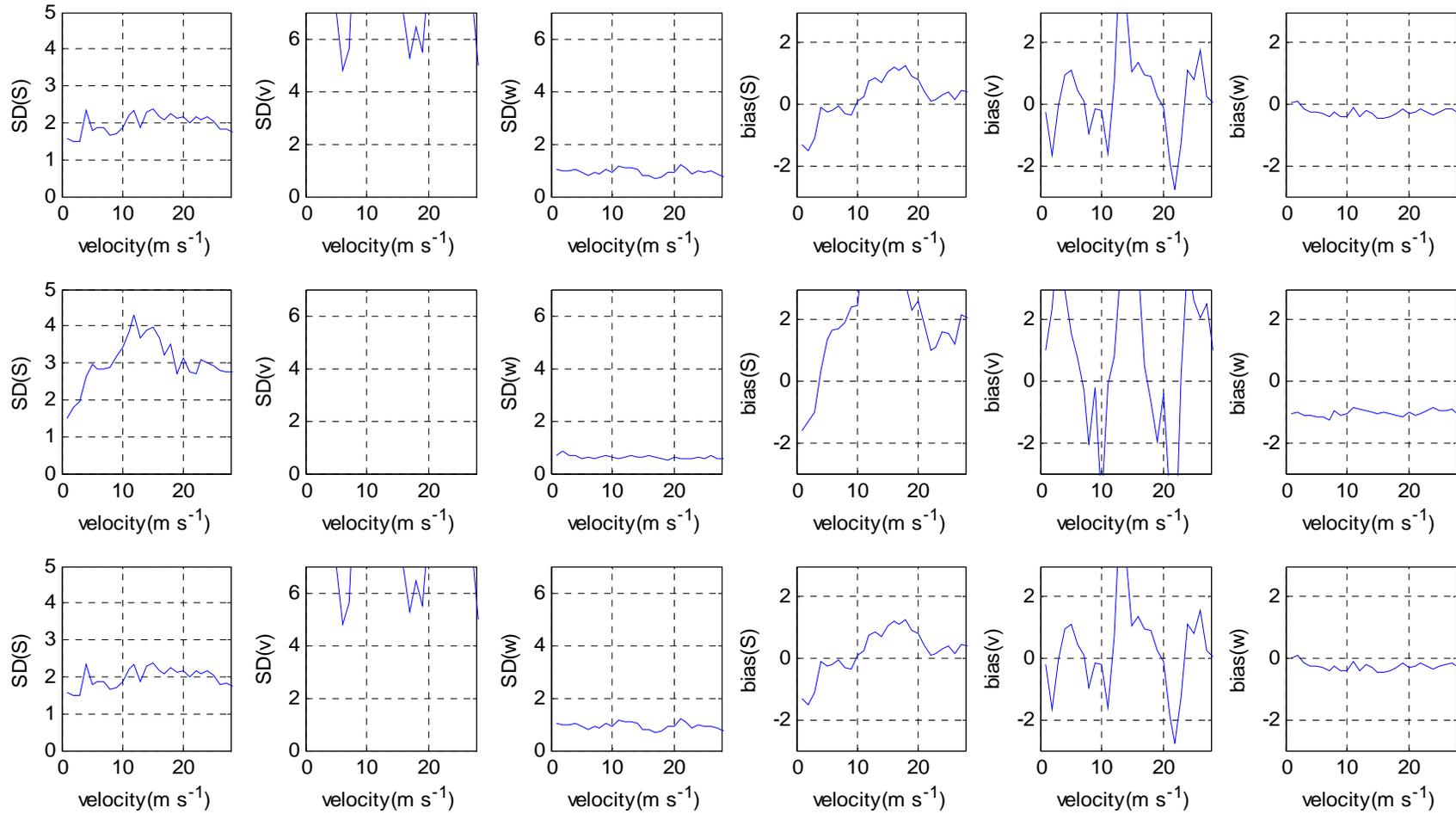
Fig.3.1.17. Standard deviations and biases of power, velocity and widths computed for the SPRT sequence filtered using (top) SACHI-GMAP, (middle) SACHI-TABL, (bottom) SACHI-q3D. The simulation parameters are 100 realizations, Blackman window, T_1=2 ms, CNR=40 dB, M_p=12 (dwell 60 ms), SNR = 20 dB, σ_v of weather 4 m s^{-1}, σ_v of clutter 0.28 m s^{-1}.
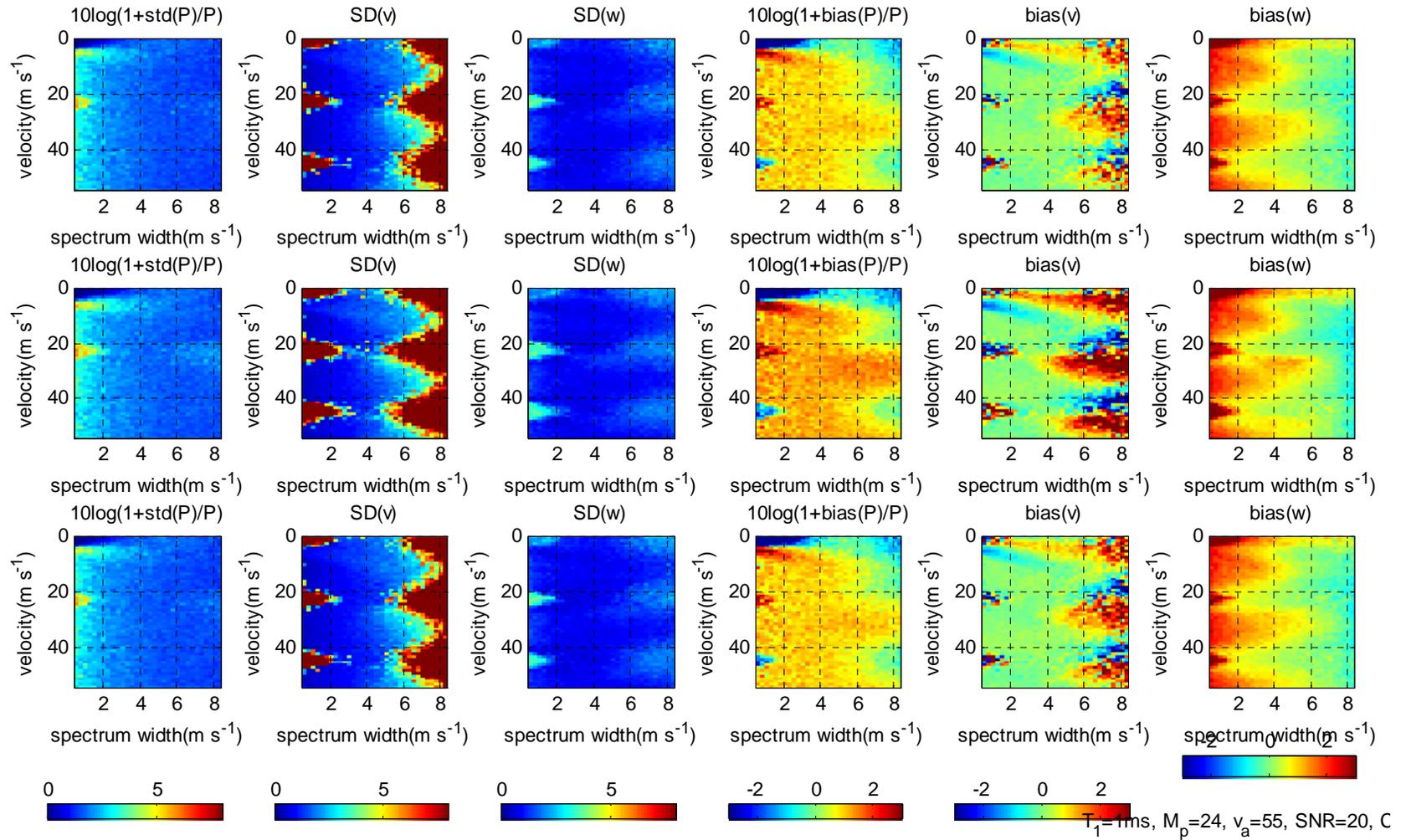
Fig.3.1.18. Standard deviations and biases of power, velocity, and widths computed for the SPRT sequence filtered using (top) SACHI-GMAP, (middle) SACHI-TABL, (bottom) SACHI-q3D. The simulation parameters are 100 realizations, Blackman window, T_1=1 ms, CNR=40 dB, M_p=24 (dwell 60 ms), SNR = 20 dB, σ_v of weather from 0.5 m s^{-1} to 8 m s^{-1}, σ_v of clutter 0.28 m s^{-1}.
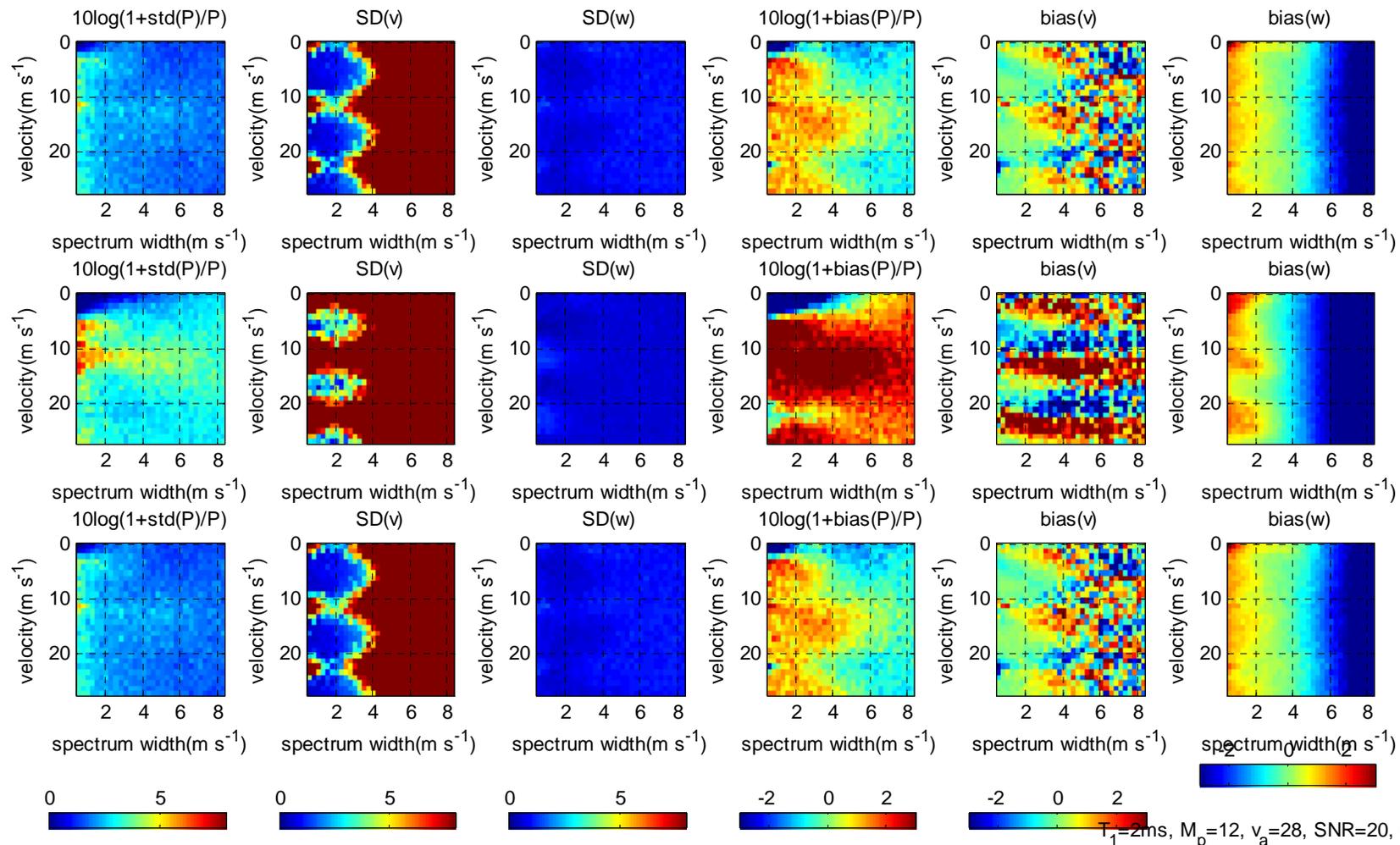
Fig.3.1.19. Standard deviations and biases of power, velocity and widths computed for the SPRT sequence filtered using (top) SACHI-GMAP, (middle) SACHI-TABL, (bottom) SACHI-q3D. The simulation parameters are 100 realizations, Blackman window, T_1=2 ms, CNR=40 dB, M_p=12 (dwell 60 ms), SNR = 20 dB, σ_v of weather from 0.5 m s^{-1} to 8 m s^{-1}, σ_v of clutter 0.28 m s^{-1}.

ii)   *Observed limitations and artifacts*

For a large spectral width (compared to v_a), small number of pairs, and small SNR the errors are large. The errors and biases of power and width are relatively small for a sufficient SNR. The velocity errors and biases can be large. The clutter replica regions are the characteristic locations that increase velocity errors. An aggressive window increases the width of clutter in the spectrum in all 5 replicas and, therefore, spreads out the regions of bad velocities. The increase in velocity errors is due to the inability of SACHI to pinpoint the correct weather replica in the SPRT spectrum. The choice of incorrect replica reflects only on the velocity errors. The width of any weather replica is the same; the power in weather replicas is comparable; therefore the width and power errors remain small.

The velocity errors are large for PRT T_1=2ms due to two reasons: 1) short dwell time dictates insufficient number of samples; 2) small unambiguous velocity and spectral width of weather 4 m s^{-1} promote self-noise and intermingling of smaller weather replicas (i.e., in a spectrum at most 3 weather replicas can be registered visually, instead of 5 replicas). Nonetheless, SACHI can recover most of the spectra in the good velocity region even for T_1=2ms. The decrease of the bad velocity region is imperative. The bad velocity regions do not depend on CNR but strongly depend on the clutter width and the type of weighting window.

The reconstructed spectrum often has gaps on the slopes (Fig.3.1.11g). Uneven location of gaps is a source of negligible power bias.

iii)   *Velocity errors*

SPRT with $T_1 = 1$ms can be successfully clutter filtered with SACHI-GMAP. To increase radar range coverage, a longer T_1 is required. A short dwell time is desirable to speed up the data acquisition process. Therefore, our first attempt increasing T_1 to 2 ms while keeping the same dwell time was natural. However, the large velocity errors observed for dwell 60 ms, $T_1 = 2$ ms, and $\sigma_v = 4$ m s^{-1} demanded an evaluation of the parameter space. Our goal was to find the PRTs for which velocity errors are within requirements. To do so, we estimate the mean of all errors in the velocity space between 0 and v_a. In other words, the mean for curve SD(v) in Fig.3.1.16 (second column first row) is estimated. Recall that each velocity error was a mean of 100 error estimates. In such manner we repeat estimation of the mean for the means for the different values of PRT and CNR and display the result in Fig.3.1.20. As for bias, it is within 2 m s^{-1} tolerance for all T_1 and CNR<55 dB. The errors are acceptable only for $T_1 < 1.3$ ms. Next, we display this result in color-scale in Fig.3.1.21. Dark red color indicates large errors, while blue color indicates small errors. The small biases are shown with light green. The computations are repeated for different dwell times 80 ms, 100 ms, and 120 ms. Doubling the original dwell time allows expanding the area with small errors in the parameter space. Nonetheless, the errors are within tolerance only for $T_1 < 1.4$ ms. The computations are repeated for the same dwell time 60 ms, but different spectral width of weather (Fig.3.1.22). The area of small errors propagates to a larger T_1 as we consider narrower spectral width of weather. The PRT $T_1 = 1.7$ ms can be used for the SPRT data acquisition scheme if the expected spectral width of weather is 3 m s^{-1}.

Generally, when weather is collocated with clutter replica, the velocity errors are large. When we estimated the mean of all errors in the velocity space between 0 and v_a (Figs. 3.1.20-22), the means were brought up by these bad velocities from clutter replica regions. Next, we reevaluate the parameter space using *percentage of acceptable error* instead of *mean error*. In other words, the values in curve SD(v) in Fig.3.1.16 (second column first row) are evaluated to be below 2 m s^{-1} for error, and within -2 m s^{-1} and 2 m s^{-1} for bias. In the case of curve SD(v) in Fig.3.1.16 (second column first row), there is 100% of acceptance of error and biases. In that manner we repeat estimation of the percent of acceptable errors and biases for the different values of PRT and CNR and display the result in Fig.3.1.23. Dark red color indicates 100% of acceptance. For dwell 60 ms only 1.1 ms PRT can be used to insure errors within tolerance level. Doubling the dwell to 120 ms allows the use of 1.4 ms PRT. We repeat the assessment for different spectral widths (Fig. 3.1.24). 1.5 ms PRT seem to be the limit if the error requirements cannot be relaxed.
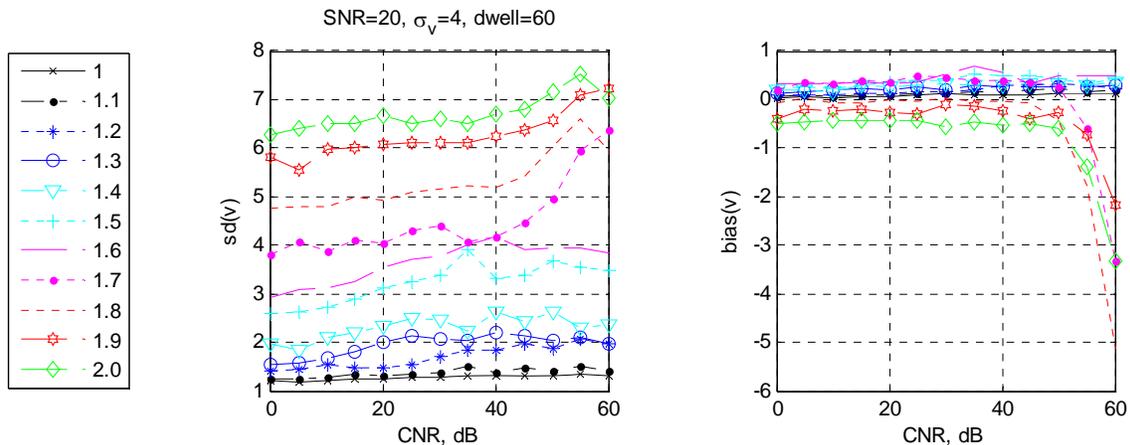
Fig.3.1.20. Mean velocity error and mean velocity bias for different PRTs.
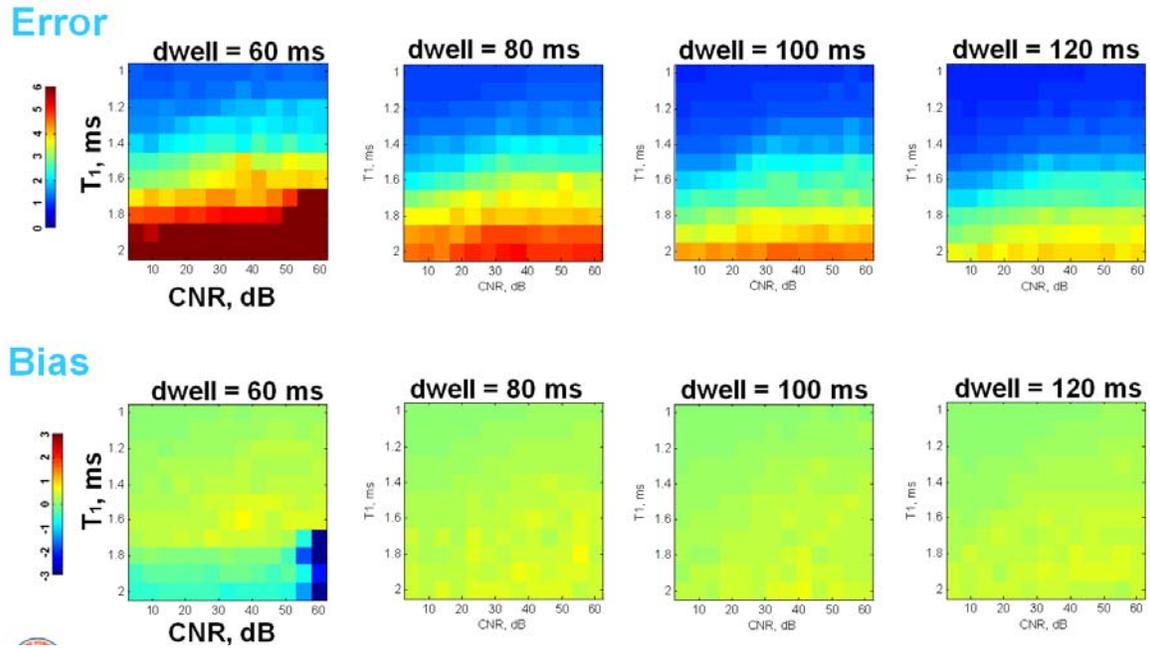
Fig.3.1.21. Mean velocity error and mean velocity bias for different dwell times. Simulation parameters: SNR=20 dB, $\sigma_v = 4$ m s^{-1}.
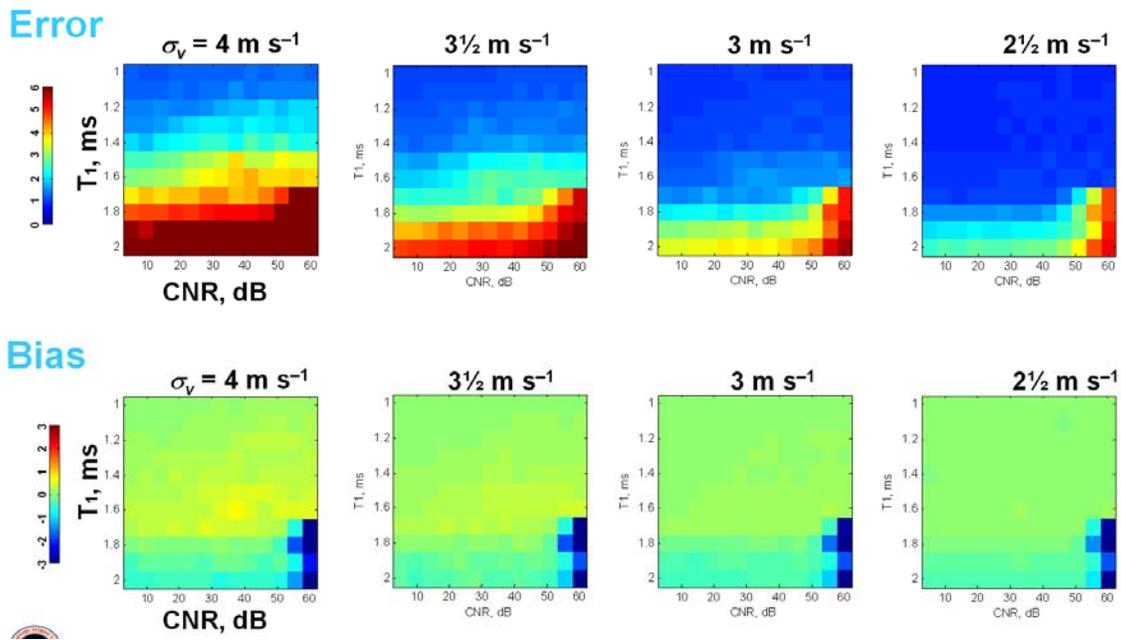
Fig.3.1.22. Mean velocity error and mean velocity bias for different σ_v. Simulation parameters: SNR=20 dB, dwell time = ~ 60 ms.
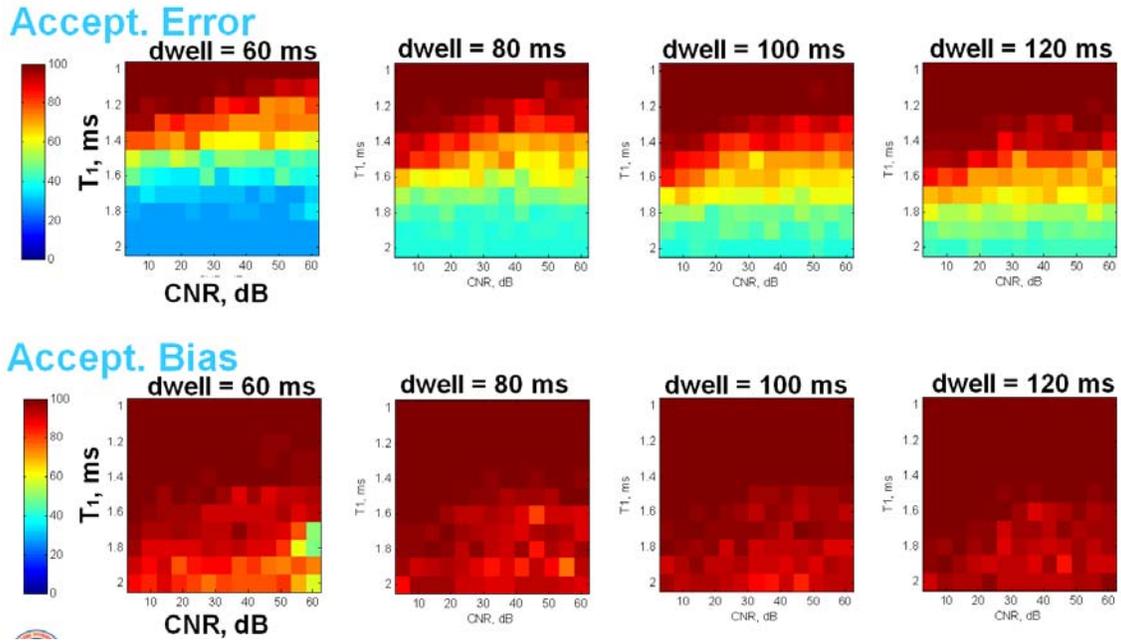
Fig.3.1.23. Percent of acceptable errors and biases for different dwell times. Simulation parameters: SNR=20 dB, σ_v. = 4 m s^{-1}.
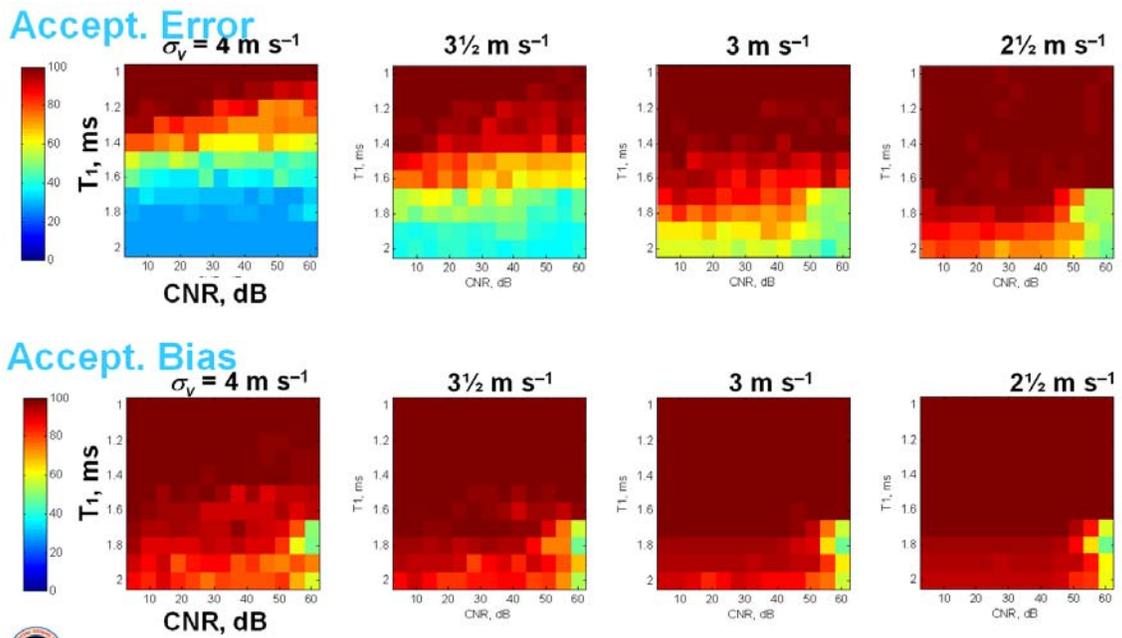
Fig.3.1.24. Percent of acceptable velocity errors and biases for different σ_v Simulation parameters: SNR=20 dB, dwell time ~ 60 m s.

iv)   *Acceptable errors with other windows (Von Hann, Rectangular).*

The percentage of acceptable errors (Figs.3.1.23-24) was assessed for the Blackman window, because this window is generally used if clutter is present. A Blackman window is considered to be an aggressive window (sidelobes at ~ 58 dB below main lobe). Blackman windows have slightly wider central lobes and less sideband leakage than equivalent length Hamming and Hann windows. The wider center lobe slightly expands the clutter contribution in a spectrum. For SPRT spectrum the expansion is 5 times wider. It was shown that in Doppler velocity the regions with clutter replicas are the main source of velocity errors. To reduce this region a less aggressive window might be preferable. We repeat the evaluation of percent of acceptable velocity errors using different weighting windows: Blackman, Von Hann, and rectangular. Fig. 3.1.25 shows the percentage of acceptable error for 60 ms dwell time. 1.4 ms PRT looks good with 60 ms dwell time and the rectangular window. Fig. 3.1.26 shows the percentage of acceptable error for 80 ms dwell time. 1.5 ms PRT looks good with 80 ms dwell time and the rectangular window. All images show a trend of fewer errors for less aggressive windows. And, last, Fig.3.1.27 shows the percentage of acceptable errors for SNR=20 dB, dwell = ~80 ms, rectangular window, and σ_v =3 m s^{-1}. In this case 1.8 ms PRT can be used for the SPRT data acquisition scheme and the errors will be within the level of tolerance.
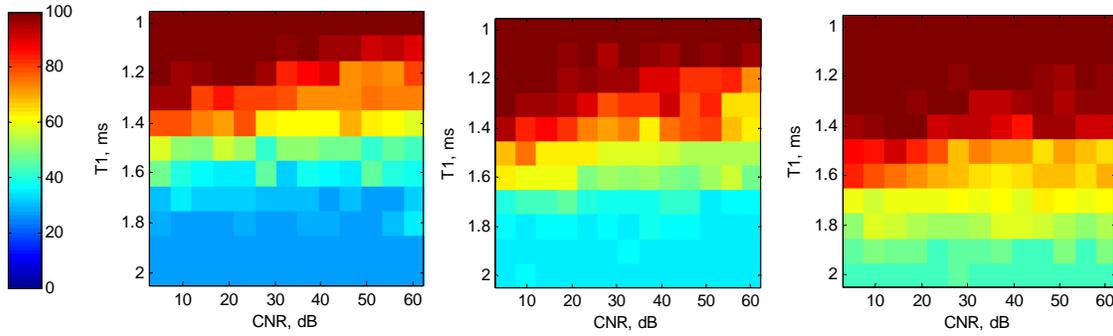
Fig.3.1.25. Percent of acceptable velocity error for different windows and dwell ~60 ms.
Simulation parameters: SNR=20 dB, σ_v =4 m s^{-1}.
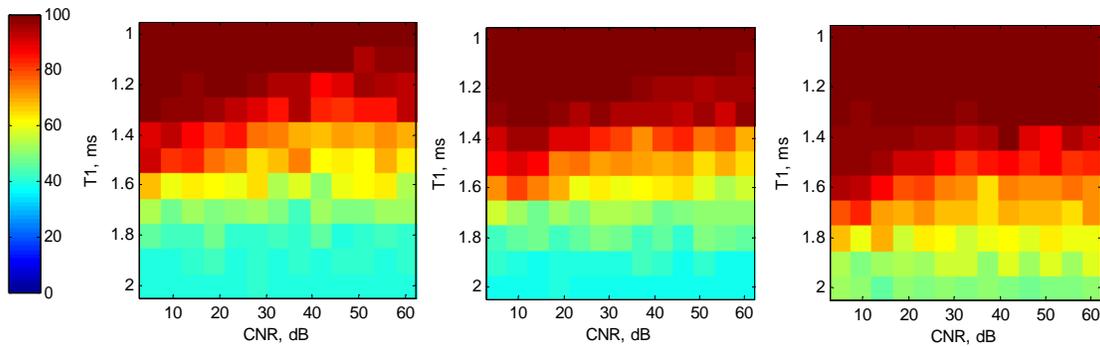
Fig.3.1.26. Percent of acceptable velocity error for different windows and dwell ~80 ms. |
Simulation parameters: SNR=20 dB, σ_v =4 m s^{-1}.
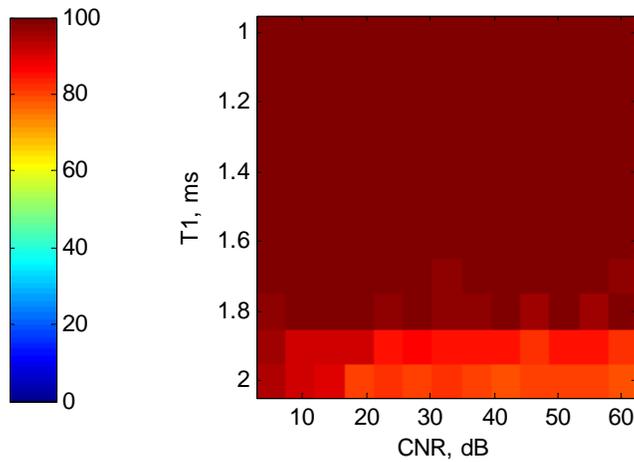
Fig.3.1.27. Percent of acceptable velocity error for a rectangular window and
σ_v = 3 m s^{-1}, (SNR=20 dB, dwell = ~80 ms).

3.1.5. *Algorithm updates*

The implementation of the SPRT GCF from NSSL report #9 into MATLAB by NSSL and ROC teams disclosed several typos and misleading notes in the functional description. Updated functional description is provided in Appendix A. The evaluation of the implemented algorithm for different simulation parameters indicated that table for clutter width parameter was not optimal due to the minimal dependence of the clutter width parameter on CNR. NSSL recommends GMAP for clutter width parameter evaluation and provides a different table that is generated by running GMAP with simulations.

A minor modification is suggested to simplify keeping the track on the window correction factor: a normalized window does not require bookkeeping. The choice of the window is rectangular for small number of pairs, and is subject of further evaluation for large number of pairs.

The algorithm is modified to accommodate the odd number of pairs M_p. The even M_p was required for the following reason. When the clutter replicas are removed from the spectrum, the initial velocity estimate is located. Only the part of the spectrum adjacent to this initial velocity (of the length M_p) is used for further processing. An equal number of spectral coefficients $M_p/2$ is used to the left and to the right from the coefficient corresponding to the initial velocity, and the remaining coefficients are removed. For the odd M_p, unequal number of spectral coefficients must be used. Therefore, a change needs to be made at the level of clutter matrixes formation. We performed only a minor modification, based on scaling down (throwing away the extra coefficient). This

approach is simple, does not require changes to clutter matrixes, but slightly increases errors, especially for large CNR. Examples of velocity errors for even and odd number of pair are shown in Fig. 3.1.28. The errors are comparable for the mid-range PRTs, slightly smaller for the small PRTs, and larger for the large PRTs. Note that even M_p, was forced by the 60 ms dwell time, and the odd M_p was artificially created by adding 1 pair to the even M_p. Therefore, the dwell times for odd M_p are longer. Consequently, the errors are larger for the odd M_p. To avoid artifacts with the current state of the algorithm, we recommend using the even number of pairs in the VCP design. Additional analyses can be performed in the future to determine if adjustment of the clutter matrices can fix the problem (slightly larger errors for odd number of pair).
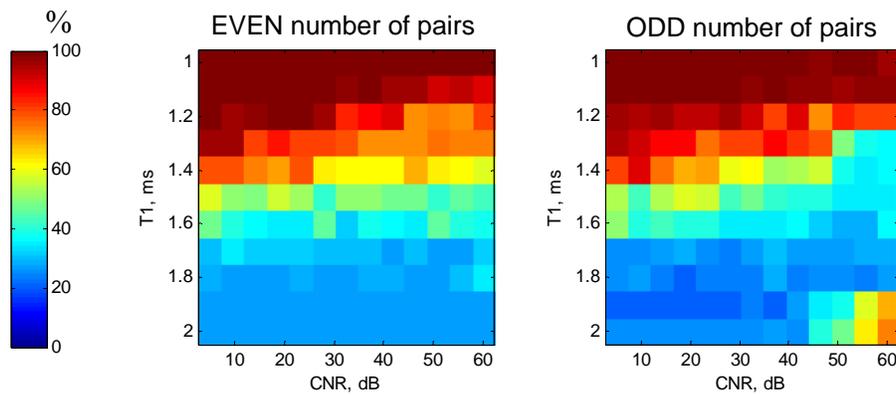
Fig.3.1.28. Percent of acceptable velocity error for even vs. odd number of pairs
$\sigma_v = 4$ m s^{-1}, SNR=20 dB, dwell time ~ 60 ms, Blackman window.

3.1.6. *Conclusions and recommendations.*

The errors and biases of power and width for SACHI-GMAP are within the requirements for a sufficient SNR. The velocity errors and biases for SACHI-GMAP depend on many factors and can be extremely large. To decrease velocity errors several aspects need to be considered: 1) a dwell time that insures a sufficient number of samples; 2) an adequate unambiguous velocity to accommodate 5 spectral replicas of width 4 m s^{-1} (unless the requirements that specify 4 m s^{-1} spectral width are relaxed); 3) a weighting function that does not spread out the main lobe. Otherwise, the velocity errors are unavoidable in the regions of clutter replicas.

With accordance to current specifications and with the desirable dwell time of 60 ms, the longest PRT that can meet the error requirements is T_1=1.1 ms (Blackman window, spectral width of 4 m s^{-1}, and SACHI-GMAP processing). A small change to the rectangular window can extend the range coverage (to about 310 km) as T_1=1.4 ms becomes usable for the given set of requirements (spectral width of 4 m s^{-1}, SACHI-GMAP processing). These assessments are performed for SNR=20 dB and CNRs from 0 dB to 60 dB. Note that 1) errors decrease as SNR increases, 2) errors do not significantly depend on CNR, and 4) errors slightly decrease if the even number of staggered pairs is used with the current version of the SACHI-GMAP algorithm.

We showed on data that SACHI-GMAP performs well with the staggered sequences and its performance is comparable to the uniform GCF. We demonstrated on simulations that SACHI-GMAP with rectangular window and even number of pairs led to a decrease in errors. Consequently, our recommendations are:

- The number of pairs must be sufficient for GMAP processing (16 and more).

- The even number of pairs is suggested.

- The elements of GMAP should be used for clutter width identification.

- Blackman window should be replaced with a less aggressive window, especially for the small number of pairs.

3.2.   VCP design for Staggered PRT

This section provides the tools for effective design of volume coverage patterns (VCP) that use staggered PRT. In designing VCPs for staggered PRT, we recommend considering the following performance indicators:

- Acquisition (or VCP) time: the goal is to preserve the acquisition times and elevation angles of existing VCPs. Hence, for the same antenna rotation rates and azimuthal resolution, preserving the VCP time is equivalent to preserving the dwell times. For staggered PRT, the dwell time (*DT*) is given by $DT = M_p(T_1 + T_2)$, where M_p is the number of staggered pairs and T_1 and T_2 are the short and long PRTs, respectively.

- Maximum unambiguous range (r_a): we need to distinguish between the maximum unambiguous range for reflectivity ($r_{a,S}$) and the one for velocity and spectrum width ($r_{a,D}$). The goal is to avoid overlaid echoes as much as possible. Ideally, we would like to pick $r_{a,D} = cT_1/2$ larger than or equal to the maximum possible range of echoes assuming storm tops at 70,000 ft (herein we will refer to this range as r_{max}). Note that if $r_{a,D}$ is larger than r_{max}, we are guaranteed that overlaid echoes will never occur. This is more practical at higher elevation angles; i.e., for smaller values of r_{max}. If this is not possible, we should at least pick $r_{a,S} = cT_2/2 \geq r_{max}$ to avoid overlaid echoes from the long PRT into the short PRT (this is an assumption in the algorithm).

- Maximum unambiguous velocity (v_a): the extended Nyquist velocity that can be achieved using staggered PRT is given by $v_a = m\lambda/4T_1 = n\lambda/4T_2$, where λ is the radar wavelength and m and n are integers forming the PRT ratio $T_1/T_2 = m/n$. The goal for this parameter is to obtain a maximum unambiguous velocity that matches or exceeds the current values using standard VCPs.

- Spectrum width saturation: measurement of wide spectrum widths is not possible due to saturation effects that depend on the PRT and the number of samples used in the estimation process (Melnikov and Zrnić, 2004). That is, spectrum widths estimates cannot exceed the saturation value $\sigma_{v,\max} = \frac{\lambda}{4\pi T_1} \sqrt{\ln M_p}$. At a minimum, the spectrum width should saturate at around 8 m/s; however, it is understood that algorithms that rely on the spectrum width such as NCAR's Turbulence Detection Algorithm may benefit from larger saturation values.

- Errors of estimates: errors can be classified as estimation errors or catastrophic errors. The worst-case scenario for estimation errors of reflectivity is when only one set of pulses can be used in the estimator (i.e., either at far ranges where only one set of pulses is available, or at close ranges in the case of overlaid echoes where only one set of pulses is clean). Estimation errors of velocity are those of the short-PRT velocity. Estimation errors should comply with NEXRAD technical requirements (NTR); however, due to the significant operational benefit realized by staggered PRT, users might accept slightly higher error levels. In addition to estimation errors, velocity estimates might exhibit "catastrophic" errors (Torres et al. 2004). These are instances in which the staggered PRT velocity dealiasing

algorithm employs the wrong dealiasing rule and the resulting "dealiased" velocity is significantly different than its true value. Catastrophic errors are usually evident as speckle noise and can be easily removed by velocity dealiasing algorithms based on field continuity. Still, the rate of catastrophic errors should be kept as low as possible to ensure that the speckling nature of these errors is preserved and that RPG continuity-based velocity dealiasing algorithms can detect and correct these problems effectively.

- Clutter suppression: performance of the SACHI clutter filter was discussed in great detail in section 3.1. Note that this spectral filter only works with the 2/3 PRT ratio and its performance is tied to that of GMAP. As a general rule, good clutter filtering performance with staggered PRT is difficult to achieve with longer PRTs and shorter dwell times. The staggered PRT clutter filter should perform as dictated by the NTR. However, these requirements might be relaxed at higher elevation angles where clutter contamination is not an overwhelming problem.

With these performance indicators in mind, design of staggered PRT VCPs consists of selecting values of T_1, T_2, and M_p such that all performance indicators are satisfied (or the proper trade-offs are achieved). With the constraint of a PRT ratio of 2/3 and maintaining the same dwell times of existing VCPs, there is only one degree of freedom; i.e., selection of T_1 determines the degree to which all performance indicators are satisfied.

Next, we consider the task of replacing all scans of three standard VCPs: VCP 11, VCP 12, and VCP 21 with staggered PRT. The process is analogous for all VCPs, and only the

one for VCP 11 is discussed in detail here. The definition of VCP 11 is repeated in table 3.2.1 for convenience; table 3.2.2 shows the staggered PRT VCP based on VCP 11. The first goal is to maintain all elevation angles and dwell times (for split cuts we used the combined dwell time for the surveillance and Doppler scans). Next, because it is not always possible to meet all the goals for the different performance indicators, selection of PRTs depends on the specific trade-offs that we accept to make. For this example, we selected T_1 such that (1) v_a at least matches the current performance of VCP 11 and (2) $r_{a,D}$ does not exceed r_{max} to use the shortest PRT possible without overlaid echoes. Note that for the first three scans, achieving the desired maximum unambiguous velocity means that we cannot have $r_{a,D}$ larger than or equal to r_{max}, and the possibility of having overlaid echoes is not entirely eliminated. It is important to realize that none of the PRTs in table 3.2.2 is any of the eight available PRTs in the system. Therefore, new PRT definitions are needed to optimize the performance of staggered PRT.

VCP 11

Angle (°)	WF Type	Surveillance PRI #	Surveillance # Pulses	Doppler PRI #	Doppler # Pulses	ra,S (km)	ra,D (km)	va (m/s)	DT (ms)
0.50	CS/CD	1	17	5	52	466	148	27.13	104.12
1.45	CS/CD	1	16	5	52	466	148	27.13	101.02
2.40	B	1	6	5	41	466	148	27.13	59.09
3.35	B	2	6	5	41	336	148	27.13	53.89
4.30	B	2	6	5	41	336	148	27.13	53.89
5.25	B	3	10	5	41	233	148	27.13	55.99
6.20	B	3	10	5	41	233	148	27.13	55.99
7.50	CDX			6	43	137	137	29.31	39.27
8.70	CDX			7	46	127	127	31.61	38.95
10.00	CDX			7	46	127	127	31.61	38.95
12.00	CDX			7	46	127	127	31.61	38.95
14.00	CDX			7	46	127	127	31.61	38.95
16.70	CDX			7	46	127	127	31.61	38.95
19.50	CDX			7	46	127	127	31.61	38.95

Table 3.2.1. Description of the standard VCP 11. Dwell times are computed for the system PRTs in the PRI Delta C set.

VCP 11

Angle (°)	Staggered max R (km)	T1 (ms)	T2 (ms)	Mp	ra,S (km)	ra,D (km)	va (m/s)	DT (ms)	σvmax (m/s)	Approximated values SD(Z) (dB)*	SD(v) (m/s)
0.50	533	1.97	2.96	21	444	296	27.13	103.60	7.53	0.44	0.78
1.45	425	1.97	2.96	20	444	296	27.13	98.67	7.47	0.45	0.80
2.40	344	1.97	2.96	12	444	296	27.13	59.20	6.81	0.58	1.04
3.35	284	1.90	2.84	11	426	284	28.23	52.15	6.96	0.61	1.09
4.30	240	1.60	2.40	13	360	240	33.46	52.00	8.53	0.60	1.07
5.25	206	1.38	2.06	16	309	206	38.92	55.01	10.32	0.58	1.04
6.20	180	1.20	1.80	19	270	180	44.55	57.08	12.17	0.56	1.04
7.50	153	1.02	1.53	15	230	153	52.41	38.30	13.73	0.67	1.30
8.70	134	0.90	1.34	17	201	134	59.78	38.06	16.02	0.67	1.33
10.00	118	0.79	1.18	20	177	118	67.84	39.46	18.69	0.66	1.35
12.00	100	0.77	1.15	20	172	115	69.82	38.34	19.23	0.66	1.38
14.00	86	0.77	1.15	20	172	115	69.82	38.34	19.23	0.66	1.38
16.70	73	0.77	1.15	20	172	115	69.82	38.34	19.23	0.66	1.38
19.50	63	0.77	1.15	20	172	115	69.82	38.34	19.23	0.66	1.38

*worst case
includes range averaging

Table 3.2.2. Description of a staggered PRT VCP based on VCP 11.

Errors of estimates are rough approximations for the benchmark conditions in the NTR document and the nominal 2.8 GHz radar frequency. Figure 3.2.1 shows the rate of catastrophic velocity errors expected for the VCP defined in table 3.2.2.
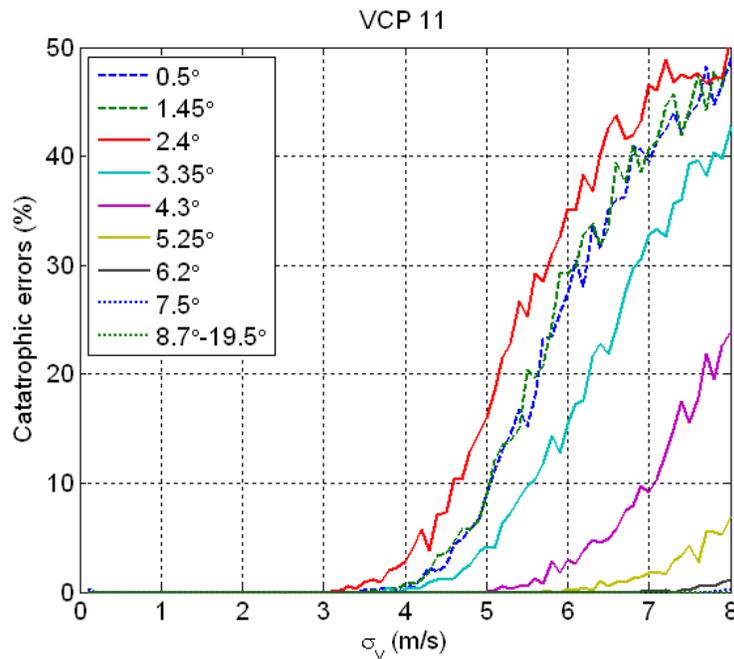
Fig. 3.2.1. Rate of catastrophic errors as a function of the spectrum width for all the scans of the VCP defined in table 3.2.2.

For this particular example, the performance of a staggered PRT VCP based on VCP 11 can be summarized as follows:

- Lower elevation scans (0.5 to 1.45 deg): these correspond to the split cuts of VCP 11. Overall, the performance in terms of maximum unambiguous range and velocity is similar to that of VCP 11 with a slightly reduced range coverage for reflectivity. Overlaid echoes are not completely avoided, and some obscuration of velocity and spectrum widths may occur within about 150 km of the radar if there are significant returns beyond about 300 km. Saturation of the spectrum width occurs at around 7.5 m/s, slightly below our goal of 8 m/s. Estimation errors are well below requirements for reflectivity, Doppler velocity, and spectrum width. Catastrophic errors are negligible for narrow spectrum widths less than about 4 m/s but increase up to 50% for spectrum widths between 4 and 8 m/s. There are enough samples in the dwell time to ensure acceptable performance of GMAP; however, the performance of SACHI may be limited due to the long PRTs required to preserve range coverage at these lower elevation angles (see section 3.1).

- Lower intermediate elevation scans (2.4 deg): this is the lowest scan using the batch mode in VCP 11. Again, the performance in terms of maximum unambiguous range and velocity is similar to that of VCP 11. Overlaid echoes are not completely avoided, and some obscuration of velocity and spectrum widths may occur within about 150 km of the radar if there are significant returns beyond about 300 km. Saturation of the spectrum width occurs at around 6.8 m/s, more than 1 m/s below our goal. Estimation errors are well below requirements for

reflectivity, but slightly above for Doppler velocity and spectrum width. Catastrophic errors are negligible for narrow spectrum widths less than about 3 m/s but increase up to 50% for spectrum widths between 3 and 8 m/s. On top of this, due to the long PRTs and the reduced number of samples in the dwell time, performance of the clutter filter may be unacceptable. Note that for VCP 11 this is the most difficult scan to replace with staggered PRT.

- Upper-intermediate elevation scans (3.35 to 6.2 deg): these comprise the remaining scans using the batch mode in VCP 11. The performance in terms of maximum unambiguous range and velocity is much superior compared to that of VCP 11, and overlaid echoes are completely avoided! Saturation of the spectrum width occurs beyond the goal of 8 m/s. Estimation errors are well below requirements for reflectivity, but slightly above for Doppler velocity and spectrum width. Catastrophic errors are negligible for narrow spectrum widths less than about 4 m/s but increase up to 40% for spectrum widths between 4 and 8 m/s. There are enough samples in the dwell time to ensure acceptable performance of GMAP, and the performance of SACHI will improve due to the shorter PRTs involved.

- Upper elevation scans (7.5 to 19.5 deg): these are the scans using the contiguous Doppler mode in VCP 11. The performance in terms of maximum unambiguous range and velocity is far superior compared to that of VCP 11, and once again, overlaid echoes are completely avoided. Saturation of the spectrum width occurs well beyond the goal of 8 m/s ($\sigma_{v,max} > 13.5$ m/s for all the scans; hence, there is

no practical saturation of the spectrum width). Estimation errors are well below requirements for reflectivity, but about 30% higher than accepted for Doppler velocity and spectrum width due to the much shorter dwell times (errors could be lowered simply by increasing the dwell time, or by other advanced signal processing techniques such as range oversampling). Catastrophic errors are negligible for spectrum widths up to about 8 m/s. There are enough samples in the dwell time to ensure acceptable performance of GMAP, and the performance of SACHI will improve significantly due to the shorter PRTs involved. However, clutter contamination may not be an issue at these elevation angles.

Analogously as with VCP 11, we can define VCPs for staggered PRT based on VCP 12 and VCP 21 (tables 3.2.3 through 3.2.6). On one hand, using the much shorter dwell times of VCP 12 results in diminish performance of staggered PRT, specially regarding to the errors of estimates. On the other hand, with the dwell times of VCP 21 it is possible to meet error requirements for all elevation angles.

VCP 12

Angle (°)	WF Type	Surveillance PRI #	# Pulses	Doppler PRI #	# Pulses	ra,S (km)	ra,D (km)	va (m/s)	DT (ms)
0.50	CS/CD	1	15	5	40	466	148	27.13	86.07
0.90	CS/CD	1	15	5	40	466	148	27.13	86.07
1.30	CS/CD	1	15	5	40	466	148	27.13	86.07
1.80	B	1	3	5	29	466	148	27.13	37.93
2.40	B	2	3	5	30	336	148	27.13	36.32
3.10	B	2	3	5	30	336	148	27.13	36.32
4.00	B	2	3	5	30	336	148	27.13	36.32
5.10	B	3	3	5	30	233	148	27.13	34.26
6.40	B	3	3	5	30	233	148	27.13	34.26
8.00	CDX			6	38	137	137	29.31	34.71
10.00	CDX			7	40	127	127	31.61	33.87
12.50	CDX			8	44	117	117	34.32	34.32
15.60	CDX			8	44	117	117	34.32	34.32
19.50	CDX			8	44	117	117	34.32	34.32

Table 3.2.3. Description of the standard VCP 12.

VCP 12

	Staggered									Approximated values	
Angle (°)	max R (km)	T1 (ms)	T2 (ms)	Mp	ra,S (km)	ra,D (km)	va (m/s)	DT (ms)	σvmax (m/s)	SD(Z) (dB)*	SD(v) (m/s)
0.50	533	1.97	2.96	17	444	296	27.13	83.87	7.27	0.49	0.87
0.90	484	1.97	2.96	17	444	296	27.13	83.87	7.27	0.49	0.87
1.30	440	1.97	2.96	17	444	296	27.13	83.87	7.27	0.49	0.87
1.80	392	1.97	2.96	8	444	296	27.13	39.47	6.23	0.70	1.27
2.40	344	1.97	2.96	7	444	296	27.13	34.53	6.02	0.74	1.36
3.10	298	1.97	2.96	7	444	296	27.13	34.53	6.02	0.74	1.36
4.00	253	1.68	2.53	9	379	253	31.78	37.90	7.50	0.70	1.26
5.10	211	1.41	2.11	10	316	211	38.05	35.17	9.19	0.72	1.31
6.40	175	1.17	1.76	12	263	175	45.75	35.11	11.48	0.71	1.33
8.00	145	0.97	1.45	14	217	145	55.47	33.78	14.34	0.71	1.39
10.00	118	0.79	1.18	17	177	118	67.84	33.54	18.17	0.71	1.46
12.50	96	0.77	1.15	18	172	115	69.82	34.50	18.89	0.70	1.45
15.60	78	0.77	1.15	18	172	115	69.82	34.50	18.89	0.70	1.45
19.50	63	0.77	1.15	18	172	115	69.82	34.50	18.89	0.70	1.45

*worst case
includes range averaging

Table 3.2.4. Description of a staggered PRT VCP based on VCP 12.

VCP 21

		Surveillance		Doppler					
Angle (°)	WF Type	PRI #	# Pulses	PRI #	# Pulses	ra,S (km)	ra,D (km)	va (m/s)	DT (ms)
0.50	CS/CD	1	28	5	88	466	148	27.13	173.82
1.45	CS/CD	1	28	5	88	466	148	27.13	173.82
2.40	B	2	8	5	70	336	148	27.13	86.99
3.35	B	2	8	5	70	336	148	27.13	86.99
4.30	B	2	8	5	70	336	148	27.13	86.99
6.00	B	3	12	5	70	233	148	27.13	87.71
9.00	CDX			7	82	127	127	31.61	69.43
14.60	CDX			7	82	127	127	31.61	69.43
19.50	CDX			7	82	127	127	31.61	69.43

Table 3.2.5. Description of the standard VCP 21.

VCP 21

	Staggered									Approximated values	
Angle (°)	max R (km)	T1 (ms)	T2 (ms)	Mp	ra,S (km)	ra,D (km)	va (m/s)	DT (ms)	σvmax (m/s)	SD(Z) (dB)*	SD(v) (m/s)
0.50	533	1.97	2.96	35	444	296	27.13	172.67	8.14	0.35	0.61
1.45	425	1.97	2.96	35	444	296	27.13	172.67	8.14	0.35	0.61
2.40	344	1.97	2.96	18	444	296	27.13	88.80	7.34	0.48	0.85
3.35	284	1.90	2.84	18	426	284	28.23	85.34	7.64	0.49	0.86
4.30	240	1.60	2.40	22	360	240	33.46	87.99	9.36	0.47	0.83
6.00	185	1.23	1.85	28	278	185	43.35	86.44	12.60	0.47	0.84
9.00	130	0.87	1.30	32	195	130	61.64	69.48	18.26	0.51	0.99
14.60	83	0.77	1.15	36	172	115	69.82	69.00	21.04	0.50	1.03
19.50	63	0.77	1.15	36	172	115	69.82	69.00	21.04	0.50	1.03

*worst case
includes range averaging

Table 3.2.6. Description of a staggered PRT VCP based on VCP 21.

3.3. Operational considerations

A complete range-and-velocity-ambiguity-mitigation strategy will include the use of systematic phase coding at the lower elevation angles, staggered PRT at the intermediate elevation angles, and the standard uniform PRT at the higher elevation angles. Currently, SZ-2 has been deployed as part of ORDA Build 9, and has been well received by the user community due to its demonstrated significant operational advantages. For the near future, staggered PRT has the potential of producing "clean" fields of reflectivity, Doppler velocity, and spectrum width where the likelihood of overlaid echoes can be minimized by selecting longer pulse repetition times (PRT). Unlike with uniform PRT, where choosing longer PRTs results in unacceptable maximum unambiguous velocities, with staggered PRT it is possible to use longer PRTs and at the same time have an extended maximum unambiguous velocity that meets most operational needs. For example, staggered PRT allows at least doubling the current maximum unambiguous ranges and increasing the maximum unambiguous velocities at the same time! Additionally, because longer PRTs are used, reflectivity errors with staggered PRT are usually much smaller than their uniform PRT counterparts. Unfortunately, the use of longer PRTs leads to earlier saturation of the spectrum width (Melnikov and Zrnić, 2004), slightly higher errors of velocity and spectrum width estimates, and the occurrence of "catastrophic" velocity dealiasing errors (Torres et al., 2004). In addition, as indicated in section 3.1, clutter filtering of staggered sequences is not as effective as with uniform PRTs (e.g., GMAP).

It is not entirely obvious if there is an operational advantage to using staggered PRT at the lowest and highest elevation angles. At lower elevation angles where clutter

contamination is more likely, the answer depends on the effectiveness of the ground clutter filter (see section 3.1 for a comprehensive performance analysis of the SACHI filter) and the performance of the velocity and spectrum width estimators with the longer PRTs that are required to satisfy larger radar coverage needs. Justification for using staggered PRT at higher elevations depends on the operational needs for high Doppler velocity measurements and the effectiveness of the current uniform PRT scheme.

Presently, it is clear that replacing the intermediate elevation scans that use the batch mode with staggered PRT will result in a marked improvement over existing range and velocity ambiguity mitigation techniques. Staggered PRTs can be selected so that there are no overlaid echoes at all, and it provides much more accurate reflectivity estimates than the batch mode in the presence of overlaid echoes. Compared to SZ-2, staggered PRT does not require a complex set of censoring rules, nor does it exhibit rings of censored data at the beginning of each of the trips. In addition, SZ-2 produces weak-trip spectrum width estimates that saturate at about 5 m/s, and weak-trip velocity estimates with larger statistical errors. Finally, "all bins" clutter filter renders the SZ-2 algorithm unusable and requires a rudimentary re-determination of the presence of clutter contamination by the algorithm. None of these issues are present with staggered PRT.

An important operational consideration is the fact that standard errors of velocity and spectrum width estimates are about 30% larger compared to using uniform PRTs on the same dwell times. We sustain that, compared to existing range and velocity ambiguity mitigation techniques in the ORDA, the operational advantages brought by staggered PRT are significant enough that they should warrant a relaxation of data quality requirements or a small increase in the dwell time to reduce the errors to acceptable

levels. A second major concern is the ability to efficiently filter clutter from staggered samples. Here, we might not be able to achieve the suppression levels required by the system specifications. However, the recommended spectral filter performs quite well and will most likely provide the required clutter suppression at intermediate to higher elevation angles (see section 3.1).

Another operational consideration is the proper selection of PRTs. Because the PRT selection in the current system is limited to a pre-determined set of 8 values, it is very unlikely that we can optimize the performance of staggered PRT with the criteria outlined in the previous section using existing PRTs (see Fig. 3.3.1). In addition, none of the existing PRTs can be used to form the PRT ratio of 2/3, which is required for the spectral clutter filter. Note that if using DC removal for clutter filtering, a PRT ratio of 2/3 is not required, but this would require a generalization of the current set of dealiasing rules (Torres et al. 2004).

A minor consideration is related to the number of staggered PRT pairs in the dwell time. Whereas the spectral filter was modified to accommodate odd number of pairs, its performance seems to be inferior in such case compared to having an even number of pairs. This might be related to the way the filter works by expecting a certain symmetry in the spectrum which is violated if the number of pairs is odd. While this problem might be fixed, we still do not have an explanation for this rather perplexing behavior. At any rate, even if we had to force the number of pairs to be even, it would not represent a significant operational constraint. Either the dwell time can be adjusted (up or down) to fit an even number of pairs with no significant change in the VCP time, or the system could use slightly overlapping radials with minimal impact.

Another minor consideration is the fact that the recommended algorithm assumes that T_1 is less than T_2. This is not a true limitation because, with additional logic and setup for the spectral clutter filter the algorithm could handle the case of $T_1 > T_2$. However, ensuring that $T_1 < T_2$ is straightforward without any changes to the staggered PRT algorithm. If every coherent processing interval is formed with $2M_p + 1$ pulses, we can always start the sequence on the short PRT with negligible azimuthal shift for the resolution volume.

The new capability of the ORDA to collect staggered PRT time-series data will enable us to identify other potential issues with staggered PRT before its operational implementation. Once operational, we maintain that, compared to existing range-and-velocity-ambiguity-mitigation techniques, staggered PRT will provide great benefits to the users of NEXRAD data by minimizing the occurrence of both purple haze obscuration and velocity dealiasing errors.

4. Updates to the SZ-2 Algorithm

In June of 2004, NSSL and NCAR provided an algorithm recommendation for the first stage of range and velocity ambiguity mitigation on the WSR-88D. The algorithm is termed SZ-2 and can be used to replace the "split cuts" in legacy VCPs. The SZ-2 algorithm has been implemented and is now operational on the ORDA providing significant reduction of obscuration (purple haze) at the lower elevation angles. Although the provided algorithm recommendation was extensively tested in a research environment, a number of issues arose during 2007, after its operational implementation. Next, we describe the specific changes suggested during this fiscal year. An updated description of the SZ-2 algorithm recommendation is included in Appendix B.

4.1. Double windowing

As documented in our previous annual report, SZ-2 uses three different data windows depending on the presence of clutter contamination and/or overlaid echoes. Generally speaking, the more aggressive the data window, the larger the errors of estimates. Therefore, one should not apply a data window unless it is really necessary. The revised June 2006 recommendation for dynamic use of data windows stated that:

1. The rectangular window should be use if there are no overlaid echoes or clutter contamination. This results in the best statistical performance that matches the one in the legacy RDA.

2. The von Hann window should be used if there are overlaid echoes but no clutter contamination. This results in an acceptable performance of the processing notch

filter (PNF) that is used to recover the weaker overlaid trip and an optimum statistical performance for the overall algorithm. Note that errors of estimates recovered from overlaid echoes are about 30% higher than those from non-overlaid echoes.

3. The Blackman window should be used if there is clutter contamination (regardless of the overlaid situation). This provides the required clutter suppression, acceptable performance of the PNF in case of overlaid echoes, but results in estimates with 50% larger errors compared to the non-overlaid, non-clutter-contaminated case.

The logic of the SZ-2 algorithm was designed assuming that the default window for the ORDA was the rectangular window (Fig. 4.1). However, this turned out not to be the case, and the recommended logic led to a case of "double windowing" in case of overlaid echoes and no clutter contamination (Fig. 4.2). The logic was changed in April of 2007, and the first data windowing rule became (Fig. 4.3):

1. The *default* window should be use if there are no overlaid echoes or clutter contamination. This is consistent with the current ORDA implementation.

Note that the default window could be any data window available in the system. Hence, as an additional benefit, this update made SZ-2 fully compatible with super resolution.

Fig. 4.1. SZ-2 logic as documented in the June 2006 interim report.
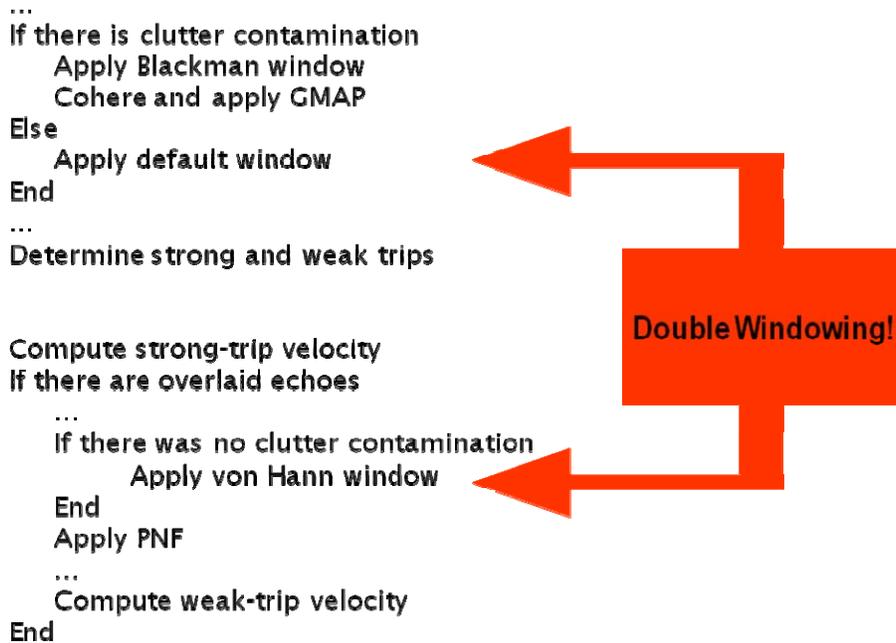
Fig. 4.2. SZ-2 logic as initially implemented in the ORDA.

68

```
…
If there is clutter contamination
    Apply Blackman window
    Cohere and apply GMAP
End
…
Determine strong and weak trips
If there was no clutter contamination
    Apply default window
End
…
Compute strong-trip velocity
If there are overlaid echoes
    …
    If there was no clutter contamination
        Apply von Hann window to original signal
    End
    Apply PNF
    …
    Compute weak-trip velocity
End
```

Fig. 4.3. Modified SZ-2 logic to avoid double windowing (April 2007).

4.2. Fourth-trip overlaid echoes

Another SZ-2 issue reported from the operational environment related to noisy velocities observed for two cases in June 2007. The common thread in these two cases was the occurrence of 4th and 1st trip overlaid echoes. The velocity field (KCRI level II data) corresponding to the 06/20/07 case is shown in Fig 4.4. For comparison, we include the same field obtained by processing the corresponding level I data in our MATLAB environment. Note that aside from a different velocity color scale, the two fields look very similar; i.e., they both exhibit the same patch of noisy velocities to the west of the radar. The reflectivity field shown in Fig. 4.5 can be used to verify that indeed, this is a case of 4th and 1st trip overlaid echoes with no significant 2nd or 3rd trips, a situation that

may be common operationally, but that had not occurred before in our test cases. With a little detective work, we can see that the patch of noisy velocities correspond to a 4th-trip strong signal and a 1st-trip weak signal; hence, the noisy velocities that we observe in the 1st trip correspond to weak-trip recovery.

Recall that the processing notch filter (PNF) is designed to remove most of the strong-trip signal while leaving two replicas of the weak-trip modulated signal for further recovery. In the case of 1st and 2nd trip overlay (herein referred to as 1-2 overlay), the modulated weak trip has eight replicas, so a PNF that removes ¾ of the spectrum and retains ¼ is ideal. In the case of 1st and 3rd trip overlay (herein referred to as 1-3 overlay), the modulated weak trip has four replicas, so the PNF has to be adjusted to remove only ½ of the spectrum to retain the required two replicas. Finally, for the case of 1st and 4th trip overlay (herein referred to as 1-4 overlay), the modulated weak trip has eight replicas and, again, a ¾ notch is feasible. Figure 4.6 depicts the placement and width of the PNF for the 1-2, 1-3, and 1-4 overlay situations. Also, this figure depicts the spectrum of the re-cohered 2nd trip weak signal in a 1-2 overlay situation. Note that the main lobe corresponds to the true placement of the weak signal spectrum; however, there are decaying sidebands that do not bias the weak-trip velocity estimate but act as white noise, increasing the errors of estimates. Closer examination to one of the gates with evident noise reveals that the recovered 1st trip spectrum (weak trip) does not seem to have the expected main lobe with decaying sidelobes! (Fig. 4.7)

KCRI Level II Data
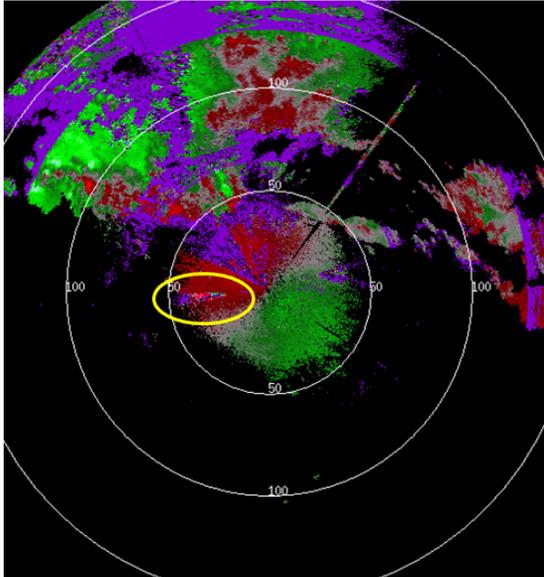
KCRI Level I Data
processed with MATLAB
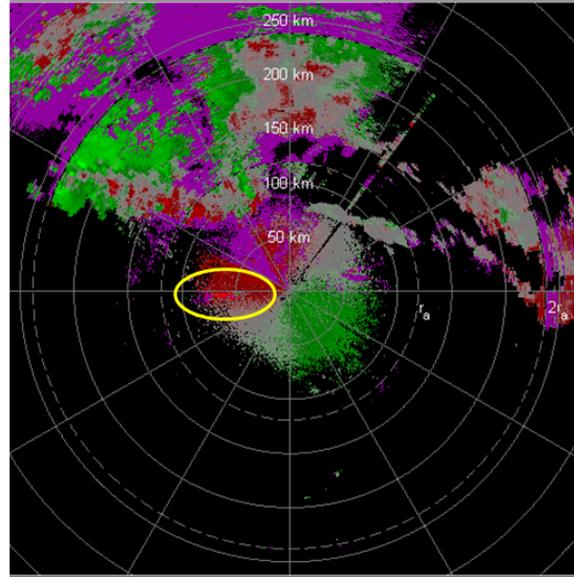
Note: Velocity color scales are different

Fig. 4.4. Doppler velocity data collected with the KCRI radar in Norman, OK on June 20, 2007. The image on the left corresponds to the KCRI level-II data, the one on the right is the KCRI level-I data processed (off-line) with our MATLAB version of SZ-2.
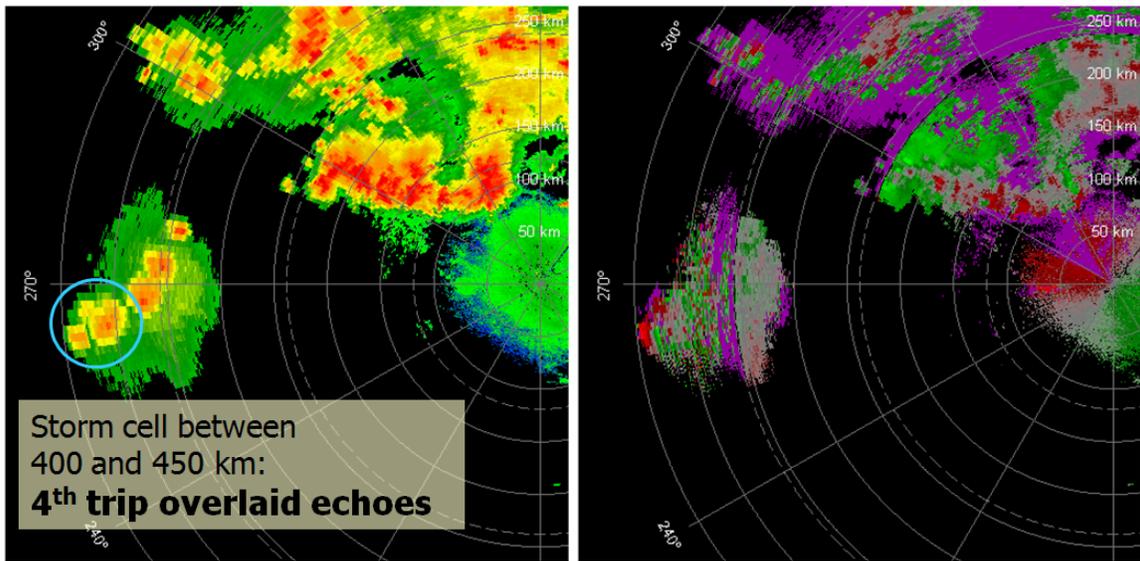
Long PRT: r_a = 471 km

Short PRT: r_a = 119 km

Fig. 4.5. Reflectivity (left) and Doppler velocity (right) for the June 20, 2007 case.

71
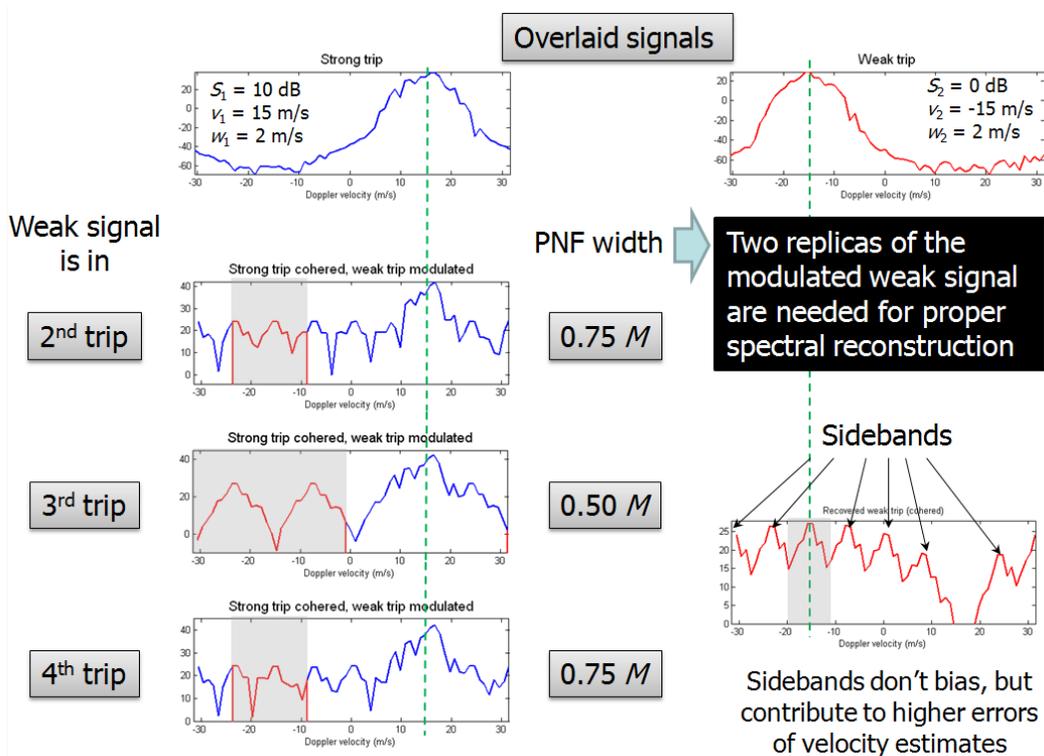
Fig. 4.6. Application of the processing notch filter (PNF) for different overlay cases in the SZ-2 algorithm to reconstruct the weak-trip signal spectrum.
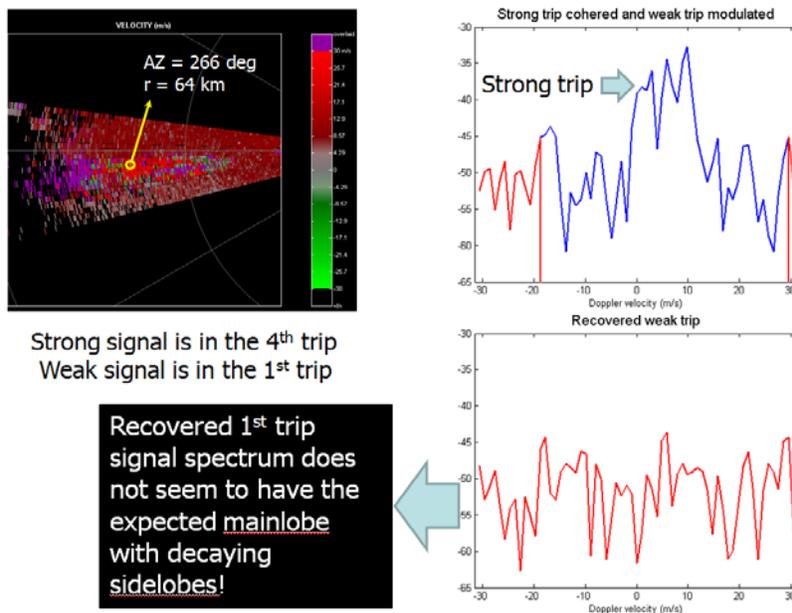
Fig. 4.7. Spectra corresponding to a range gate with noisy velocity. The top-right panel shows the spectrum of the strong-trip cohered signal and the lower-right panel shows the spectrum of the recovered weak-trip signal.

A closer look to the spectra of the recovered weak trip in the 1-2, 1-3, and 1-4 overlay situations turns out to be the key to this problem (Fig 4.8). Whereas, the 1-2 and 1-3 overlay cases exhibit *decaying* sidebands, this is not true for the 1-4 overlay case. Further, a statistical analysis of the recovery of weak-trip velocities shown in Fig. 4.9 reveals that if strong and weak signals are 3 trips apart (e.g., 1st and 4th trips), recovery of the weak-trip velocity is not possible (i.e., errors of estimates are very large). This can be intuitively explained by computing the normalized spectrum width of the modulation code of the recovered weak trip signal. Note that the normalized spectrum width computed this way is not the true spectrum width of the code because the Gaussian assumption obviously does not hold. However, this number is a good indicator of the "spread" of the spectrum, which in turn is associated with the errors of velocity estimates. For the 1-2, 1-3, and 1-4 overlay cases, the normalized spectrum width (σ_{vn}) is 0.1855, 0.1855, and 0.5305, respectively. Hence, the normalized spectrum width in the 1-4 overlay case is about 3 times larger than in the 1-2 or 1-3 cases, which explains the much larger errors of estimates observed both with simulations and real data.

An easy solution to this problem consists on reducing the PNF notch width to reduce the normalized spectrum width of the modulation code of the recovered weak signal. A PNF notch width of $5M/8$ results in an even larger value, $\sigma_{vn} = 0.5610$, whereas a notch width of $M/2$ (same as in the 1-3 overlay case) results in $\sigma_{vn} = 0.2637$, which is much closer to the values observed in the 1-2 and 1-3 overlay cases. Fig 4.10 shows the same statistical analysis of Fig. 4.9 but with a PNF notch width of $M/2$ for the 1-4 overlay instead of the old $3M/4$. With this simple change, it is now possible to recover the weak-trip velocity if the overlaid signals are three trips apart.

1st to 2nd trip mod. code	1st to 3rd trip mod. code	1st to 4th trip mod. code

$$\phi_k^{1 \to 2} = \frac{\pi}{8} k^2$$

$$\phi_k^{1 \to 3} = \frac{\pi}{8}[k^2 + (k-1)^2]$$

$$\phi_k^{1 \to 4} = \frac{\pi}{8}[k^2 + (k-1)^2 + (k-2)^2]$$

Cohere to strong ➜ Apply von Hann window ➜ Apply PNF ➜ Cohere to weak
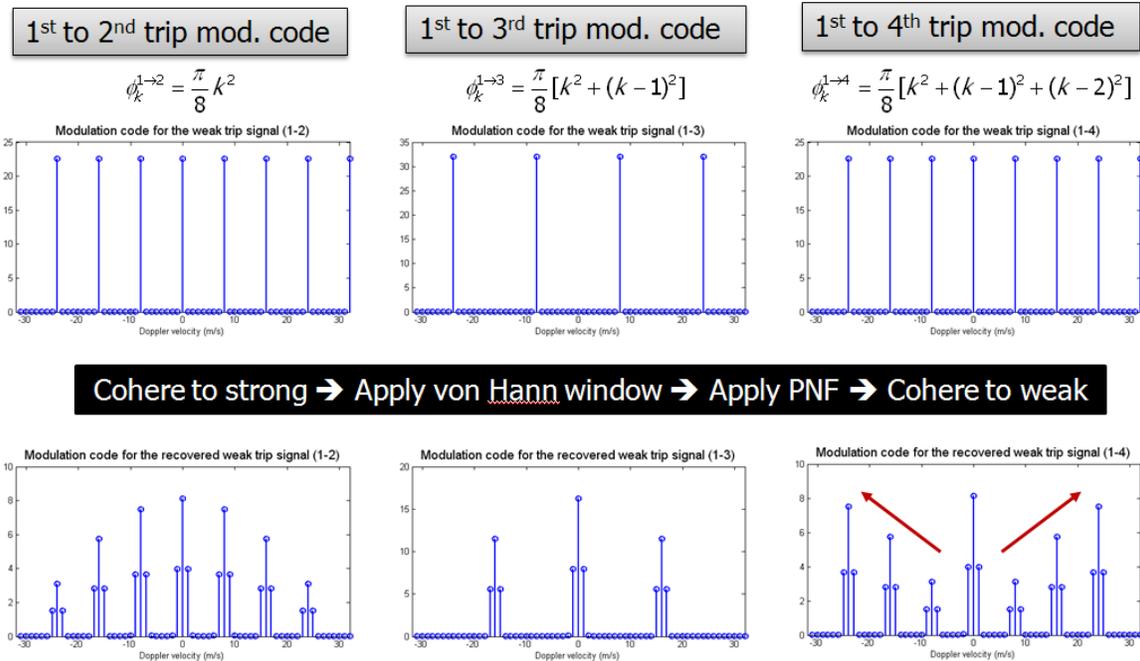
Fig. 4.8. Spectra of the modulated code for the weak-trip signal and for the recovered weak-trip signal after windowing, notching, and re-cohering for different overlay cases

In summary, proper recovery of the weak trip in the case of 1-4 overlay requires a processing notch filter narrower than initially assumed. The SZ-2 algorithm can be easily modified to use a 50% notch in this case by changing one line of code in step 14.ii of the algorithm (see Appendix B for an updated functional description). We recommend that the ROC implements this change as soon as possible. The change will improve the recovery of weak overlaid echoes in those cases where the strong-to-weak trip difference is three. Fig 4.11 shows the 06/20/07 case as processed with this change. It is evident that recovery of the weak 1st trip velocities is now feasible. However, we can still observe noisy velocities in this and in other areas of the field. This issue is addressed next.

74
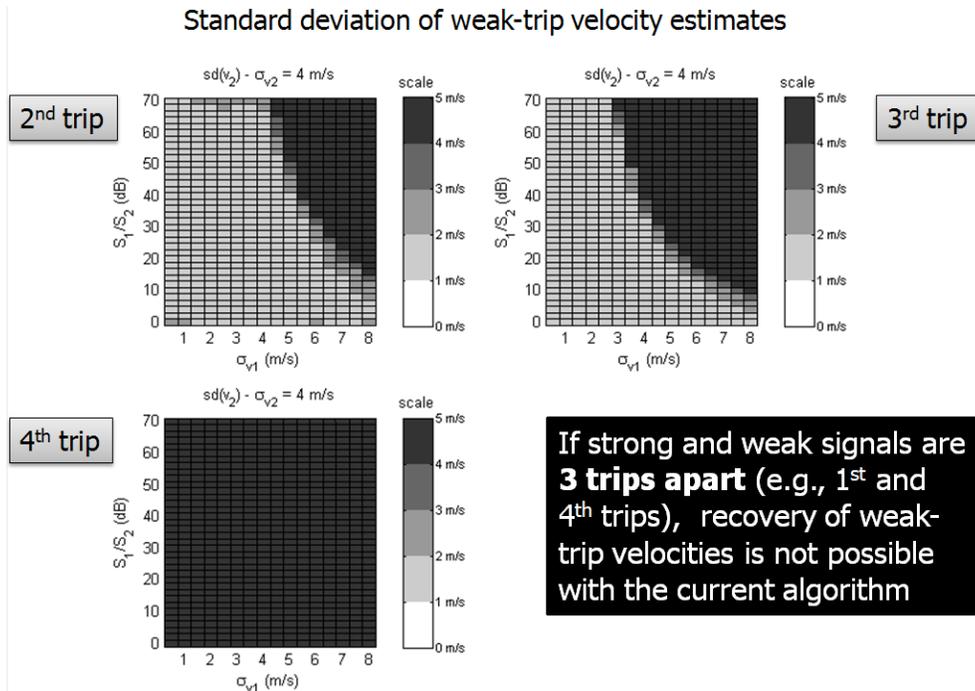
Fig. 4.9. Standard deviation of weak-trip velocities for the current SZ-2 algorithm as a function of the power ratio (S_1/S_2) and the strong-trip spectrum width (σ_{v1}) for different overlay cases, high signal-to-noise ratio, and a 4 m/s weak-trip spectrum width (σ_{v2}).
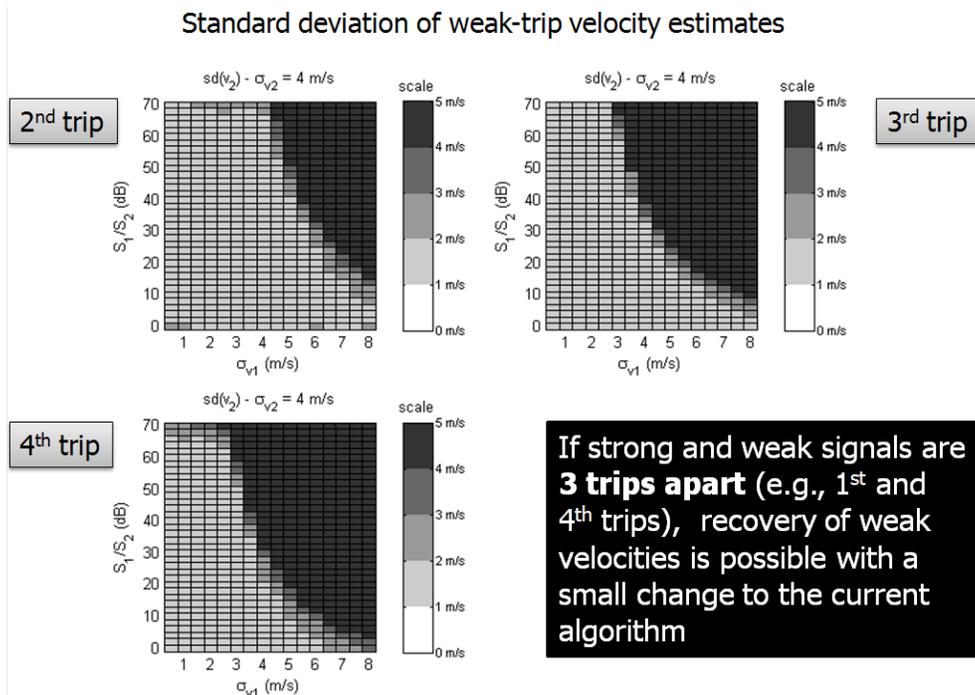
Fig. 4.10. Standard deviation of weak-trip velocities for the *proposed* SZ-2 algorithm as a function of the power ratio (S_1/S_2) and the strong-trip spectrum width (σ_{v1}) for different overlay cases, high signal-to-noise ratio, and a 4 m/s weak-trip spectrum width (σ_{v2}).
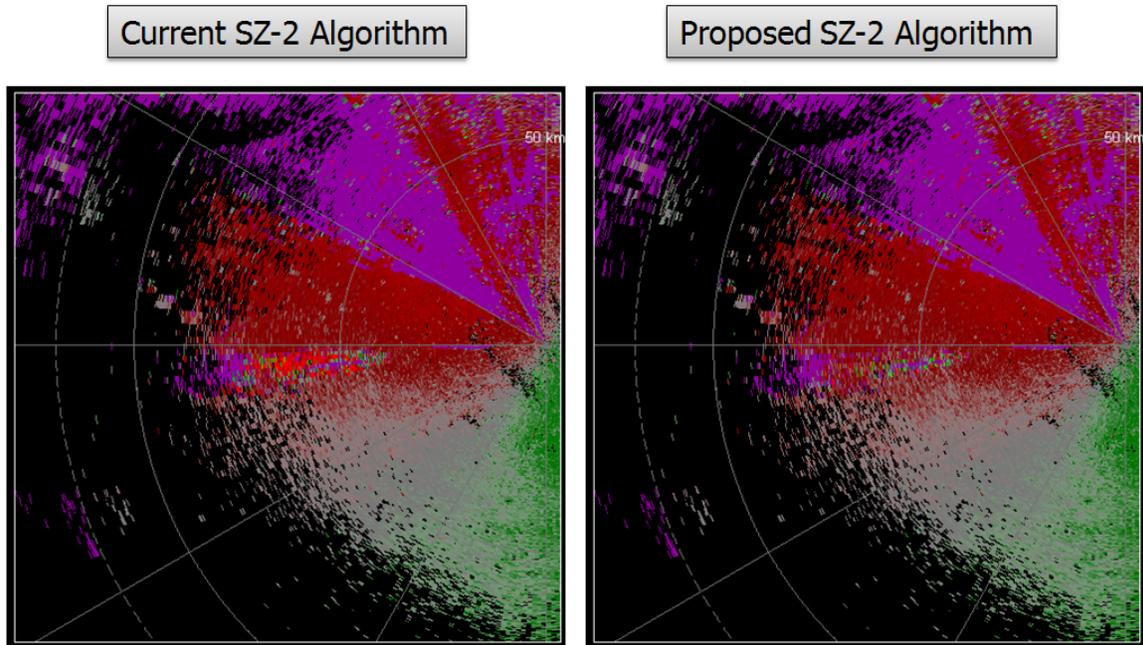
Fig. 4.11. Doppler velocity fields for the June 20, 2007 case for the current (left) and proposed (right) SZ-2 algorithms.

4.3. Recovery region censoring

Since its implementation, Doppler velocity fields produced with the SZ-2 algorithm have been characterized as "noisier". On one hand, it was accepted that errors of weak-trip velocity estimates would be larger. In fact, never before had the NEXRAD system been able to recover Doppler velocities of weak-trip overlaid echoes. Due to the great operational gain associated with the SZ-2 algorithm, the NEXRAD Technical Requirement (NTR) for errors of weak-trip velocity estimates was waived. The normal requirement of standard errors of velocity less than 1 m/s for a true spectrum width of 4 m/s and a signal-to-noise ratio larger than 8 dB was changed to a maximum allowable standard error of 2 m/s. On the other hand, even with the increased level of errors, it looks like estimates with errors much larger than that are being produced by the SZ-2 algorithm (see Fig 4.11).

A closer look at the weak trip number for the 06/20/07 case reveals that most of the noisy velocities come from the weak trip. Therefore, any censoring that should occur would be given by the power-ratio recovery-region censoring rules (see Appendix B). Originally, the thresholds for this type of censoring were based on plots of errors of weak-trip velocity as a function of the strong-to-weak trip power ratio and the strong-trip spectrum width, with the weak-trip spectrum width as a parameter (Hubbert et al. 2003, 2005). However, those plots only considered the 1-2 overlay case.

A more thorough analysis is presented next. Fig. 4.12 through 4.14 show the standard error of weak-trip velocity estimates on the strong-to-weak power ratio vs. strong-trip spectrum width plane, with the weak-trip spectrum width as a parameter (ranging from 1 to 8 m/s) for the 1-2, 1-3, and 1-4 overlay situations, respectively. These statistics were computed for the nominal transmitter frequency of 2800 MHz, a short PRT of 780 μs, and large SNR. Comparing these figures, it is evident that the different overlay situations exhibit different power-ratio recovery regions. Furthermore, for wide weak-trip spectrum widths, acceptable recovery of weak-trip velocities is not possible (i.e., errors of weak-trip velocity are unacceptably large).
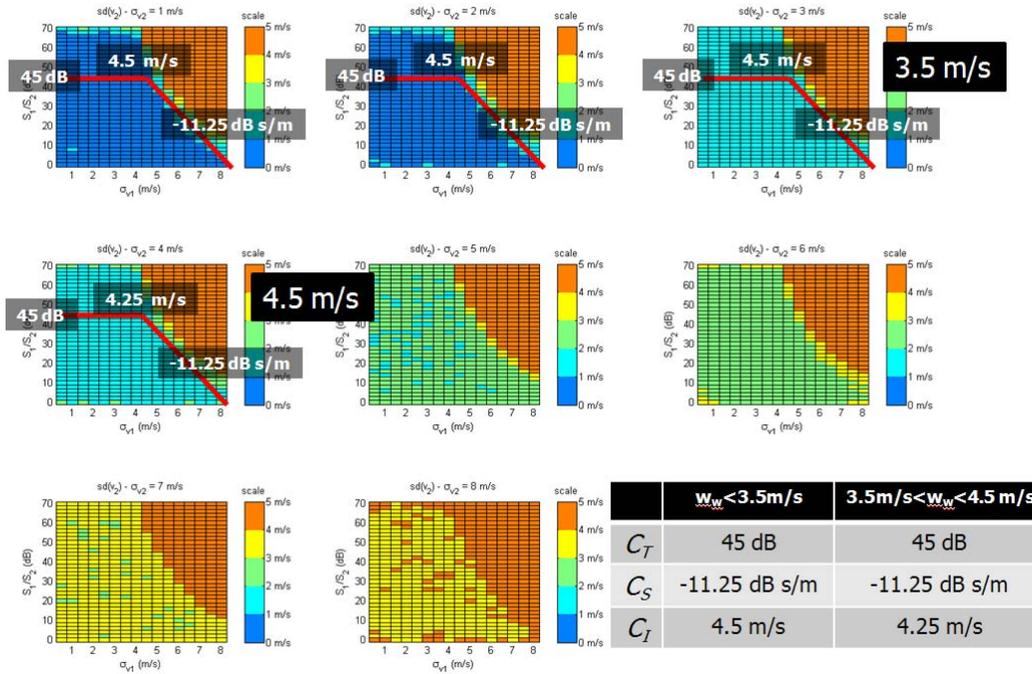
Fig. 4.12. Standard deviation of weak-trip velocities for the SZ-2 algorithm as a function of the power ratio (S_1/S_2) and the strong-trip spectrum width (σ_{v1}) for the 1-2 overlay case, high SNR, and weak-trip spectrum widths (σ_{v2}) between 1 and 8 m/s.
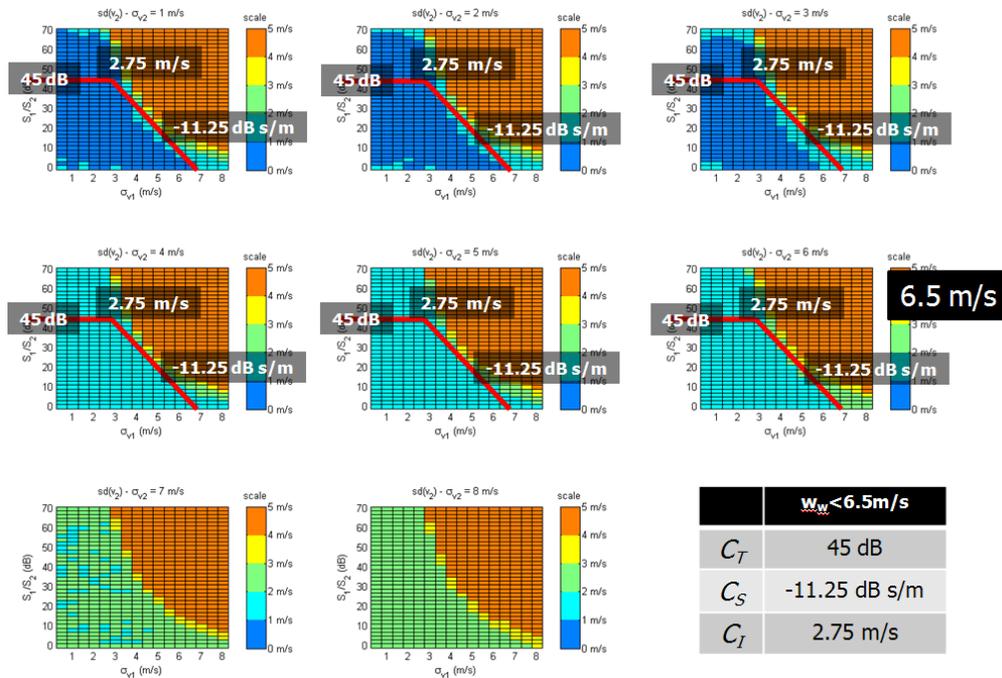
Fig. 4.13. Standard deviation of weak-trip velocities for the SZ-2 algorithm as a function of the power ratio (S_1/S_2) and the strong-trip spectrum width (σ_{v1}) for the 1-3 overlay case, high SNR, and weak-trip spectrum widths (σ_{v2}) between 1 and 8 m/s.
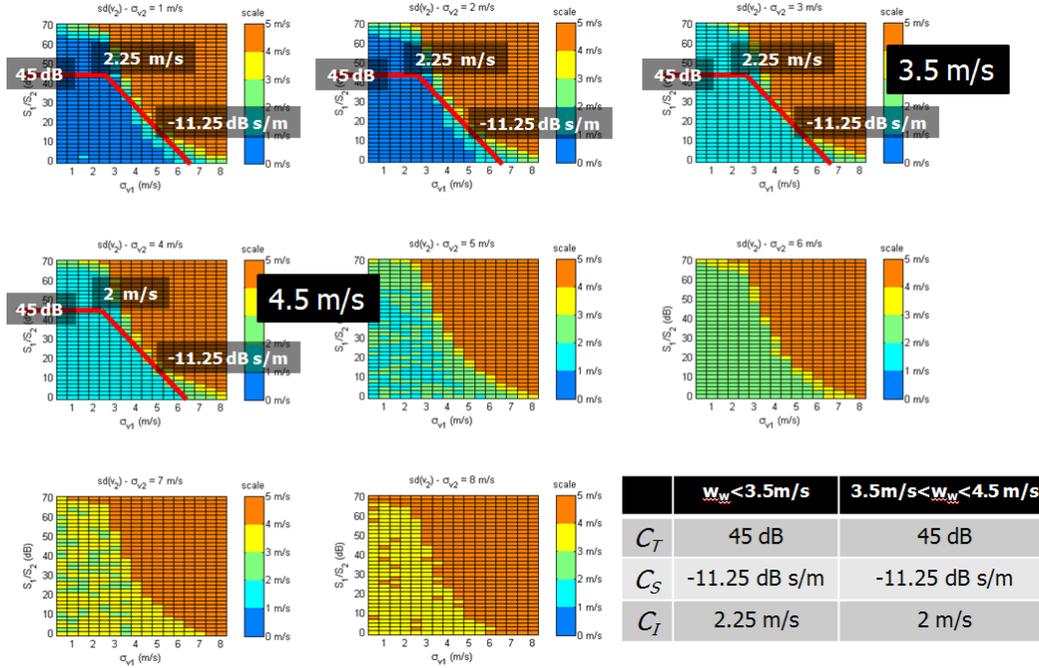
Fig. 4.14. Standard deviation of weak-trip velocities for the SZ-2 algorithm as a function of the power ratio (S_1/S_2) and the strong-trip spectrum width (σ_{v1}) for the 1-4 overlay case, high SNR, and weak-trip spectrum widths (σ_{v2}) between 1 and 8 m/s.

Closer examination of these plots indicates that the current recovery region thresholds are not aggressive enough. We propose expanding the set of thresholds to accommodate all expected overlay cases and to modify the rules so that three weak-trip spectrum width regions are considered: narrow, medium, and wide. For the narrow and medium weak-trip spectrum widths, thresholds should be different, and for wide weak-trip spectrum widths, immediate censoring should be applied. Current thresholds and preliminary recommended thresholds are in Table 4.1. Note that even for the 1-2 overlay case, the new thresholds result in more aggressive censoring of weak trip echoes. Fig. 4.15 through 4.17 depict the effects of different censoring approaches on the 06/20/07 case. Note that the current censoring scheme is not aggressive enough, producing a large number of noisy velocities. The proposed censoring scheme mitigates this problem but not

completely. A more aggressive set of thresholds is shown for comparison. Evidently, there is a trade-off between preserving data quality by censoring unreliable gates and recovering as much as we can by not censoring valid data.

A comprehensive analysis is needed before establishing a permanent set of censoring thresholds. Ideally, we should examine a variety of cases collected from operational radars. However, this type of analysis requires level-I phase-coded data which is not easily available. Whereas the determination of optimum censoring thresholds would take significant time, the SZ-2 code can be modified right away to include the upgraded rules for recovery region censoring. Having the additional functionality in place, we could set the thresholds so that the algorithm behaves exactly the same as in the ORDA B10 implementation. The thresholds could be updated in later builds with little impact to the system. The functional description of the SZ-2 algorithm in Appendix B has been updated with the proposed changes and thresholds. We recommend that the ROC implements these changes and conducts a censoring threshold evaluation with assistance of the Data Quality team as soon as possible. This would minimize the occurrence of noisy velocities when using SZ-2 at the expense of increasing the number of gates with purple haze.

Current thresholds Same for every type of overlay			$w_{Wn} < 0.243$	$w_{Wn} \geq 0.243$
K_r		C_T	45 dB	45 dB
		C_S	−429 dB	−429 dB
		C_I	0.0699	0.0544

Proposed thresholds
Depend on type of overlay

		$w_{Wn} < w_0$	$w_0 < w_{Wn} < w_1$	$w_W > w_1$
One-trip difference $w_0 = 0.2032$ $w_1 = 0.2612$	C_T	45 dB	45 dB	$-\infty$
	C_S	-772	-772	N/A
	C_I	0.0656	0.0619	N/A
Two-trip difference $w_0 = 0$ $w_1 = 0.3773$	C_T	N/A	45 dB	$-\infty$
	C_S	N/A	-772	N/A
	C_I	N/A	0.0401	N/A
Three-trip difference $w_0 = 0.2032$ $w_1 = 0.2612$	C_T	45 dB	45 dB	$-\infty$
	C_S	-772	-772	N/A
	C_I	0.0328	0.0291	N/A

Table 4.1. Current and proposed SZ-2 power-ratio recovery-region censoring thresholds.
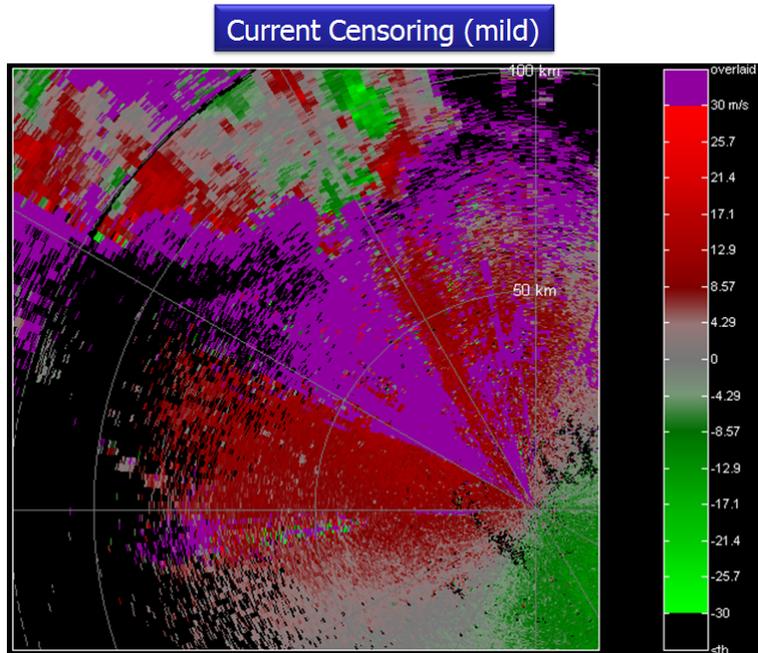
Fig. 4.15. Doppler velocity field for the June 20, 2007 case using current recovery region censoring thresholds.
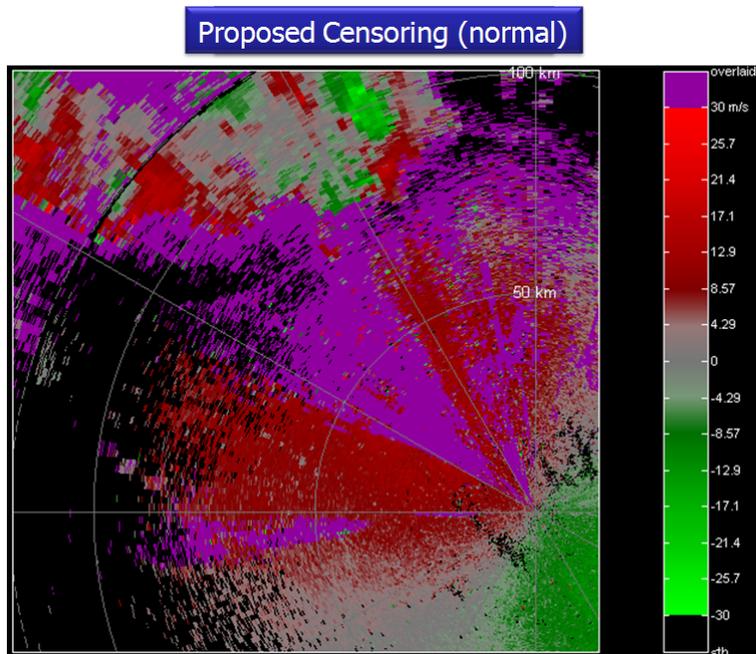
Fig. 4.16. Doppler velocity field for the June 20, 2007 case using proposed recovery region censoring thresholds.
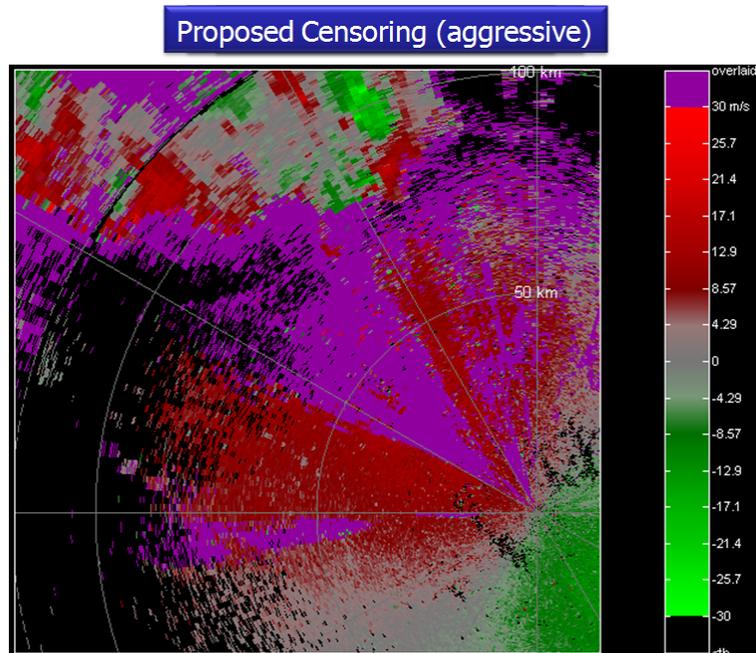
Fig. 4.17. Doppler velocity field for the June 20, 2007 case using aggressive recovery region censoring thresholds.

5. References

Hubbert, J., S. Ellis, G. Meymaris, and M. Dixon, 2003: NEXRAD Range-Velocity Mitigation: SZ(8/64) Phase Coding for the RVP8 Processor, NCAR Annual Report, 54 pp.

Hubbert, J., C. Kessinger, M. Dixon, S. Ellis, G. Meymaris, and J. Van Andel, 2005: NEXRAD Data Quality: SZ Phase Coding Enhancements and Radar Echo Classification Advances, NCAR Annual Report, 138 pp.

Melnikov, V. M., and D. S. Zrnić, 2004: Estimates of large spectrum width from autocovariances. *J. Atmos. Oceanic Technol.*, **21**, 969-974.

Torres, S., Y. Dubel, and D. S. Zrnić, 2004: Design, implementation, and demonstration of a staggered PRT algorithm for the WSR-88D. *J. Atmos. Oceanic Technol.*, **21**, 1389-1399.

Torres S., M. and D. Zrnić, 2006: Signal Design and Processing Techniques for WSR-88D Ambiguity Resolution: Evolution of the SZ-2 Algorithm. NOAA/NSSL Report, Part 10, 71 pp.

M. Sachidananda, D. Zrnic, and R. Doviak, "Signal Design and processing techniques for WSR-88D ambiguity resolution – Part 3: Staggered PRT Technique," *NSSL / OAR / NOAA report*, Norman OK, p. 103, 1999. Available online cimms.ou.edu/rvamb/Documents/Report_3.pdf

M. Sachidananda, and D. S. Zrnic**,** "Clutter filtering and spectral moment estimation for doppler weather radars using staggered pulse repetition time (PRT)," *Journal of Atmospheric and Oceanic Technology*, **17**, 323-331, 2000.

S. Torres, M. Sachidananda, and D. Zrnic, "Signal Design and processing techniques for WSR-88D ambiguity resolution – Part 9: Phase Coding and Staggered PRT," NSSL / *OAR / NOAA report*, Norman OK, p. 103, 2005. Available online cimms.ou.edu/rvamb/Documents/Report_9.pdf .

M. Sachidananda, and D. S. Zrnic, "Ground Clutter Filtering Dual polarized, Staggered PRT Sequence," *Journal of Atmospheric and Oceanic Technology*, **23**, 1114-1130, 2006.

S. Torres, "Processing of Staggered PRT Sequences on the KOUN Research Radar," AMS *International Radar Conference*, August 2003.

A. D. Siggia, and R. E. Passareli, Jr., "Gaussian Model Adaptive Processing (GMAP) for improved ground clutter cancellation and moment calculation," Proc., *European radar conf.*, 67-73, 2004.

R.L. Ice, R.D. Rhoton, D. S. Saxion, C.A. Ray, N. K. Patel, D. A. Warde, A. D. Free, O.E. Boydstun, D. S. Berkowitz, J. N. Chrisman, J. C. Hubbert, C. Kessinger, M. Dixon, S. Torres, "Optimizing clutter filtering in the WSR-88D," *AMS Proc. 23d Conf on IIPS*, P2.11, 2007.

Radar Operation Center, *Commerce-defense-transportation. Doppler meteorological radar WSR-88D. WSR-88D System specification.* Document number 2810000G, identification code 0WY55, May 2007. Available online www.roc.noaa.gov/security/files/other/2810000G.pdf

LIST OF NSSL REPORTS FOCUSED ON POSSIBLE UPGRADES

TO THE WSR-88D RADARS

Zrnić, D.S., Melnikov, V. M., J. K. Carter, and I. Ivić, 2007: Calibrating differential reflectivity on the WSR-88D, (Part 2). NOAA/NSSL Report, 34 pp.

Torres S., M. and D. Zrnić, 2006: Signal Design and Processing Techniques for WSR-88D Ambiguity Resolution: Evolution of the SZ-2 Algorithm. NOAA/NSSL Report, Part 10, 71 pp.

Torres S., M. Sachidananda, and D. Zrnić, 2005: Signal Design and Processing Techniques for WSR-88D Ambiguity Resolution: Phase coding and staggered PRT. NOAA/NSSL Report, Part 9, 112 pp.

Zrnić, D.S., Melnikov, V.M., and J.K. Carter, 2005: Calibrating differential reflectivity on the WSR-88D. NOAA/NSSL Report, 34 pp.

Torres S., M. Sachidananda, and D. Zrnić, 2004: Signal Design and Processing Techniques for WSR-88D Ambiguity Resolution: Phase coding and staggered PRT: Data collection, implementation, and clutter filtering. NOAA/NSSL Report, Part 8, 113 pp.

Zrnić, D., S. Torres, J. Hubbert, M. Dixon, G. Meymaris, and S. Ellis, 2004: NEXRAD range-velocity ambiguity mitigation. SZ-2 algorithm recommendations. NCAR-NSSL Interim Report.

Melnikov, V, and D Zrnić, 2004: Simultaneous transmission mode for the polarimetric WSR-88D – statistical biases and standard deviations of polarimetric variables. NOAA/NSSL Report, 84 pp.

Bachman, S., 2004: Analysis of Doppler spectra obtained with WSR-88D radar from non-stormy environment. NOAA/NSSL Report, 86 pp.

Zrnić, D., S. Torres, Y. Dubel, J. Keeler, J. Hubbert, M. Dixon, G. Meymaris, and S. Ellis, 2003: NEXRAD range-velocity ambiguity mitigation. SZ(8/64) phase coding algorithm recommendations. NCAR-NSSL Interim Report.

Torres S., D. Zrnić, and Y. Dubel, 2003: Signal Design and Processing Techniques for WSR-88D Ambiguity Resolution: Phase coding and staggered PRT: Implementation, data collection, and processing. NOAA/NSSL Report, Part 7, 128 pp.

Schuur, T., P. Heinselman, and K. Scharfenberg, 2003: Overview of the Joint Polarization Experiment (JPOLE), NOAA/NSSL Report, 38 pp.

Ryzhkov, A, 2003: Rainfall Measurements with the Polarimetric WSR-88D Radar, NOAA/NSSL Report, 99 pp.

Schuur, T., A. Ryzhkov, and P. Heinselman, 2003: Observations and Classification of echoes with the Polarimetric WSR-88D radar, NOAA/NSSL Report, 45 pp.

Melnikov, V., D. Zrnić, R. J. Doviak, and J. K. Carter, 2003: Calibration and Performance Analysis of NSSL's Polarimetric WSR-88D, NOAA/NSSL Report, 77 pp.

NCAR-NSSL Interim Report, 2003: NEXRAD Range-Velocity Ambiguity Mitigation SZ(8/64) Phase Coding Algorithm Recommendations.

Sachidananda, M., 2002: Signal Design and Processing Techniques for WSR-88D Ambiguity Resolution, NOAA/NSSL Report, Part 6, 57 pp.

Doviak, R., J. Carter, V. Melnikov, and D. Zrnić, 2002: Modifications to the Research WSR-88D to obtain Polarimetric Data, NOAA/NSSL Report, 49 pp.

Fang, M., and R. Doviak, 2001: Spectrum width statistics of various weather phenomena, NOAA/NSSL Report, 62 pp.

Sachidananda, M., 2001: Signal Design and Processing Techniques for WSR-88D Ambiguity Resolution, NOAA/NSSL Report, Part 5, 75 pp.

Sachidananda, M., 2000: Signal Design and Processing Techniques for WSR-88D Ambiguity Resolution, NOAA/NSSL Report, Part 4, 99 pp.

Sachidananda, M., 1999: Signal Design and Processing Techniques for WSR-88D Ambiguity Resolution, NOAA/NSSL Report, Part 3, 81 pp.

Sachidananda, M., 1998: Signal Design and Processing Techniques for WSR-88D Ambiguity Resolution, NOAA/NSSL Report, Part 2, 105 pp.

Torres, S., 1998: Ground Clutter Canceling with a Regression Filter, NOAA/NSSL Report, 37 pp.

Doviak, R. and D. Zrnić, 1998: WSR-88D Radar for Research and Enhancement of Operations: Polarimetric Upgrades to Improve Rainfall Measurements, NOAA/NSSL Report, 110 pp.

Sachidananda, M., 1997: Signal Design and Processing Techniques for WSR-88D Ambiguity Resolution, NOAA/NSSL Report, Part 1, 100 pp.

Sirmans, D., D. Zrnić, and M. Sachidananda, 1986: Doppler radar dual polarization considerations for NEXRAD, NOAA/NSSL Report, Part I, 109 pp.

Sirmans, D., D. Zrnić, and N. Balakrishnan, 1986: Doppler radar dual polarization considerations for NEXRAD, NOAA/NSSL Report, Part II, 70 pp.

Appendix A. Staggered PRT Algorithm: Functional Description Update

Assumptions:

(a) The switching sequence is $[T_1,T_2,T_1,T_2, \ldots]$.

(b) $T_1 < T_2$, $T_1 / T_2 = \kappa = 2/3$, and $(T_2 - T_1) = T_u$.

(c) M is the number of staggered PRT samples. $M/2$ is the number of staggered pairs.

M divisible by 4 is recommended (but not required).

(d) $N = 5M/2$, number of DFT coefficients.

(e) Ground clutter is present.

(f) No overlaid signal.

Inputs:

(a) complex time series, g_i, i=1, 2, 3, ... M.

(b) ground clutter filter map.

(c) M, T_1, T_2, radar frequency, radial, range, p_noise (receiver noise).

Pre-compute: the following are pre-computed and supplied to the algorithm. These need to be re-computed only if M changes.

(a) Normalized window coefficients for N points, b_i , i $=$ 1, 2, 3, ..., N.

(b) Re-arranged (5x5) convolution matrix, $\mathbf{C_r}$.

(c) Magnitude de-convolution matrix, $\{abs(\mathbf{C_r})\}^{-1}$.

(d) Matrices $\mathbf{C_{f1}}$, and $\mathbf{C_{f2}}$.

(e) Matrix $\mathbf{Z} = [1111...(M/2),\xi_2,\xi_2,\xi_2...(M),\xi_3,\xi_3,\xi_3,...(M) \quad ,\xi_2,\xi_2,\xi_2...(M),111...(M/2)]$

{ the numbers in ( ) brackets indicate number of time to repeat the element.}

{...

How to compute C_r, C_{f1}, and C_{f2}:

(1) form code sequence of length 5 only, [10100].

(2) take x = DFT([10100]), normalize power to unity (divide each element by the square root of the total power in the spectrum)

(3) form matrix C_r with these 5 coefficients as the first column, and form the second and subsequent columns by down shifting cyclically by one coefficient at a time.

(4) C_{f1}, and C_{f2} are computed using 1st and 5th columns, C_1, and C_5 of C_r.

$C_{f1} = C_1 \, C_1^{t*}$ and $C_{f2} = C_5 \, C_5^{t*}$

...}

The clutter filter algorithm: {explanation/details is given in {} brackets.}

Input time series, radial, range:

if clutter is **not** present for the range gate {determine from the clutter filter map}

go to the pulse pair algorithm {given in report-7 or updated AEL, delete the clutter filtering part}.

elseif **overlaid** signal present

go to the pulse pair algorithm (report-7 or updated AEL)

else {ground **clutter present** and **no overlay**} apply the algorithm below:

1. Form derived time series,

{insert zeros: $e = [g_1, 0, g_2, 0, 0, g_3, 0, g_4, 0, 0, ..., g_M, 0, 0]$ } }

2. Apply normalized window {multiply, $e.*b = e_i*b_i$; $i=1,2,...N$}

{if the *CNR* is known from the clutter map, one may select appropriate optimum window. However, the Blackman window should be replaced with a less aggressive window. For small number of pairs and long PRT the rectangular window is recommended}.

3. Compute $\mathbf{V} = \text{DFT}(e.*b)$. {$\mathbf{V}$ is a row vector}

4. (skip this step)

5. Determine clutter filter width parameter, q.

{If GMAP is available: Make sure that GMAP is modified to return the number of coefficient identified as clutter. Take the 5th of the Doppler spectrum containing the main clutter replica and whichever weather replica; initialize GMAP for spectra with $v_a/5$; pass this 5th of Doppler spectrum to GMAP; and get the number of coefficients i_gap_from_GMAP identified as clutter to estimate q}.

$$q = (\text{i\_gap\_from\_GMAP} + 1)/2$$

{If GMAP is not available, choose an approximate q from table q3D based on *CNR*, number of pairs $M/2$, and v_a}.

Compute approximate *CNR*:

$$CNR\_aprox = [(V_1 + V_2 + V_N) (5/2)(5/2)] / (p\_noise).$$

{The two 5/2 factors are to account for: (a) the inserted zeros, and (b) the spread of the clutter spectral amplitude. The staggered PRT spectrum has 5 unequal replicas, with the main one having 2/5th of the power}.

{If the table q3D has dimensions [30x50x10], where *CNR* spans 1:2:60, number of pairs spans 10:1:59, and the unambiguous velocity spans 20:5:65; then, estimate the corresponding cell in the table as follows ..}

x = round((CNRdb_aprox/2)); if $x<1$ $x=1$; end; if $x>30$ $x=30$; end;

y = round((M/2-9)); if $y<1$ $y=1$; end; if $y>50$ $y=50$; end;

z = round(v_a/5-3); if $z<1$ $z=1$; end; if $z>10$ $z=10$; end;

{.. and load the value from the chosen cell}.

q = round(q3D(x, y, z));

6. Compute clutter filter matrices, $\mathbf{I_{f1}}$, $\mathbf{I_{f2}}$, $\mathbf{I_1}$, $\mathbf{I_2}$. {all are row matrices}

$\mathbf{I_{f1}}$ = [1,1,... (q times),0,0, ...(N-q times)],

$\mathbf{I_{f2}}$ = [0,0,...(N-q+1 times),1,1,...(q-1 times)].

$\mathbf{I_2}$ = [($\mathbf{I_{f1}}$+ $\mathbf{I_{f2}}$),... repeat 5 times],

$\mathbf{I_1}$ = complement of $\mathbf{I_2}$, (interchange 0s and 1s).

{ [$\mathbf{I_{f1}}$+$\mathbf{I_{f2}}$] has M/2 elements (first q and last q-1 elements are ones and the rest zeros), and $\mathbf{I_1}$ and $\mathbf{I_2}$ have N elements each.}

7. Row-wise re-arrange $\mathbf{V}$ into a (5x(M/2)) matrix $\mathbf{V_r}$. {see Eq.3.15 in report-9}

8. Filter the clutter: compute the spectrum, $\mathbf{V_f}$, after the clutter is filtered

$\mathbf{V_f}$ = $\mathbf{V_r}$ - $\mathbf{C_{f1}}$ $\mathbf{V_r}$ diag ($\mathbf{I_{f1}}$) - $\mathbf{C_{f2}}$ $\mathbf{V_r}$ diag ($\mathbf{I_{f2}}$)

9. Magnitude de-convolution

$\mathbf{E_r}$ = $[abs\{\mathbf{C_r}\}]^{-1} abs\{\mathbf{V_f}\}$.

10. Row-wise unfold $\mathbf{E_r}$ into a single row matrix, $\mathbf{E_s}$.

11. Compute the autocorrelation $R(T_u)$, and *initial* velocity

$$R(T_u) = \frac{\sum_{1}^{N} |E_{sk}|^2 e^{j2\pi(k-1)/N}}{\frac{1}{N}\sum_{1}^{N-1} b_k b_{k+1}}$$

{E_{sk} are the elements of $\mathbf{E_s}$, b is the data window }

$$v_{initial} = \frac{v_a}{\pi}\arg[R(T_u)]; \qquad v_a = \frac{\lambda}{4T_u}.$$

12. Compute row matrix $\mathbf{I_v}$ {$M/2$ ones centered on $v_{initial}$ }

{Round to the nearest spectral coefficient velocity estimate. Choose symmetric window of coefficients around it. }

$$k_0 = round\left[\frac{-v_{initial}N}{2v_a}\right]; \qquad\qquad \text{if } k_0 < 1 \text{ , } k_0 = k_0 + N,$$

$$k_1 = k_0 - floor(M/4); \qquad\qquad \text{if } k_1 < 1 \text{ , } k_1 = k_1 + N,$$

$$k_2 = k_0 + floor(M/4); \qquad\qquad \text{if } k_2 > N \text{ , } k_2 = k_2 - N,$$

{k_0 is the DFT index corresponding to $v_{initial}$, and k_2 specify the portion of M spectral coefficients centered on the mean velocity. The function *round* gives the nearest integer. If $k_1 > k_2$, the ones will span from k_1 to N, and 1 to k_2}

$\mathbf{I_v} = [0,0, ...,1,1,1,...,0,0,...]$

{In the N element row matrix,

if $k_1 < k_2$, element # k_1 to k_2 are ones and the rest are zeros in $\mathbf{I_v}$.

if $k_2 < k_1$, element # (k_2+1) to $(k_1 -1)$ are zeros and the rest are ones in $\mathbf{I_v}$.}

13. Interpolate the elements for the region-1 in $\mathbf{E_s}$.

Let $s_1 = |E_s(q+1)|^2$, and $s_2 = |E_s(N-q+1)|^2$, the $(q+1)^{th}$, and $(N-q+1)^{th}$ element powers of $\mathbf{E_s}$. The elements in the *velocity_region*-(1) are replaced with interpolated values from s_1 and s_2.

$$E_s(k) = [s_2 + (s_1 - s_2) (q + k - 1) / 2q]^{1/2}, \quad k = 1 \text{ to } q;$$

and $E_s(k) = [s_2 + (s_1 - s_2) (q + k - 1 - N) / 2q]^{1/2}, \quad k = N-q+2 \text{ to } N.$

14. Compute the corrected spectrum, $\mathbf{E_c}$.

$$\mathbf{E_c} = \mathbf{E_s} \bullet \mathbf{I_1} + \mathbf{E_s} \bullet \mathbf{I_2} \bullet \mathbf{I_v} \bullet \mathbf{Z}$$

{ all are row matrices, and the $\bullet$ represents the element by element multiplication ($\bullet$* of MATLAB}

15. Re-compute the autocorrelation $R(T_u)$ using $\mathbf{E_c}$, and compute bias corrected mean velocity, v, from the phase of the autocorrelation. The mean power, p, is also computed from this spectrum. Add *win_cor* to p mean power to correct for the loss due to window. Compute reflectivity, z, in dBZ units. (need *syscal*, *noise*, *range*, and atmospheric attenuation)

16. Retain only M coefficients centered on the mean velocity, v, and delete the rest from $\mathbf{E_c}$.

$$k_0 = round\left[\frac{-vN}{2v_a}\right]; \qquad \text{if } k_0 < 1 , k_0 = k_0 + N,$$

$$k_1 = k_0 - floor(M/2); \qquad \text{if } k_1 < 1 , k_1 = k_1 + N,$$

$$k_2 = k_0 + floor(M/2); \qquad \text{if } k_2 > N , k_2 = k_2 - N.$$

if $k_1 < k_2$, set the elements of $\mathbf{E_c}$ from 1 to (k_1-1), and (k_2+1) to N, to zero to get $\mathbf{E_{cm}}$.

if $k_2 < k_1$, set the elements of $\mathbf{E_c}$ from (k_2+1) to (k_1-1) to zero to get $\mathbf{E_{cm}}$.

17. Compute spectrum width from $\mathbf{E_{cm}}$ (modified spectrum) using the width estimator (Eq. 6.27 of Doviak and Zrnic, 1983). Note that the $R(T_u)$ and the mean power, S, used in that expression has to be computed from $\mathbf{E_{cm}}$, and not from $\mathbf{E_c}$.

18. Output the spectral parameters, p (or reflectivity z), v, and w.

19. Go to the next data set.

Appendix B. SZ-2 Algorithm: Functional Description Update

1. Introduction

This appendix includes the latest revision to the SZ-2 algorithm from November 2007. The update covers a simple fix for the 4th trip overlay case (step 14.ii) and improved power-ratio recovery-region censoring rules and thresholds (step 24 and updated table with censoring thresholds).

2. SZ-2 Algorithm Description

The SZ-2 algorithm was first introduced by Sachidananda et al. (1998) in a study of range-velocity ambiguity mitigation using phase coding. Unlike the stand-alone SZ-1 algorithm, SZ-2 relies on power and spectrum width estimates obtained using a long pulse repetition time (PRT). The SZ-2 algorithm is computationally simpler than its stand-alone counterpart as it only tries to recover the Doppler velocities associated with strong- and weak-trip signals and the spectrum widths associated with the strong-trip signal. Analogous to the legacy "split cut", the volume coverage pattern (VCP) is designed such that a non-phase-coded scan using a long PRT is immediately followed by a scan with phase-coded signals using a short PRT at the same elevation angle. Hence, determination of the number and location of overlaid trips can be done by examining the overlay-free long-PRT powers.

The following is a functional description of the SZ-2 algorithm tailored for insertion into the signal processing pipeline of the RVP-8. The description is divided into two parts: long PRT processing and short PRT processing with emphasis given to the latter. The algorithm is specified in a general manner and is not constrained to specific PRT values.

2.1. Long-PRT Processing

2.1.1. Assumptions

1) There is no phase modulation of the transmitted pulses.
2) There are no overlaid echoes.
3) The number of pulses transmitted in the dwell time is M_L.
4) The number of range cells is $N_L = T_{s,L}/\Delta t$, where $T_{s,L}$ is the pulse repetition time (long PRT) and Δt is the range-time sampling period (e.g., in the legacy WSR-88D $\Delta t = 1.57$ μs).
5) The algorithm operates on one range cell of time-series data at a time (M_L samples).

2.1.2. Inputs

1) Time series data for range cell n: $V_{n,L}(m) = I_{n,L}(m) + jQ_{n,L}(m)$, for $0 \leq m < M_L$, where m indexes the samples (or pulses).

2.1.3. Internal Outputs

These outputs are saved internally for later use during the short-PRT processing:

1) Clutter filtered powers: $P_L(n)$, for $0 \leq n < N_L$
2) GMAP removed powers: $C_L(n)$, for $0 \leq n < N_L$
3) Spectrum widths: $w_L(n)$, for $0 \leq n < N_L$

2.1.4. External Output

1) Reflectivity: $Z_L(n)$, for $0 \leq n < N_L$

2.1.5. Algorithm

SZ-2 processing in the long-PRT scan is an extension of the processing performed in any of the operational surveillance scans. Time-series data are clutter filtered using the GMAP clutter filter only in those locations where the bypass map indicates ground clutter contamination. Clutter-filtered time-series data are used to compute total power and lag-one correlation (R_L) estimates. The signal power (P_L) is obtained after subtracting the noise power from the total power, and spectrum width (w_L) is estimated from the P_L/R_L ratio. P_L, w_L, and the powers removed by GMAP (C_L) are saved internally to be used later during the short-PRT processing. A reflectivity estimate, Z_L, is obtained from P_L after proper censoring and scaling as usual.

2.2. Short-PRT Processing

2.2.1. Assumptions

1) The phases of the transmitted pulses are modulated with the SZ(8/64) switching code.
2) Regardless of the number of pulses transmitted in the dwell time $M = 64$ pulses worth of data are supplied to the algorithm.
3) The number of range cells is $N = T_s/\Delta t$, where T_s is the pulse repetition time (short PRT) and Δt is the range-time sampling period (e.g., in the legacy WSR-88D $\Delta t = 1.57$ μs).
4) Range cells in the short-PRT scan are **perfectly aligned** with range cells in the long-PRT scan. This is important for determining short-PRT trips within the long-PRT data. Note: Misalignments may occur, for example, due to $T_s/\Delta t$ not being an integer number or due to one or more samples being dropped.
5) Long- and short-PRT radials are perfectly aligned in azimuth. This is true for the ORDA system, which collects data on indexed radials.
6) The algorithm operates on one range cell (M samples) of time-series data at a time, but requires all cells to perform strong-point clutter suppression.

2.2.2. Inputs

1) Phase-coded time series data cohered to the 1st trip: $V_n(m) = I_n(m) + jQ_n(m)$, for $0 \le m < M$, where m indexes the samples (or pulses) and n indexes the range gates.
2) Ground-clutter-filtered powers and spectrum widths from the long-PRT scan: P_L and w_L. These vectors correspond to the long-PRT scan radial that has the same (or closest) azimuth to the phase-coded radial in (1).
3) GMAP removed powers: C_L. This vector corresponds to the long-PRT scan radial that has the same (or closest) azimuth to the phase-coded radial in (1).
4) Range-dependent ground clutter filter bypass map corresponding to the long- and short-PRT radials (B). B can be either `FILTER` or `BYPASS`, indicating the presence or absence of clutter, respectively.
5) Measured SZ(8/64) switching code: $\psi(m)$, for $-3 \le m < M$.
6) Censoring thresholds:
   $K_{SNR,Z}$: signal-to-noise (SNR) threshold for determination of significant returns for reflectivity,
   $K_{SNR,V}$: signal-to-noise (SNR) threshold for determination of significant returns for velocity,
   K_{IGN}: power ratio threshold to ignore trips with small total powers,
   K_s: signal-to-noise ratio (SNR) threshold for determination of strong trip recovery,
   K_w: signal-to-noise ratio (SNR) threshold for determination of weak trip recovery,
   $K_r(w_{Sn}, w_{Wn}, t_{diff})$: maximum strong-to-weak power ratios (P_S/P_W) for recovery of the weaker trip for different values of trip number difference ($t_{diff} = |t_S - t_W|$), strong- and weak-trip normalized spectrum widths ($w_{Sn} = w_S/2v_a$ and $w_{Wn} = w_W/2v_{a,L}$, where v_a and $v_{a,L}$ are the maximum unambiguous velocities corresponding to the short and long PRT, respectively). The value of K_r is determined using the spectrum-width-dependent constants C_T (threshold), C_S (slope), and C_I (intercept).

K_{CSR1}: clutter-to-strong-signal ratio (CSR) threshold for determination of strong trip recovery,

K_{CSR2}: clutter-to-weak-signal ratio (CSR) threshold for determination of weak trip recovery,

K_{CSR3}: clutter-to-signal ratio (CSR) threshold for determination of clutter presence,

$w_{n,max}$: maximum valid normalized spectrum width estimated from the long-PRT data.

$K_{x0}, K_{x1}, K_{s0}, K_{s1}$: clutter-to-noise ratio region definitions and correction slopes.

   The table below shows the recommended values for the censoring thresholds in the SZ-2 algorithm. These are expected to be refined during the testing and validation stages of the SZ-2 algorithm implementation.

Censoring threshold	Recommended value					Notes
$K_{SNR,Z}$	Value from VCP definition					
$K_{SNR,V}$	Value from VCP definition					
K_{IGN}	100					20 dB
K_s	0.5012					−3 dB
K_w	1.5849					2 dB
K_r	$t_{diff}=1$		$w_{Wn} < 0.2032$	$0.2032 \leq w_{Wn} < 0.2612$	$w_{Wn} \geq 0.2612$	Step 24 describes the computation of K_r based on C_T, C_S, and C_I. Note that these thresholds depend on the trip number difference of the overlaid trips (t_{diff}).
		C_T	45 dB	45 dB	$-\infty$	
		C_S	−772 dB	−772 dB	0	
		C_I	0.0656	0.0619	∞	
	$t_{diff}=2$		$w_{Wn} < 0$	$0 \leq w_{Wn} < 0.3773$	$w_{Wn} \geq 0.3773$	
		C_T	45 dB	45 dB	$-\infty$	
		C_S	−772 dB	−772 dB	0	
		C_I	0	0.0401	∞	
	$t_{diff}=3$		$w_{Wn} < 0.2032$	$0.2032 \leq w_{Wn} < 0.2612$	$w_{Wn} \geq 0.2612$	
		C_T	45 dB	45 dB	$-\infty$	
		C_S	−772 dB	−772 dB	0	
		C_I	0.0328	0.0291	∞	
K_{CSR1}	31622.8					45 dB
K_{CSR2}	1000					30 dB
K_{CSR3}	31.6228					15 dB
$w_{n,max}$	0.25					This is equivalent to ~4.5 m s^{-1} for PRT #1
K_{x0}	Same as in ORDA					
K_{x1}	Same as in ORDA					
K_{s0}	Same as in ORDA					
K_{s1}	Same as in ORDA					

2.2.3. Outputs

1) Doppler velocities for 4 trips: $v(n), 0 \leq n < 4N$
2) Spectrum widths for 4 trips: $w(n), 0 \leq n < 4N$
3) Return types for Doppler velocity and spectrum width for 4 trips: $type_v(n)$ and $type_w(n)$, $0 \leq n < 4N$. As in the legacy WSR-88D, $type$ can take the values NOISE_LIKE, SIGNAL_LIKE, or OVERLAID_LIKE. These are used to qualify the base data moments sent to the RPG as being non-significant returns, significant returns, or unrecoverable overlaid echoes, respectively.

2.2.4. Algorithm

. Compute autocorrelation normalization factors
For $0 \leq n < N$
   . Determine overlaid trips
  If $t_{Ao} \neq -1$
      (There is at least one trip to recover based on long-PRT powers)
      . Determine ground clutter location
      If $t_A \neq -1$
         (There is at least one trip to recover based on clutter location and long-PRT powers)
         If $t_C \neq -1$
            (There is clutter contamination)
            winType = WIN_BLACKMAN
            . Apply data window
            If $t_C \neq 0$
               (Clutter is not in the 1st trip)
               . Cohere to ground clutter trip
            End
            . Filter ground clutter
         Else
            (There is no clutter contamination)
            $k_{GMAP} = 0$
            $clutter_{GMAP} = 0$
            winType = WIN_RECT
            $V_w = V$
         End
         . Cohere to trips A and B
         . Compute lag-one autocorrelations for trips A and B
         . Determine strong and weak trips
         If $t_C = -1$
            (There is no clutter contamination)
            winType = WIN_DEFAULT
            If *winType* $\neq$ WIN_RECT
               . Apply data window
               . Compute lag-one autocorrelation for strong trip
            End
         End
         . Compute total power
         . Compute strong-trip velocity
         If $t_W \neq -1$
            (There are overlaid echoes)
            . Compute strong-trip lag-two autocorrelation
            If $t_C = -1$
               (There was no clutter contamination)
               winType = WIN_VONHANN

. Apply data window to original strong-trip cohered signal
End
. Compute discrete Fourier transform
. Apply processing notch filter
. Compute inverse discrete Fourier transform
. Compute weak-trip power
. Cohere to weak trip
. Compute weak-trip lag-one autocorrelation
. Retrieve weak-trip spectrum width
. Adjust powers
. Compute strong-trip spectrum width using R_1/R_2 estimator
Else
(There are no overlaid echoes)
. Adjust powers
. Compute strong-trip spectrum width using R_0/R_1 estimator
End
Else
(There are no trips to recover based on clutter location)
$clutter_{GMAP} = 0$
$t_S = t_W = -1$
End
Else
(There are no trips to recover based on long-PRT powers)
$clutter_{GMAP} = 0$
$t_S = t_W = t_C = -1$
End
. Compute SNR threshold adjustment factors
. Determine censoring and moments
End
. Filter strong point clutter
. Determine outputs

1) Compute autocorrelation normalization factors (Outputs: nf_0, nf_1, nf_2)

Three normalization factors (for autocorrelation computations at lags 0, 1, and 2) are computed for each data window (rectangular, von Hann, and Blackman) as follows:

For i = WIN_RECT, WIN_VONHANN, WIN_BLACKMAN
$\quad h$ = WINDOW(i)

$$nf_0(i) = \left[\sum_{m=0}^{M-1} h^2(m) \right]^{-1}$$

$$nf_1(i) = \left[\sum_{m=0}^{M-2} h(m)h(m+1) \right]^{-1}$$

$$nf_2(i) = \left[\sum_{m=0}^{M-3} h(m)h(m+2) \right]^{-1}$$

End

It is assumed that the function WINDOW(.) returns a sequence $h(m)$, $0 \leq m < M$ with the corresponding data window (with or without scaling).

2) Determine overlaid trips (Inputs: P_L, C_L. Outputs: t_{Ao}, t_{Bo}, r, t, P, Q)

The signal powers (after noise and clutter have been removed) from trips 1 to 4, i.e., $P_L(n)$, $P_L(n + N)$, $P_L(n + 2N)$, and $P_L(n + 3N)$, are used to determine t_{Ao} and t_{Bo}, the recoverable trips, according to the following algorithm (note that this assumes **perfect alignment** of range cells between the long and short PRTs).

(Collect long-PRT filtered and unfiltered powers for 4 trips)
For $0 \leq l < 4$
$\quad$ If $n + lN < N_L$
$\qquad$ *(Within the long-PRT range)*
$\qquad$ *(Filtered power)*
$\qquad$ $P(l) = P_L(n + lN)$
$\qquad$ *(Unfiltered or total power)*
$\qquad$ $Q(l) = P(l) + C_L(n + lN)$
$\quad$ Else
$\qquad$ *(Outside the long-PRT range)*
$\qquad$ $P(l) = 0$
$\qquad$ $Q(l) = 0$
$\quad$ End
$\quad$ *(Trip number)*
$\quad$ $t(l) = l$
End

(Rank long-PRT filtered powers)
Sort vectors *P, Q,* and *t* so that powers $P(0)$, $P(1)$, $P(2)$, and $P(3)$ are in descending order
with their corresponding total powers as $Q(0)$, $Q(1)$, $Q(2)$, and $Q(3)$ and trip numbers as $t(0)$,
$t(1)$, $t(2)$, and $t(3)$. Note that trip numbers are 0, 1, 2, or 3. In what follows, a −1 will be used to
indicate an invalid trip number.

(Determine trip-to-rank mapping)
For $0 \leq l < 4$
    $r[t(l)] = l$
End

Note: $t(rank)$ will be used to get the trip number for a given rank and $r(trip)$ to get the rank of a
given trip.

(Determine potentially recoverable trips based on long-PRT filtered powers)
If $P(0) > NOISE.K_{SNR,V}$
    (The strongest trip signal is a significant return; therefore, it is recoverable)
    $t_{Ao} = t(0)$
    If $P(1) > NOISE.K_{SNR,V}$
        (The second strongest trip signal is a significant return; therefore, it is recoverable)
        $t_{Bo} = t(1)$
    Else
        *(The second strongest trip signal is not a significant return; therefore, it is not
        recoverable)*
        $t_{Bo} = -1$
    End
Else
    *(The strongest trip signal is not a significant return; therefore, none of the trips are
    recoverable)*
    $t_{Ao} = -1$
    $t_{Bo} = -1$
End

In the above algorithm, $K_{SNR,V}$ is the SNR threshold to determine significant returns for velocity
and spectrum width estimates. This should be obtained from the VCP definition.

Note: If $t_{Bo} = -1$, only one trip is recoverable. If $t_{Ao} = -1$, no trips are recoverable.

3) Determine ground clutter location (Inputs: B, P_L, C_L, P, Q, r, t, t_{Ao}, t_{Bo}. Outputs: t_A, t_B, t_C)

In the case of overlaid clutter, an additional check is made using the long-PRT powers to prevent a catastrophic failure of the algorithm due to an incorrectly defined clutter map.

(Determine trips with clutter)
$n_C = 0$
For $0 \leq l < 4$
    If $n + lN < N_L$
        (Within the long-PRT range)
        If $B(n + lN) = $ FILTER
            (There is clutter in the l-th trip; therefore, store clutter trip number and increment clutter trip count)
            $clutterTrips(n_C) = l$
            $n_C = n_C + 1$
        End
    End
End
If $n_C > 1$
    (According to the Bypass map there is overlaid clutter; therefore, re-determine trips with clutter using both Bypass map and long-PRT powers)
    $n_C = 0$
    For $0 \leq l < 4$
        If $n + lN < N_L$
            (Within the long-PRT range)
            If $B(n + lN) = $ FILTER and $C_L(n + lN) > P_L(n + lN) \, K_{CSR3}$
                (There is clutter in the l-th trip)
                 $clutterTrips(n_C) = l$
                $n_C = n_C + 1$
            End
        End
    End
End

(Handle clutter)
If $n_C = 0$
    (No clutter anywhere; therefore, clutter filter will not be applied)
    $t_C = -1$
ElseIf $n_C = 1$
    (Non-overlaid clutter)
    $t_C = clutterTrips(0)$
    If $t_C \neq t_A$
        (The strong trip does not contain clutter)
        If $t_C = t_B$

(The weak trip contains clutter)

If $P(0) > Q(1) K_{IGN}$

(Strong signal is K_{IGN}-times larger than the total signal in the trip with clutter; therefore, clutter can be ignored and the weak signal is not recoverable)

$t_B = -1$

$t_C = -1$

End

Else

(One of the unrecoverable trips contains clutter)

If $P(0) > Q[r(t_C)] K_{IGN}$

(Strong signal is K_{IGN}-times larger than the total signal in the trip with clutter; therefore, clutter can be ignored)

$t_C = -1$

End

End

End

ElseIf $n_C = 2$

(Overlaid clutter in two trips)

$CwS = $ FALSE　　*(clutter with strong signal)*

$CwW = $ FALSE　　*(clutter with weak signal)*

$CwU = $ FALSE　　*(clutter with unrecoverable signals)*

For $0 \leq l < n_C$

If $clutterTrips(l) = t_A$

(The trip with the strong signal contains clutter)

$CwS = $ TRUE

ElseIf $clutterTrips(l) = t_B$

(The trip with the weak signal contains clutter)

$CwW = $ TRUE

Else

(One of the trips with unrecoverable signals contains clutter)

$CwU = $ TRUE

$t_{CU} = clutterTrips(l)$

End

End

If CwS and CwW

(Clutter is with the strong and weak trips, weak signal cannot be recovered)

$t_B = -1$

If $P(0) > Q(1) K_{IGN}$

(Trip with weak signal can be ignored)

$t_C = t_A$

Else

(None of the trips can be recovered, ignore clutter)

$t_A = -1$

$t_C = -1$

End

ElseIf CwS and CwU

(Clutter is with the strong and one of the unrecoverable trips)
If $P(0) > Q[r(t_{CU})]\ K_{IGN}$
    (Trip with unrecoverable signal can be ignored)
    $t_C = t_A$
Else
    (None of the trips can be recovered, ignore clutter)
    $t_A = -1$
    $t_B = -1$
    $t_C = -1$
End
ElseIf *CwW* and *CwU*
  (Clutter is with the strong and one of the unrecoverable trips)
  If $P(0) > \{Q(1) + Q[r(t_{CU})]\}\ K_{IGN}$
    (All trips with clutter can be ignored and weak signal cannot be recovered)
    $t_B = -1$
    $t_C = -1$
  ElseIf $P(0) > Q[r(t_{CU})]\ K_{IGN}$
    (Trip with unrecoverable signal can be ignored)
    $t_C = t_B$
  ElseIf $P(0) > Q(1)\ K_{IGN}$
    (Trip with weak signal can be ignored and weak signal cannot be recovered)
    $t_B = -1$
    $t_C = t_{CU}$
  Else
    (None of the trips can be recovered, ignore clutter)
    $t_A = -1$
    $t_B = -1$
    $t_C = -1$
  End
ElseIf *CwU*
  (Clutter is with both of the unrecoverable trips)
  If $P(0) > [Q(2) + Q(3)]\ K_{IGN}$
    (All trips with clutter can be ignored)
    $t_C = -1$
  ElseIf $P(0) > Q(2)\ K_{IGN}$
    (One of the trips with unrecoverable signals can be ignored)
    $t_C = t(3)$
  ElseIf $P(0) > Q(3)\ K_{IGN}$
    (One of the trips with unrecoverable signals can be ignored)
    $t_C = t(2)$
  Else
    (None of the trips can be recovered, ignore clutter)
    $t_A = -1$
    $t_B = -1$
    $t_C = -1$
  End

End
ElseIf $n_C = 3$
    (Overlaid clutter in three trips)
    $CwS = \text{FALSE}$
    $CwW = \text{FALSE}$
    $CwU = \text{FALSE}$
    For $0 \leq l < n_C$
        If $clutterTrips(l) = t_A$
            (The trip with the strong signal contains clutter)
            $CwS = \text{TRUE}$
        ElseIf $clutterTrips(l) = t_B$
            (The trip with the weak signal contains clutter)
            $CwW = \text{TRUE}$
        Else
            (One of the trips with unrecoverable signals contains clutter)
            $CwU = \text{TRUE}$
            $t_{CU} = clutterTrips(l)$
        End
    End
    If CwS and CwW and CwU
        (Weak trip is unrecoverable)
        $t_B = -1$
        If $P(0) > \{Q(1) + Q[r(t_{CU})]\}\ K_{IGN}$
            (Trips with weak and unrecoverable signals can be ignored)
            $t_C = t_A$
        Else
            (None of the trips can be recovered, ignore clutter)
            $t_A = -1$
            $t_C = -1$
        End
    ElseIf CwS and CwU
        If $P(0) > [Q(2) + Q(3)]\ K_{IGN}$
            (Trips with unrecoverable signals can be ignored)
            $t_C = t_A$
        Else
            (None of the trips can be recovered, ignore clutter)
            $t_A = -1$
            $t_B = -1$
            $t_C = -1$
        End
    Else
        If $P(0) > [Q(1) + Q(2) + Q(3)]\ K_{IGN}$
            (All trips with clutter can be ignored and weak trip is unrecoverable)
            $t_B = -1$
            $t_C = -1$

ElseIf $P(0) > [Q(1) + Q(2)]\,K_{IGN}$
  (Trips with weak and one unrecoverable signal can be ignored and weak trip is unrecoverable)
  $t_B = -1$
  $t_C = t(3)$
ElseIf $P(0) > [Q(1) + Q(3)]\,K_{IGN}$
  (Trips with weak and one unrecoverable signal can be ignored and weak trip is unrecoverable)
  $t_B = -1$
  $t_C = t(2)$
ElseIf $P(0) < [Q(2) + Q(3)]\,K_{IGN}$
  (Both trips with unrecoverable signals can be ignored)
  $t_C = t_B$
Else
  (None of the trips can be recovered, ignore clutter)
  $t_A = -1$
  $t_B = -1$
  $t_C = -1$
End
    End
Else ($n_C = 4$)
  (Overlaid clutter in four trips)
  (Weak trip is unrecoverable)
  $t_B = -1$
  If $P(0) > [Q(1) + Q(2) + Q(3)]\,K_{IGN}$
    (Trips with weak and both unrecoverable signals can be ignored)
    $t_C = t_A$
  Else
    (None of the trips can be recovered, ignore clutter)
    $t_A = -1$
    $t_C = -1$
  End
End

Note: If $t_A = -1$, none of the trips are recoverable.

4) Apply data windowing (Input: *V, winType*. Output: V_W)

$h = \text{WINDOW}(winType)$
$V_W(m) = V(m)h(m)$, for $0 \le m < M$,

where *h* is either the rectangular, von Hann, or Blackman window function.

5) Cohere to ground clutter trip (Inputs: V_W, t_C, ψ. Output: V_{CW})

Time series data are cohered to trip t_C to filter ground clutter:

$$V_{CW}(m) = V_W(m)\exp[-j\phi_{t_C,0}(m)], \text{ for } 0 \leq m < M,$$

where ϕ_{k_1,k_2} is the modulation code for the k_1-th trip with respect to the k_2-th trip, obtained from the measured switching code ψ. In general,

$$\phi_{k_1,k_2}(m) = \psi(m-k_1) - \psi(m-k_2), \text{ for } 0 \leq m < M.$$

6) Filter ground clutter (Inputs: V_{CW}. Outputs: V_{CF}, k_{GMAP})

Time series data V_{CW} are filtered using the GMAP ground clutter filter to get V_{CF} as follows:

i) Discrete Fourier Transform

$$F_{CW}(k) = \frac{1}{M}\sum_{m=0}^{M-1} V_{CW}(m)e^{-j\frac{2\pi mk}{M}}, \text{ for } 0 \leq k < M.$$

ii) Power spectrum

$$S_{CW}(k) = |F_{CW}(k)|^2, \text{ for } 0 \leq k < M.$$

iii) Ground Clutter Filtering

$$S_{CF} = \text{GMAP}(S_{CW})$$

Note: The receiver noise power is not provided to GMAP. In addition to the filtered power spectrum, GMAP returns the amount of clutter power removed (*clutter$_{GMAP}$*). Moreover, GMAP should be modified to return the number of spectral coefficients with clutter (k_{GMAP}). Note that k_{GMAP} is `iGapPoints` in SIGMET's `fSpecFilterGMAP()` function.

iv) Phase reconstruction

Use the original phases except in those spectral components notched and reconstructed by GMAP:

$$\varphi_{CF}(k) = \begin{cases} 0, & k_{GMAP} > 0 \text{ and} \\ & \left[k \le (k_{GMAP}-1)/2 \text{ or } k \ge M - (k_{GMAP}-1)/2\right], \text{ for } 0 \le k < M, \\ Arg[F_{CW}(k)], & \text{otherwise} \end{cases}$$

where $Arg(.)$ indicates the complex argument or phase.

v) Inverse Discrete Fourier Transform

$$V_{CF}(m) = \sum_{k=0}^{M-1} \sqrt{S_{CF}(k)} e^{j\varphi_{CF}(k)} e^{j\frac{2\pi mk}{M}}, \text{ for } 0 \le m < M.$$

7) Cohere to trips A and B (Inputs: V_W, V_{CF}, t_A, t_B, t_C, ψ. Outputs: V_A, V_B)

The original (cohered to the 1st trip: $t = 0$) or ground-clutter-filtered (cohered to trip t_C) signal is now cohered (if necessary) to trips t_A and t_B using the proper modulation codes.

(Get trip to cohere from)
If $t_C \ne -1$
    $t_X = 0$
Else
    $t_X = t_C$
End
If $t_A \ne -1$
    (Strongest trip is recoverable; therefore, cohere to trip A if needed)
    If $t_A \ne t_X$
        (Cohere to trip A)
        $V_A(m) = V_W(m)\exp[-j\phi_{t_A,t_X}(m)]$, for $0 \le m < M$
    Else
        (Cohering is not needed)
        $V_A(m) = V_{CF}(m)$, for $0 \le m < M$
    End
Else
    (Signal was unrecoverable)
    $V_A(m) = 0$, for $0 \le m < M$
End

If $t_B \ne -1$
    (Strongest trip is recoverable; therefore, cohere to trip B if needed)
    If $t_B \ne t_X$
        (Cohere to trip B)
        $V_B(m) = V_W(m)\exp[-j\phi_{t_B,t_X}(m)]$, for $0 \le m < M$
    Else

(Cohering is not needed)
$V_B(m) = V_{CF}(m)$, for $0 \le m < M$
    End
Else
    (Signal was unrecoverable)
    $V_B(m) = 0$, for $0 \le m < M$
End

In the previous algorithm, ϕ_{k_1,k_2} is the modulation code for the k_1-th trip with respect to the k_2-th trip, obtained from the switching code ψ as in step 5.

8) Compute total power (Inputs: V_A, *winType*. Output: $\tilde{P}_T$)

$$K = nf_0(winType)$$
$$\tilde{P}_T = K \sum_{m=0}^{M-1} |V_A(m)|^2 .$$

Note: ideally, this is the short-PRT total power in all trips with the clutter power in trip t_C removed; i.e., $\tilde{P}_T \approx P(0) + P(1) + P(2) + P(3) + NOISE$ (this assumes no overlaid clutter).

9) Compute lag-one autocorrelations for trips A and B (Inputs: V_A, V_B, t_A, t_B, *winType*. Outputs: R_A, R_B)

$$K = nf_1(winType)$$
If $t_A \ne -1$
    (Strongest trip is recoverable; therefore, compute lag-one autocorrelation)
$$R_A = K \sum_{m=0}^{M-2} V_A^*(m) V_A(m+1)$$
Else
    (Strongest trip is not recoverable)
    $R_A = 0$
End
If $t_B \ne -1$
    (Second strongest trip is recoverable; therefore, compute lag-one autocorrelation)
$$R_B = K \sum_{m=0}^{M-2} V_B^*(m) V_B(m+1)$$
Else
    (Second strongest trip is not recoverable)
    $R_B = 0$
End

10) Determine strong and weak trips (Inputs: V_A, V_B, R_A, R_B, t_A, t_B. Outputs: V_S, R_S, t_S, t_W)

The final strong/weak trip determination is done using the magnitude of the lag-one autocorrelation estimates (equivalent to using the spectrum widths) from the actual phase-coded data.

If $|R_A| \geq |R_B|$
    (Trip A is strong, trip B is weak)
    $t_S = t_A$
    $t_W = t_B$
    $R_S = R_A$
    $V_S(m) = V_A(m)$, for $0 \leq m < M$
Else
    (Trip B is strong, trip A is weak)
    $t_S = t_B$
    $t_W = t_A$
    $R_S = R_B$
    $V_S(m) = V_B(m)$, for $0 \leq m < M$
End

11) Compute strong-trip velocity (Input: R_S. Output: v_S)

$$v_S = -\frac{v_a}{\pi} Arg(R_S),$$

where v_a is the maximum unambiguous velocity corresponding to the short PRT ($v_a = \lambda/4T_s$, and λ is the radar wavelength).

12) Compute the strong-trip lag-two autocorrelation (Input: V_S, *winType*. Output: R_{S2})

$$K = nf_2(winType)$$
$$R_{S2} = K \sum_{m=0}^{M-3} V_S^*(m) V_S(m+2).$$

13) Compute discrete Fourier transform (DFT) (Input: V_S. Output: F_S)

$$F_S(k) = \frac{1}{M} \sum_{m=0}^{M-1} V_S(m) e^{-j\frac{2\pi mk}{M}}, \text{ for } 0 \leq k < M.$$

14) Apply processing notch filter (Inputs: F_S, v_S, t_S, t_W, t_C, k_{GMAP}. Outputs: F_{SN}, NW)

The PNF is an ideal bandstop filter in the frequency domain; i.e., it zeroes out the spectral components within the filter's cutoff frequencies (stopband) and retains those components outside the stopband (passband). With the PNF center (v_S) in m s^{-1} units, the first step consists of mapping the center velocity into a spectral coefficient number. Next, the stopband is defined by moving half the notch width above and below the central spectral coefficient (these are wrapped around to the fundamental Nyquist interval) and adjusting the position to always include those coefficients that originally had ground clutter. However, the notch width depends on the strong- and weak-trip numbers. For strong and weak trips that are one or three trips away from each other, the modulation code is the one derived from the SZ(8/64) switching code. On the other hand, for strong and weak trips that are two trips away from each other, the modulation code is the one derived from the SZ(16/64) switching code. While the processing with a SZ(8/64) code requires a notch width of 3/4 of the Nyquist interval, the SZ(16/64) is limited to a notch width of one half of the Nyquist interval.

   i)   Central spectral coefficient computation:

$$k_o = \begin{cases} -v_S \frac{M}{2v_a}, & \text{if } v_S \leq 0 \\ M - v_S \frac{M}{2v_a}, & \text{if } v_S > 0 \end{cases}$$

k_o should be rounded to the nearest integer.

   ii) Notch width determination:

$$NW = \begin{cases} M/2, & \text{if } |t_S - t_W| \neq 1 \text{ and } t_W \neq -1 \\ 3M/4, & \text{otherwise} \end{cases}$$

   iii) PNF center adjustment (perform only if clutter was with the strong signal)

If $t_C = t_S$ and $k_{GMAP} > 0$
     $k_{ADJ} = (k_{GMAP} - 1)/2 + k_{GMAP\_EXTRA}$
     if $\left\lfloor \frac{NW-1}{2} \right\rfloor - k_{ADJ} < k_o < \frac{M}{2}$
         $k_o = \left\lfloor \frac{NW-1}{2} \right\rfloor - k_{ADJ}$
     ElseIf $\frac{M}{2} \leq k_o < M - \left\lceil \frac{NW-1}{2} \right\rceil + k_{ADJ}$
         $k_o = M - \left\lceil \frac{NW-1}{2} \right\rceil + k_{ADJ}$
     End
End

Note: The computation of k_{ADJ} includes an empirical constant k_{GMAP_EXTRA}. Simulations suggest that k_{GMAP_EXTRA} should be set to 1 to obtain better results.

iv) Cutoff frequency computation:

$$k_a = \begin{cases} k_o - \lfloor \frac{NW-1}{2} \rfloor, & \text{if } k_o - \lfloor \frac{NW-1}{2} \rfloor \geq 0 \\ k_o - \lfloor \frac{NW-1}{2} \rfloor + M, & \text{if } k_o - \lfloor \frac{NW-1}{2} \rfloor < 0 \end{cases},$$

$$k_b = \begin{cases} k_o + \lceil \frac{NW-1}{2} \rceil, & \text{if } k_o + \lceil \frac{NW-1}{2} \rceil < M \\ k_o + \lceil \frac{NW-1}{2} \rceil - M, & \text{if } k_o + \lceil \frac{NW-1}{2} \rceil \geq M \end{cases}.$$

v) Notch filtering:

$$F_{SN}(k) = \begin{cases} \dfrac{F_S(k)}{\sqrt{1 - \frac{NW}{M}}}, & \begin{array}{l} \text{if } k_b < k < k_a \text{ for } k_b < k_a \text{ or} \\ \text{if } 0 \leq k < k_a \text{ or } k_b < k < M \text{ for } k_a < k_b \end{array}, \text{ for } 0 \leq k < M. \\ 0, & \text{otherwise} \end{cases}$$

Note: The factor $\sqrt{1 - \frac{NW}{M}}$ normalizes the filtered signal in order to preserve its power.

In the previous equations $\lfloor x \rfloor$ is the nearest integer to x that is smaller than x, and $\lceil x \rceil$ is the nearest integer to x that is larger than x; k_o, k_a, and k_b are zero-based indexes.

15) Compute inverse discrete Fourier transform (IDFT) (Input: F_{SN}. Output: V_{SN})

$$V_{SN}(m) = \sum_{k=0}^{M-1} F_{SN}(k) e^{j\frac{2\pi mk}{M}}, \text{ for } 0 \leq m < M.$$

16) Compute weak-trip power (Input: V_{SN}, $winType$. Output: $\tilde{P}_W$)

$$K = nf_0(winType)$$
$$\tilde{P}_W = K \sum_{m=0}^{M-1} |V_{SN}(m)|^2.$$

Note: ideally, this would be the short-PRT total power in all trips except the strong trip; i.e., $\tilde{P}_W \approx P[r(t_W)] + P(2) + P(3) + NOISE$ (this assumes no overlaid clutter and that the PNF completely removed the strong trip).

17) Cohere to weak trip (Inputs: V_{SN}, t_S, t_W, ψ. Output: V_W)

$$V_W(m) = V_{SN}(m) \exp\left[-j\phi_{t_W, t_S}(m)\right], \text{ for } 0 \leq m < M,$$

where ϕ_{k_1,k_2} is the modulation code for the k_1-th trip with respect to the k_2-th trip, obtained from the switching code ψ as in step 5.

18) Compute weak-trip lag-one autocorrelation (Input: V_W, *winType*. Output: R_W)

$$K = nf_1(winType)$$

$$R_W = K \sum_{m=0}^{M-2} V_W^*(m)V_W(m+1).$$

19) Retrieve weak-trip spectrum width (Input: w_L, t_W. Output: w_W, *wAlgo*)

(Flag spectrum width computation method for final step)
$wAlgo(n + t_W N) = $ LONG_PRT_ESTIMATOR
(Retrieve long-PRT spectrum width estimate)
$w_W = w_L(n + t_W N)$.

20) Adjust powers (Inputs: P, $\tilde{P}_T$, $\tilde{P}_W$, t_W. Outputs: P_S, P_W)

    i) Strong-trip power adjustment:

If $t_W \neq -1$
    (Subtract short-PRT out-of-trip powers and noise power from total power)
    $P_S = \tilde{P}_T - \tilde{P}_W$
Else
    (Subtract long-PRT out-of-trip powers and noise power from total power)
    $P_S = \tilde{P}_T - [P(1) + P(2) + P(3) + NOISE]$
End
If $P_S < 0$
    (Clip negative powers to zero)
    $P_S = 0$
End

    ii) Weak-trip power adjustment:

If $t_W \neq -1$
    (Weak trip is recoverable; therefore, subtract long-PRT out-of-trip powers and noise power from weak power)
    $P_W = \tilde{P}_W - [P(2) + P(3) + NOISE]$
    If $P_W < 0$

(Clip negative powers to zero)
$P_W = 0$
    End
  Else
    $P_W = 0$
End

In the previous equations *NOISE* is the receiver noise power.
Note: while P_S is used both for censoring and in the computation of the strong-trip spectrum width, P_W is used solely for censoring purposes.

21) Compute strong-trip spectrum width using the R_0/R_1 estimator (Inputs: P_S, R_S. Output: w_S, *wAlgo*)

(Flag spectrum width computation method for final step)
$wAlgo(n + t_S N) = \texttt{R0\_R1\_ESTIMATOR}$

(Compute spectrum width)
If $|R_S| = 0$

  (Lag-one correlation is zero; therefore, signal is like white noise having the maximum possible spectrum width)
  $w_S = v_a / \sqrt{3}$

ElseIf $P_S < |R_S|$

  (Lag-one correlation is larger than the power; therefore, signal is very coherent having the minimum possible spectrum width)
  $w_S = 0 \ (\mathrm{m\ s}^{-1})$

Else

  (Spectrum width computation)
$$w_S = \frac{v_a}{\pi}\left[2\ln\left(\frac{P_S}{|R_S|}\right)\right]^{1/2}$$

End
If $w_S > v_a / \sqrt{3}$

  (Clip large values of spectrum width)
  $w_S = v_a / \sqrt{3}$

End

Here v_a is the maximum unambiguous velocity corresponding to the short PRT ($v_a = \lambda/4T_s$ and λ is the radar wavelength).

22) Compute strong-trip spectrum width using the R_1/R_2 estimator (Inputs: R_S, R_{S2}. Output: w_S, wAlgo)

(Flag spectrum width computation method for final step)
$wAlgo(n + t_SN) = \texttt{R1\_R2\_ESTIMATOR}$

(Compute spectrum width)
If $|R_{S2}| = 0$

    (Lag-two correlation is zero; therefore, signal is like white noise having the maximum possible spectrum width)
    $w_S = v_a / \sqrt{3}$

ElseIf $|R_S| < |R_{S2}|$

    (Lag-two autocorrelation is larger than lag-one autocorrelation; therefore, signal is very coherent having the minimum possible spectrum width)
    $w_S = 0$ (m s^{-1})

Else

    (Spectrum width computation)

$$w_S = \frac{v_a}{\pi}\left[\frac{2}{3}\ln\left(\frac{|R_S|}{|R_{S2}|}\right)\right]^{1/2}$$

End
If $w_S > v_a / \sqrt{3}$

    (Clip large values of spectrum width)
    $w_S = v_a / \sqrt{3}$

End

Here v_a is the maximum unambiguous velocity corresponding to the short PRT ($v_a = \lambda/4T_s$ and λ is the radar wavelength).

23) Compute SNR threshold adjustment factors (Inputs: C_L, $clutter_{GMAP}$, Outputs: $AdjK_{SNR}Short$, $AdjK_{SNR}Long$)

This is also referred to as dB-for-dB or log-for-log censoring.

Apply the following algorithm twice with the following sets of parameters:
    1) $C = C_L(n + t_CN)$ and $AdjK_{SNR}Long = AdjK_{SNR}$,
    2) $C = clutter_{GMAP}$ and $AdjK_{SNR}Short = AdjK_{SNR}$.

(Compute CNR)
If $C > 0$

    $CNRdB = 10\log_{10}(C/NOISE)$

Else

$CNRdB = 0$

End

(Compute SNR threshold adjustment in dB depending on CNR region)
If $CNRdB \leq K_{x0}$

    $deltaTh = 0$

ElseIf $CNRdB \leq K_{x1}$

    $deltaTh = K_{s0}(CNRdB - K_{x0})$

Else

    $deltaTh = K_{s0}(K_{x1} - K_{x0}) + K_{s1}(CNRdB - K_{x1})$

End

(Compute SNR threshold adjustment factor)
$AdjK_{SNR} = 10^{deltaTh/10}$

24) Determine censoring and moments (Inputs: P, Q, t, r, P_S, P_W, R_S, R_W, R_{S2}, w_S, w_W, t_S, t_W, t_C, t_{Ao}, t_{Bo}, $AdjK_{SNR}Short$, $AdjK_{SNR}Long$, $clutter_{GMAP}$. Outputs: T_0, R_0, R_1, R_2, $type_v$, $type_w$)

(Adjust powers based on clutter filtering)
For $0 \leq l < 4$

    If $t_C = t(l)$

        $PQ(l) = P(l)$

    Else

        $PQ(l) = Q(l)$

    End

End

(Go through 4 trips)
For $0 \leq l < 4$

    (Initially tag for no censoring)
    $CENSOR = $ `NO_CENSORING`

    (Check for significant long-PRT power)
    If $CENSOR = $ `NO_CENSORING` and $P[r(l)] < NOISE.K_{SNR,V}$

        $CENSOR = $ `SNR_LONG_PRT`

    End

    (Strong-trip censoring)
    If $t_S = l$

        (Short-PRT SNR censoring)
        If $CENSOR = $ `NO_CENSORING` and $P_S < NOISE.K_{SNR,V}$

            $CENSOR = $ `SNR_SHORT_PRT_STRONG_TRIP`

        End

        (Short-PRT CNR censoring)
        If $CENSOR = $ `NO_CENSORING` and $P_S < NOISE.K_{SNR,V}.AdjK_{SNR}Short$

            If $t_W = -1$

$CENSOR = $ CNR_SHORT_PRT_STRONG_TRIP_NON_OVLD
   Else
      If $P[r(t_W)] < NOISE.K_{SNR,Z}.AdjK_{SNR}Long$
         $CENSOR = $ CNR_SHORT_PRT_STRONG_TRIP_NON_OVLD
      Else
         $CENSOR = $ CNR_SHORT_PRT_STRONG_TRIP_OVLD
      End
   End
End

(Long-PRT CSR censoring)
If $CENSOR = $ NO_CENSORING and $t_C \neq -1$ and $\{Q[r(t_C)] - P[r(t_C)]\} > P[r(t_S)]\, K_{CSR1}$
   If $t_W = -1$
      $CENSOR = $ CSR_LONG_PRT_STRONG_TRIP_NON_OVLD
   Else
      If or $P[r(t_W)] < NOISE.K_{SNR,Z}.AdjK_{SNR}Long$
         $CENSOR = $ CSR_LONG_PRT_STRONG_TRIP_NON_OVLD
      Else
         $CENSOR = $ CSR_LONG_PRT_STRONG_TRIP_OVLD
      End
   End
End

(SNR* censoring)
If $t_W \neq -1$
   (Weak trip was recovered)
   If $CENSOR = $ NO_CENSORING and
   $PQ[r(t_S)] < \{PQ[r(t_W)] + PQ(2) + PQ(3) + NOISE\}K_s$
      $CENSOR = $ SNRS_LONG_PRT_STRONG_TRIP
   End
Else
   If $CENSOR = $ NO_CENSORING and
   $PQ[r(t_S)] < [PQ(1) + PQ(2) + PQ(3) + NOISE]K_s$
      $CENSOR = $ SNRS_LONG_PRT_STRONG_TRIP
   End
End

(Weak trip censoring)
ElseIf $t_W = l$
   (Short-PRT SNR censoring)
   If $CENSOR = $ NO_CENSORING and $P_W < NOISE.K_{SNR,V}$
      $CENSOR = $ SNR_SHORT_PRT_WEAK_TRIP
   End

(Short-PRT CNR censoring)
If $CENSOR = $ `NO_CENSORING` and $P_W < NOISE.K_{SNR,V}.AdjK_{SNR}$
   $CENSOR = $ `CNR_SHORT_PRT_WEAK_TRIP`
End

(Long-PRT CSR censoring)
If $CENSOR = $ `NO_CENSORING` and $t_C \neq -1$ and $Q[r(t_C)] - P[r(t_C)]\} > P[r(t_W)] K_{CSR2}$
   $CENSOR = $ `CSR_LONG_PRT_WEAK_TRIP`
End

(SNR* censoring)
If $CENSOR = $ `NO_CENSORING` and $PQ[r(t_W)] < [PQ(2) + PQ(3) + NOISE]K_w$
   $CENSOR = $ `SNRS_LONG_PRT_WEAK_TRIP`
End

(Power-ratio recovery-region censoring)
If $CENSOR = $ `NO_CENSORING` and $P[r(t_S)] > P[r(t_W)] K_r(w_S/2v_a, w_W/2v_{a,L}, |t_S - t_W|)$
   $CENSOR = $ `RECOV_REGION`
End

(Clutter-not-with-strong-trip censoring)
If $CENSOR = $ `NO_CENSORING` and $t_C \neq -1$ and $t_C \neq t_S$
   $CENSOR = $ `CLUTTER_LOCATION`
End

(Long-PRT saturated spectrum width censoring)
If $CENSOR = $ `NO_CENSORING` and $w_W/2v_{a,L} > w_{n,max}$
   $CENSOR = $ `SATURATED_WIDTH`
End

(Unrecoverable censoring)
Else
   If $CENSOR = $ `NO_CENSORING`
      (Check for censoring due to clutter location in step 3)
      If $t_{Ao} = l$ or $t_{Bo} = l$
         $CENSOR = $ `CLUTTER_LOCATION`
      Else
         $CENSOR = $ `UNRECOVERABLE`
      End
   End
End

(Handle censoring)
Switch *CENSOR*
   Case   `NO_CENSORING`

(Do not censor data)

$type_v(n + lN) = $ SIGNAL_LIKE

$type_w(n + lN) = $ SIGNAL_LIKE

If $t_S = l$

   $R_0(n + lN) = P_S$

   $R_1(n + lN) = R_S$

   $R_2(n + lN) = R_{S2}$

Else

   $R_0(n + lN) = P_W$

   $R_1(n + lN) = R_W$

   $R_2(n + lN) = 0$

End

$T_0(n + lN) = R_0(n + lN) + clutter_{GMAP}$

Case   SNR_LONG_PRT,

      SNR_SHORT_PRT_STRONG_TRIP,

      SNR_SHORT_PRT_WEAK_TRIP,

      CSR_LONG_PRT_STRONG_TRIP_NON_OVLD,

      CNR_SHORT_PRT_STRONG_TRIP_NON_OVLD

(Censor as noise-like data)

$type_v(n + lN) = $ NOISE_LIKE

$type_w(n + lN) = $ NOISE_LIKE

$R_0(n + lN) = P[r(l)]$

$R_1(n + lN) = 0$

$R_2(n + lN) = 0$

$T_0(n + lN) = Q[r(l)]$

Case   SNRS_LONG_PRT_STRONG_TRIP,

      SNRS_LONG_PRT_WEAK_TRIP,

      CNR_SHORT_PRT_WEAK_TRIP,

      CSR_LONG_PRT_WEAK_TRIP,

      CSR_LONG_PRT_STRONG_TRIP_OVLD,

      CNR_SHORT_PRT_STRONG_TRIP_OVLD,

      RECOV_REGION,

      CLUTTER_LOCATION,

      UNRECOVERABLE

(Censor as overlaid-like data)

$type_v(n + lN) = $ OVERLAID_LIKE

$type_w(n + lN) = $ OVERLAID_LIKE

$R_0(n + lN) = P[r(l)]$

$R_1(n + lN) = 0$

$R_2(n + lN) = 0$

$T_0(n + lN) = Q[r(l)]$

Case   SATURATED_WIDTH

(Censor weak-trip spectrum width only)

$type_v(n + lN) = $ SIGNAL_LIKE

$type_w(n + lN) = $ OVERLAID_LIKE

$R_0(n + lN) = P_W$

$$R_1(n + lN) = R_W$$
$$R_2(n + lN) = 0$$
$$T_0(n + lN) = R_0(n + lN) + clutter_{GMAP}$$

    End

End

In the previous algorithm, $K_{SNR,Z}$ and $K_{SNR,V}$ are the SNR thresholds to determine significant returns for reflectivity and velocity, respectively. These should be obtained from the VCP definition as in the legacy WSR-88D. K_s and K_w are the minimum SNRs needed for recovery of the strong and weak trips, respectively. Here, the noise consists of the whitened out-of-trip powers plus the system noise. K_r is the maximum P_S/P_W ratio for recovery of the weaker trip. K_r is a function of the trip number difference t_{diff}, the normalized strong and weak trip spectrum widths $w_{Sn} = w_S/2v_a$ and $w_{Wn} = w_W/2v_{a,L}$, and is defined as

$$K_r(w_{Sn}, w_{Wn}, t_{diff}) = \begin{cases} 10^{C_T(w_{Wn}, t_{diff})/10}, & w_{Sn} < C_I(w_{Wn}, t_{diff}) \\ 10^{\left\{C_S(w_{Wn}, t_{diff})\left[w_{Sn} - C_I(w_{Wn}, t_{diff})\right] + C_T(w_{Wn}, t_{diff})\right\}/10}, & w_{Sn} \geq C_I(w_{Wn}, t_{diff}) \end{cases}$$

where C_T is the threshold, C_S is the slope and C_I is the intercept all of which depend on t_d and w_{Wn} as listed in the table of recommended censoring thresholds. v_a and $v_{a,L}$ are the maximum unambiguous velocities corresponding to the short and long PRT, respectively. K_{CSR1} and K_{CSR2} are the clutter-to-signal ratio (CSR) thresholds for determination of recovery of the strong and weak trip, respectively ($K_{CSR2} \leq K_{CSR1}$). K_2 is the power ratio threshold for the determination of significant clutter in the overlaid case. Lastly, $w_{n,max}$ is the maximum valid normalized spectrum width estimated from the long-PRT data.

25) Filter strong point clutter (Inputs: T_0, R_0, R_1, R_2. Outputs: T_0, R_0, R_1, R_2)

The algorithm is the same as in the legacy RDA (this is also implemented in the ORDA).

26) Determine outputs (Inputs: R_0, R_1, R_2, $wAlgo$. Outputs: v, w)

    i) Compute Doppler velocity

    For $0 \leq n < 4N$

$$v(n) = -\frac{v_a}{\pi} Arg\left[R_1(n)\right]$$

    End

where v_a is the maximum unambiguous velocity corresponding to the short PRT ($v_a = \lambda/4T_s$, where λ is the radar wavelength).

    ii) Compute spectrum width

For $0 \le n < 4N$

    Switch $wAlgo(n)$

        Case 0

            (Spectrum width was not computed for this gate. This assumes that wAlgo is set to zero for all gates at the beginning of each radial)

            $w(n) = 0$

        Case `LONG_PRT_ESTIMATOR`

            $w(n) = w_L(n)$

        Case `R0_R1_ESTIMATOR`

            If $|R_1(n)| = 0$

$$w(n) = v_a / \sqrt{3}$$

            ElseIf $R_0(n) < |R_1(n)|$

                $w(n) = 0$

            Else

$$w(n) = \frac{v_a}{\pi} \left[2 \ln \left(\frac{R_0(n)}{|R_1(n)|} \right) \right]^{1/2}$$

            End

        Case `R1_R2_ESTIMATOR`

            If $|R_2(n)| = 0$

$$w(n) = v_a / \sqrt{3}$$

            ElseIf $|R_1(n)| < |R_2(n)|$

                $w(n) = 0$

            Else

$$w(n) = \frac{v_a}{\pi} \left[\frac{2}{3} \ln \left(\frac{|R_1(n)|}{|R_2(n)|} \right) \right]^{1/2}$$

            End

    End

    If $w(n) > v_a / \sqrt{3}$

        $w(n) = v_a / \sqrt{3}$

    End

End

Appendix C. Periodic Phase Codes for Mitigating Ambiguities in Range and Velocity

1. Introduction

Inherent limitation in pulsed Doppler weather radars operating at centimeter wavelengths is the coupled ambiguity in velocity and range. No perfect solution to this problem has been found and it is unlikely that one exists. Furthermore, although several mitigation strategies have been proposed, the optimum one has yet to be determined. This is because the strategies depend on the type and extent of the observed weather phenomena. Moreover, demands on the techniques increase to a point of breakdown in precisely the situation when they are needed the most. This is in widespread outbreaks of severe weather with storm covering huge areas and producing echoes of excessive dynamic range. Two somewhat complimentary approaches have become part in some mitigation strategies and have been (or will be) implemented on operational Doppler radars (Cho 2005). One is a variation of the pulsed sequence, such as in staggered pulse repetition time (PRT) technique, to separate returns in time. The other is separation of overlaid echoes in the frequency domain (Doviak and Zrnić 2006) exemplified by phase coding techniques. When combined to cover a volume, these kinds of techniques constitute the mitigation strategy. Herein, we study issues pertaining to systematic phase codes and properties thereof.

Random phase of transmitted pulses, inherently present in magnetrons, benefited early users of Doppler radars by providing a degree of protection against ambiguous returns

(i.e., second or higher trip echoes). These appear as white noise in the spectrum of the cohered first trip signal. An improved protection (Zrnić 1989) for two overlaid signals involves cohering one, filtering it, and then reconstructing the second one from the residue, or vice versa. This random phase scheme has been analyzed, and advanced by Laird (1981) and Siggia (1983). Furthermore, it has been implemented on commercial Doppler weather radars.

Two issues affect the recovery of the weaker signal in the random phase scheme. These are: 1) contamination of the weak signal by the residue of the strong filtered signal, and 2) loss of the weak signal part that shares the same Doppler band with the strong signal (see Zrnić and Mahapatra 1985 for quantitative analysis) and results in "self noise".

To overcome the self noise, Sachidananda and Zrnić (1999) proposed systematic phase codes. Further, they studied sequence lengths of 64 (and other powers of two) and codes that fit well these lengths. Although the general information for constructing these codes is contained in that paper and reports (Sachidananda et al. 1997, 1998), specifics dealing with periodicities and choices of sequence length are not explicitly addressed. Neither are discussed the peculiarities concerning protection and reconstruction of higher than second trip echoes. Herein, we review issues concerning these codes and justify reasons for further exploration of their properties.

2.   The SZ systematic phase code

In the phase coding technique, the transmitted pulses are phase shifted in a systematic code sequence given by $a_k = exp(j\psi_k)$, and the received echo samples are multiplied by a_k^* (* represents complex conjugate) to restore the phases. Consequently, the 1st trip

signal is made coherent and the 2nd trip signal is phase modulated by the code $c_k = a_{k-1} a_k^*$. The signals from the third and higher-order trips are modulated by codes $(a_{k-2}a_k^*)$, $(a_{k-3}a_k^*)$, etc., respectively. The 2nd trip signal can be made coherent by multiplying the incoming sequence with a_{k-1}^*, in which case the 1st trip signal is modulated by the code c_k^*. In general, any one of the overlaid trip signals can be cohered leaving the rest modulated by different codes. By a proper choice of the code, it is possible to spread the spectra of the overlaid signals in a desirable number of replicas.

Sachidananda and Zrnić (1999) designed the code, a_k, so that upon decoding the first trip signal, the phase of the second trip signal φ_k satisfies

$$\varphi_k = \psi_{k-1} - \psi_k = n\pi k^2/M; \; k=0,1,2,... \; M-1, \tag{1}$$

where the integers n and M are selected appropriately. M is equal to the number of samples which ensures that the code cycles through one or more full cycles in the sample sequence. Depending on the choice of n, the periodicity of the code is M or sub-multiples of M. This composite code is derived from a code which has zero autocorrelation for all lags except zero and multiples of M (Chu 1972). This property is obtained by selecting n prime to M. Selection of n such that M is divisible by n, gives the code a periodicity of M/n; its autocorrelation is unity for lags in multiples of M/n, and is zero for all other lags.

Sachidananda and Zrnić (1999) proposed $M = 64$ and $n = 8$ for estimating the spectral parameters of the overlaid 1st and the 2nd trip signals. The modulation code (of the second trip signal) corresponding to this choice is $c_k = exp(j\varphi_k) = exp(j\pi k^2/8)$; its spectrum has 8 non-zero coefficients spaced $M/8$ apart. Thus, the modulated signal has 8 spectral peaks

uniformly spread across the Nyquist interval because it is the convolution of the signal and the code spectra.

There are few issues not explicitly addressed by Sachidananda and Zrnić (1999) which savvy readers could deduce after some labor. The list and explanation follows.

1) One is constructing the code from the ratio M/n which, in general, can be awkward because for a given M there might not be a suitably dividing n.

2) The well studied sequence has length 64 (or some other power of 2) mainly because computation of discrete Fourier transform is most efficient on such lengths. The number of samples for estimating spectral moments is rarely a power of two; it typically ranges between 16 and 128. The required number is a compromise: it is sufficiently large to maintain statistical errors at acceptable level and small enough to provide moments at spacing equal to the radar beam width (for the usual rotating antenna). In the current implementation of the systematic code on the WSR-88D, the number of samples is 64 and the spacing in azimuth is 1 deg. For most of the volume coverage patterns the antenna rotation rate and PRT are such that there are fewer than 64 returns within one degree of spacing in azimuth. Therefore to use the SZ(8/64) code, the antenna rotation rate is reduced or sequences are weighted by window functions and overlapped so that the spacing of spectral moments is at 1 deg intervals. This somewhat constrains the flexibility in the choice of sequence lengths.

3) For filtering strong trip echo in the SZ(8/64) code ,the notch width (in Doppler velocity domain) should be integer multiple m of $0.25v_a$, where m can be 1 to 6. The highest $m = 6$ leaves two replicas of the week signal in the spectrum and that is the

128

minimum required for reconstruction of the original week signal. If the spectrum spread of the weak signal exceeds $0.25v_a$, the retrieval of its spectral moments degrades because the spectral replicas overlap; at substantial overlaps it becomes impossible to retrieve the first and second Doppler spectral moment. Other codes of the same family but with fewer replicas would reduce the amount of mutual overlap and therefore extend the recovery of week trip signals.

4) The modulation codes for different trip echoes do not generate the same number of spectral replicas. Hence the separation of two overlaid echoes depends on the relative trip distance between the two. Separation and recovery is best for signals from two adjacent trips, as the code was designed with this in mind.

5) The SZ(8/64) code is vulnerable to the fifth trip echo and therefore might be unfit for the short-wavelength radars that routinely experience similar and higher order ambiguities.

With the listed limitations in mind, we continue our review of the systematic phase code and set out to find the ones that minimize these deficiencies. To construct the code of desired length M, it is relatively simple to start with some L which if multiplied with an integer would give a number close to the desired M; thus rather than use M/n in (1) it is advantageous to use $2M/n$ and the reason for 2 in the denominator is so that 2π appears in the numerator. Further, a good starting point is to define the code kernel modulating the second trip echo as the sequence of phases over the 2π interval satisfying

$$\varphi_{2,k} = \psi_{k\text{-}1} - \psi_k = 2\pi k^2/L; \, k = 0, 1, 2,\ldots, p-1, \qquad (2)$$

where p is the period, L is an integer, and the first subscript 2 indicates that the second trip is modulated. The code is constructed from this kernel by periodically repeating the kernel m times. The kernel length specifies the code properties and is the critical design parameter.

The code period p is defined as the length of smallest subsequence in M which repeats. It is found from the equation

$$(k + p)^2/L - k^2/L = \text{integer},$$

therefore

$$(2pk + p^2)/L = \text{integer}. \tag{3}$$

It follows that if L is divisible by 4 the period $p = L/2$ otherwise $p = L$. In the case of the SZ(8/64) code, $L=16$ which is divisible by 4, hence the period $L/2 = 8$. The results in this text for codes with $p = L$ are obtained from congruence relations, that is modular (L) arithmetic.

For a chosen L, the code period is p and the discrete Fourier transform C_m of the kernel $c_{2,k} = exp(j\varphi_{2,k})$ of length p, has p equal spectral coefficients. Illustrated in Fig. 1 are the relations between the code kernel, and the code sequence in time and frequency domains. Magnitudes of the complex Fourier coefficients are plotted for a hypothetical case in which the code modulates a constant (DC values). For a sinusoids with a frequency $k/(mLT)$ the L coefficients are each shifted by k positions.

To see how returns from other trips are coded (upon decoding for the first trip) start with

the modulation code for the second trip,

$$\varphi_{2,1} = \psi_0 - \psi_1$$

$$\varphi_{2,2} = \psi_1 - \psi_2$$

$$\varphi_{2,3} = \psi_2 - \psi_3$$

$$........................$$

$$\varphi_{2,k} = \psi_{k-1} - \psi_k .$$

By inspection it then follows that a sum of two adjacent phases in (4) produces the phase

of the modulation code for the third trip. Sum of three adjacent phases in (4) is the code

for the fourth trip and so on. This can be written concisely as

$$\forall k : \varphi_{n,k} = \sum_{i=0}^{n-2} \varphi_{2,k+i} \tag{5}$$

which expressed explicitly is

1st trip $\qquad\qquad\qquad\qquad \varphi_{1,k} = 0 \qquad\qquad\qquad$ coherent

2nd trip $\qquad\qquad\qquad \varphi_{2,k} = \psi_{k-1} - \psi_k = 2\pi k^2/L$

3rd trip $\qquad\qquad\qquad \varphi_{3,k} = \psi_{k-2} - \psi_k = 2\pi[k^2 + (k\text{-}1)^2]/L$

$$.....................$$

nth trip $\qquad \varphi_{n,k} = \psi_{k-n+1} - \psi_k = 2\pi[k^2 + (k\text{-}1)^2 + .. (k\text{-}n+2)^2] / L \tag{6}$

In (6) n is the trip number (i.e., $n = 1$ is first trip etc.).

Some properties follow. If the modulation code period is L, (L not divisible by 4) it will produce L spectral replicas of second trip signal. If L is even, then the modulation code for the third trip has period $L/2$ and thus would produce $L/2$ spectral replicas of the third trip signal (if decoding is for the first trip). It is obvious that if decoding is for the second trip, the third trip phase would be modulated by $\varphi_{2,k}$ and the first trip phase by $-\varphi_{2,k}$.

For optimum protection of first trip signal, as is desirable on the terminal Doppler weather radar, the protection from out-of-trip echoes should be equally good regardless of which trip is overlaid. Therefore, one is motivated to find modulations $\varphi_{n,k}$ (for as many trips n as possible) that would equally affect the spectra of the week signals. Such protection might be achieved if the period of $\varphi_{n,k}$ is L for all trips (it will be demonstrated latter that the notch filter width should be adaptive for retrieving accurately the mean velocity.) Obviously, there is no protection whatsoever against the $L+1$ trip because the corrected phases for it and the first trip are equal. But, if L is sufficiently large (> 4) such protection might not be needed.

Following equation (3) one can pose the problem of periodicity for codes that modulate signals from any of the trips. To find periodicity add p to each k in (6), subtract (6) without the added p, and equate to an integer. The result is

$$\{2pk(n-1) - (n-2)(n-1)p + (n-1)\,p^2\}/L = \text{integer.} \tag{7}$$

Periodicities shorter than L (i.e., $p = L/a$) reduce the number of spectral replicas of the modulated signal from L to p and might be undesirable for some applications as will be explained shortly. From (7) it follows that if L is divisible by $(n-1)$ then the period will be $L/(n-1)$.

If $L = p_1 p_2$: p_1 and p_2 are prime numbers then the $1+p_1$ modulation has period p_2.

Codes with periods $< L$ do not produce the same number of spectral replicas for each of the $(L-1)$ trips and thus offer uneven protection. It turns out that even codes with the same number of replicas do not offer the same protection. The SZ(8/64) has different periodicities (or number of replicas) for some trips (report by Sachidananda et al. 1998) and therefore the effect of overlaid echo depends on the relative trip distance between the desired trip (whose signal has been cohered) and the trip of the overlaying signal.

If the first element of the code kernel is appended to the last one (so that there are $L+1$ terms) the resulting sequence is symmetric with respect to its middle point. This can be deduced by observing that

$$\forall\, k \colon k^2 \equiv (L\text{-}k)^2 \ (\text{mod } L).$$

Because the kernel length is L and $k \in 0,\ 1,...L\text{-}1$; it follows from (8) that first term (for $k=0$) equals the last term of the extended sequence ($k=L$), the second term ($k=1$) is the same as the $(L\text{-}1)$ term, the third term equals the $(L\text{-}2)$ term, and so on.

From this discussion it follows that in practice good choices of L are small prime numbers like 5 and 7. Integer multiples of these two produce a dance set of numbers between say 30 and 90 which cover well the range of desirable sequence lengths. Five

offers equal protection for four out of trip echoes and seven increases this to six trips. The notch filter widths of 3/5 and 5/7 for the two kernels are sufficiently large to eliminate most of leakage due to the strong trip signal, although these are slightly smaller than the 6/8 of the SZ(8/64) code (for second trip recovery). With 5 and 7 spectral replicas and assuming the same PRTs the amount of spectral overlap of the replicas would be smaller than in the case of the SZ(8/64) code (for the second trip signal).
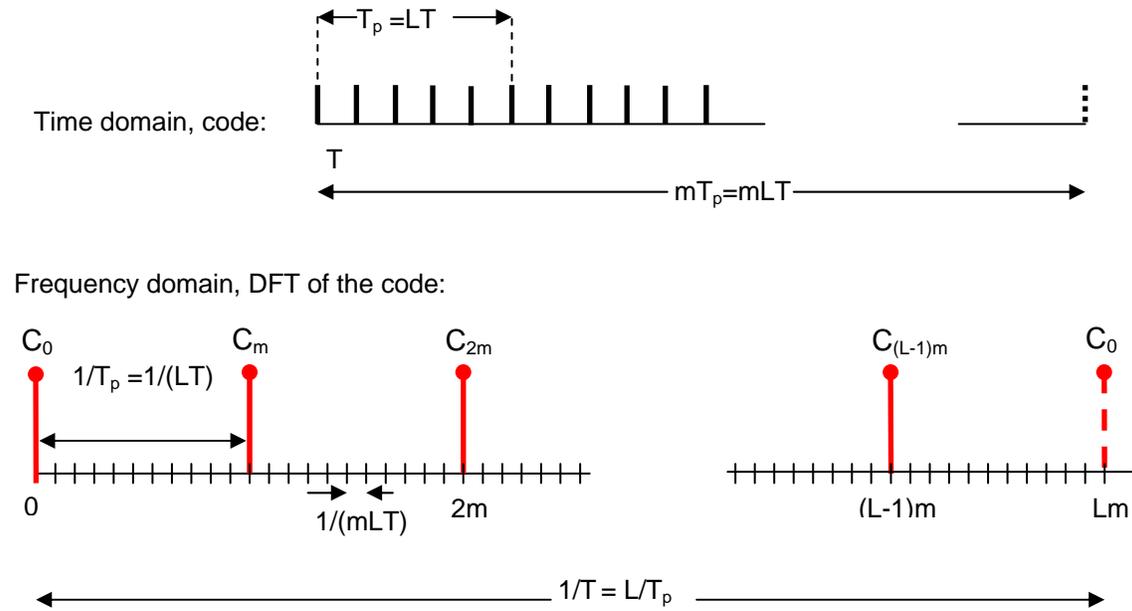
Fig. 1. Time domain and frequency domain representation. Code kernel length is L, spacing of pulses is T, and period is T_p (here $p=5$). The length of the code sequence is mL, and the Fourier coefficients of the code sequence are C_m.

3. Another code kernel

Code kernel with $n/M = 2h/L$ where L is not divisible by h is also suitable for separating overlaid echoes. The equations for periodicities etc., are obtained if h is inserted in the nominators of equations (2) to (7); $h =1$ is the special case that has merits. The code with

h/L has different phase sequence otherwise all the properties about periodicity etc are the same as when *h*=1. The 12/64 has h=6, L=32. So period is L/2 = 16 and that is the number of spectral replicas; in M=64 the periodic part repeats 4 times. The normalized notch width for the 12/64 code is $n_w/16$= 0.625, hence, n_w = 10 coefficients. Therefore 6 replicas are kept. But how are these spread? They must overlap a lot? Still, the question is "does the h/L code have the same protection for several consecutive trips as does the L code?, i.e., is the 3d on top of 1st and 4th on top of 1st same type code as is 2nd on top of 1st?

4. Quantitative measures of improvement

Qualifiers of improvement – comparison of the code with *L*=7 to the code with L=16 (i.e., SZ(8/64)) are discussed here. Consider the second trip signal residue after the strong first trip signal has been removed with a notch filter of width n_w as explained in Sachidananda and Zrnić (1999). Further, let the first trip strong signal have Gaussian spectrum, then the effective signal to noise ratio of the second trip is (eq. 6 in Sachidananda and Zrnić (1999)):

$$\mathrm{SNR}_{2e} = P_2(1-n_w)/[P_1(1-erf\{n_w v_a/w_1\sqrt{2}\} +P_2(1-n_w)/\mathrm{SNR}_2]. \qquad (9)$$

Here P_1 and P_2 are the signal power of first and second trip; SNR_2 is the second trip signal to noise power ratio; v_a is the unambiguous velocity, and w_1 is the spectrum width of the first trip signal. It is instructive to compare SNR_{2e} for the case for the notch width of 5/7 (L=7 code) and 6/8 (L=16 code). Take the same parameters as in Sachidananda and Zrnić (1999), that is, P_1/P_2 = 20 dB, v_a = 32 m s^{-1}, SNR_2 = 20 dB. For spectrum

widths of the first trip signal, w_1, less that 4 m s^{-1}, the improvement in (8) is about 2 dB if the L = 7 code is used.
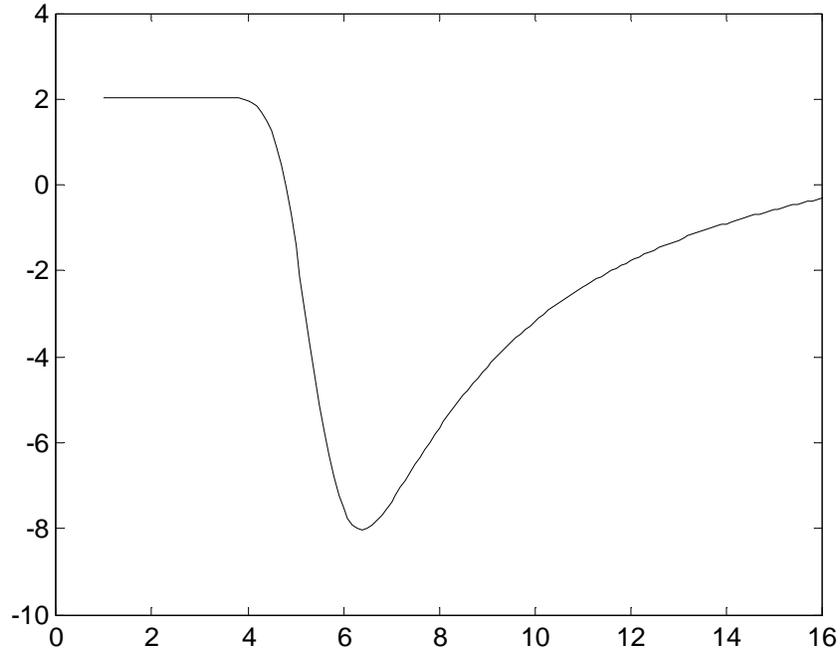
Fig. 1 Improvement in SNR2e vs spectrum width of strong signal (first trip).

Equation (9) does not consider the self noise of the weak (second trip signal). This self noise is from the spectral skirts that overlap the main lobe of the second trip spectrum. Because two replicas are required for reconstruction of the second trip signal the width occupied by a single lobe of the replica is

$$n_r = (1-n_w)/2. \tag{10}$$

Hence the "clean' signal power is

$$P_2' = P_2 \, erf(n_r v_a/w_2\sqrt{2}), \tag{11}$$

and the self noise power is

$$N_{2s} = P_2 \, erfc(n_r v_a / w_2 \sqrt{2}),$$ (12)

with the compliment error function given by $erfc(x) = 1 - erf(x)$.

Thus equation (9) becomes

$$SNR_{2e} = P_2(1-n_w)erf(n_r v_a / w_2 \sqrt{2}) / [P_1 erfc(n_w v_a / w_1 \sqrt{2}) + P_2(1-n_w)/SNR_2 + P_2 \, erfc(n_r v_a / w_2 \sqrt{2})].$$

(13)

The plot of this equation for larger SNR_2 (100 or more linear units) is in the figure 2.
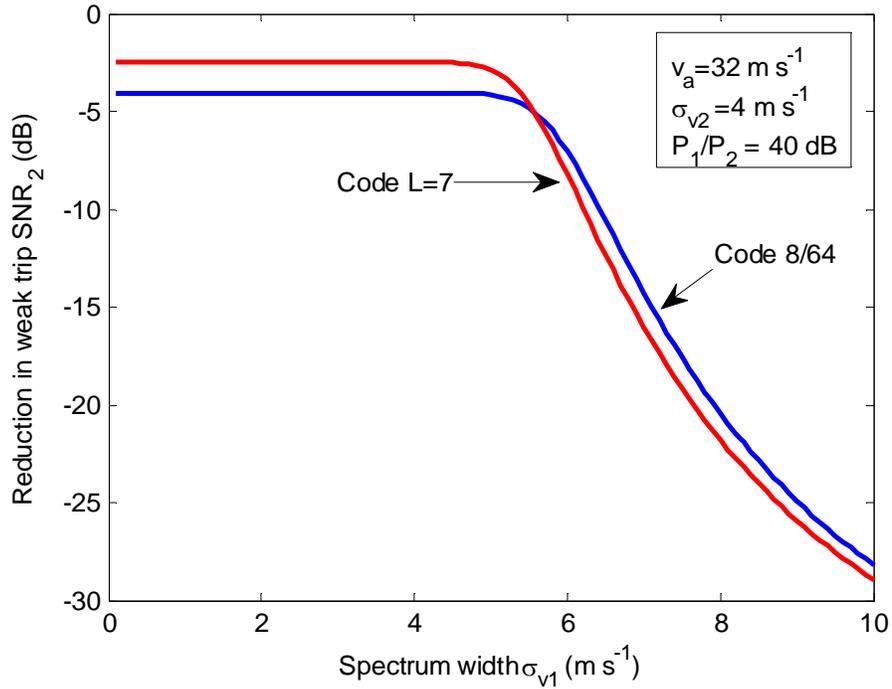
Fig.2 Reduction in SNR_2

The larger negative numbers (reduction) mean that more of the SNR2 is lost. Two regimes of SNR2 reduction are evident. The flat part is due to the self noise of the second trip signal whereas the decreasing part is due to the non filtered first trip signal. Note that the self noise is smaller for the $L=7$ code because the width of the replication region is larger by 8/7 and therefore the ratios or the *erfc*'s in dB units is 2 dB.

Figure 3 presents the residual power ratio P_1/P_r that determines the region of recovery of the week trip signal. It is given by (Sachidananda and Zrnić 1999):

$$P_1/P_r = 3/[(3 - \varepsilon^2)\ erfc(n_w v_a/w_1\sqrt{2}) + \varepsilon^2(1 - n_w)], \tag{14}$$

where ε^2 is the rms value of phase fluctuations (in radians).
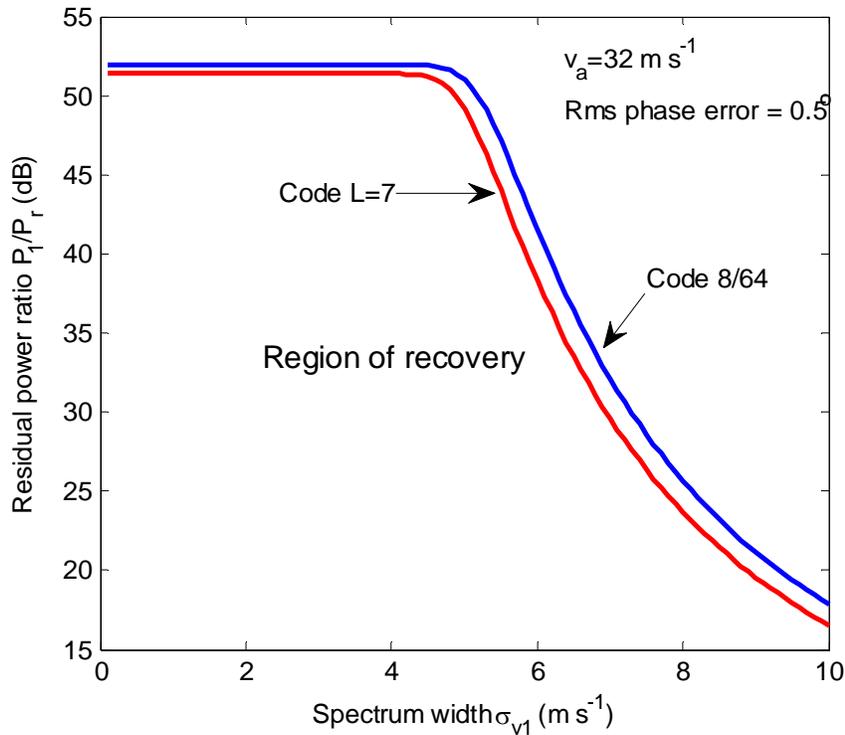
Fig. 3 Residual power ratio

138

Note that the region of recovery is somewhat smaller for the $L = 7$ code. This is because its slightly smaller notch width removes less of phase fluctuations than the 0.75 width of the 8/64 code.

5. The code kernel with $L=7$

This kernel is attractive because the spacing of spectral replicas is sufficiently large so that they seldom overlap. Yet filtering of first trip returns is effective as will be demonstrated next.

Consider the process of reconstructing the week trip echo if two spectral replicas are retained. These can be any two replicas but in practice one would take two adjacent ones furthest removed from the strong trip echo spectrum. It suffices to examine the effects on the kernel as extensions to longer lengths have the same properties. For $L=7$ the phase sequence (modulation of the second trip) is produced by multiplying $2\pi/7$ with {0, 1, 4, 2, 2, 4, 1}. Discrete Fourier Transform of this sequence produces seven spectral coefficients. Removal of two followed by inverse discrete Fourier Transform returns the code into time domain. Decoding by adjusting the phases (taking them out of the sequence) partially reconstructs the DC value. Discrete Fourier transform of the partial reconstruction (Fig. 4) produces a spectrum with the peak at DC and sidebands.
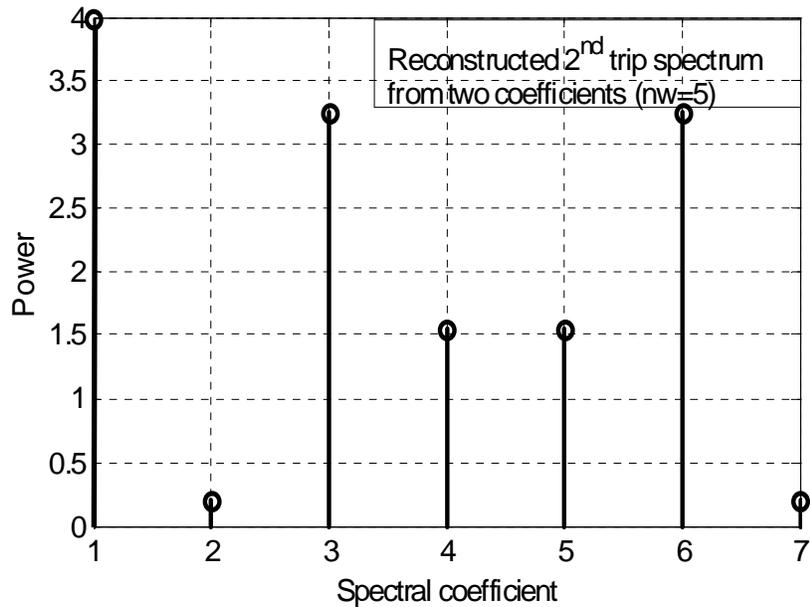
Fig.4 Reconstructed spectral coefficients of a 2nd trip DC signal after removing five replicas and recohering the signal (code). Standard deviation (width) of this spectrum with respect to the DC value is 1.97.

In the phase code scheme the position of the peak (or mean value of the spectrum) must be determined to obtain the mean Doppler velocity. For that reason the difference in power between the spectral peak and the strongest replica is important and well as the separation of the strongest side band from the peak of the spectrum.

At low signal to noise ratios a small difference between the peak and side band would create large errors in velocity estimates because noise could often cause one or the other side band to exceed the main spectral peak. In this code peak to strongest sideband power is 4/3.25 (0.9 dB) which would not be always acceptable. The reconstructed spectral distributions of the third and fourth trip echoes have replicas with the same values as the

ones in Fig. 4 except the locations of the replicas differ as follows. Third trip: the replica No 2 is shifted to the 3rd position, No 3 to the 4th position and No 4 to the 2nd position, the replicas 5, 6, and 7 become symmetric to the cyclic shift in the first tree replicas (Fig. 5). Fourth trip: the same shifts in coefficients as from the second to third tip apply to the shifts from the third to fourth trip (Fig. 6). Further note that because of the symmetry property (8) the spectral of the reconstructed 2nd and 7th trip signal are conjugate pairs and so are the spectra of the 3rd, 6th and 4th, 5th trip signals.
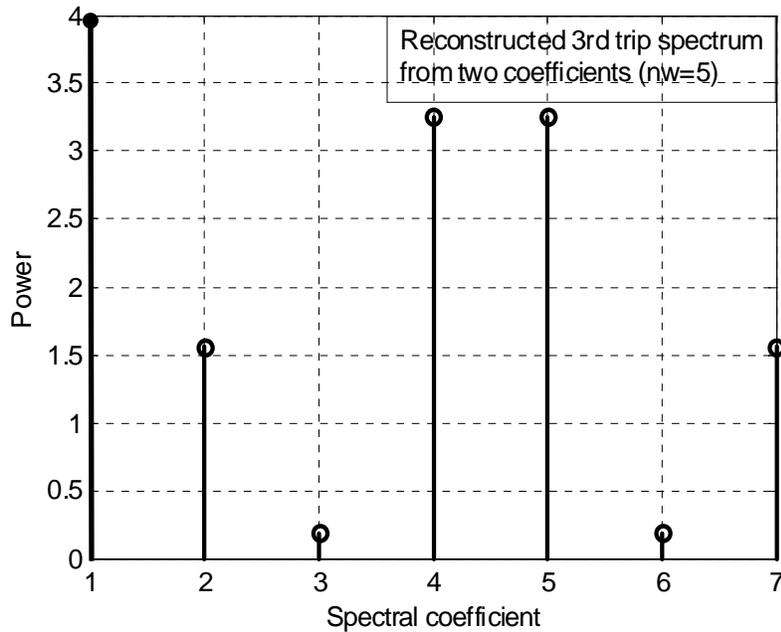
Fig. 5 Reconstructed spectral coefficients of a 3nd trip DC signal after removing five replicas and recohering the signal (code). Standard deviation (width) of this spectrum with respect to the DC value is 2.12.
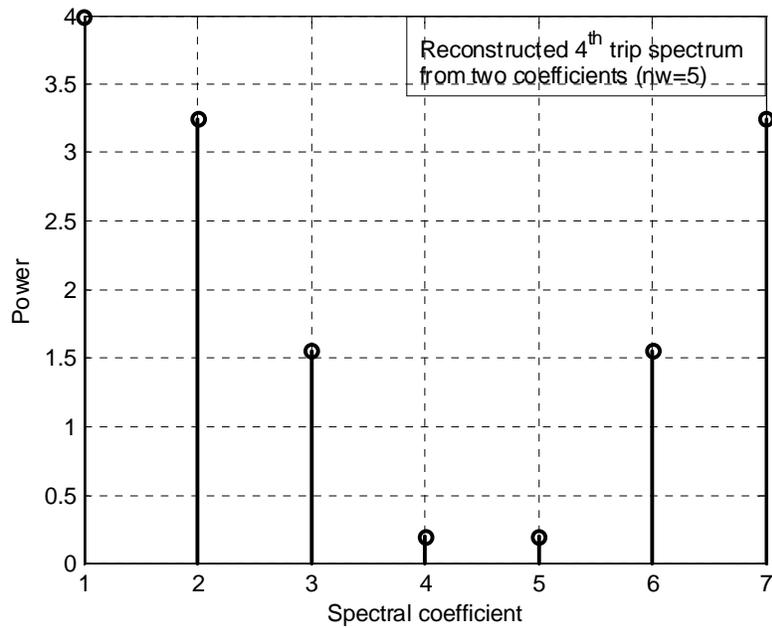
Fig. 6 Reconstructed spectral coefficients of a 4nd trip DC signal after removing five replicas and recohering the signal (code). Standard deviation (width) of this spectrum with respect to the DC value is 1.27.

To reduce sensitivity to the SNR a smaller notch width (by one replica region) is advised for the case of 2nd and even smaller for the 3rd trip signals. That is removal of four spectral coefficients (for 2nd) and three coefficients (for 3rd). That way the remaining coefficients add to the coherent reconstruction of the signal, hence less power is redistributed to the sidebands (Fig. 7).
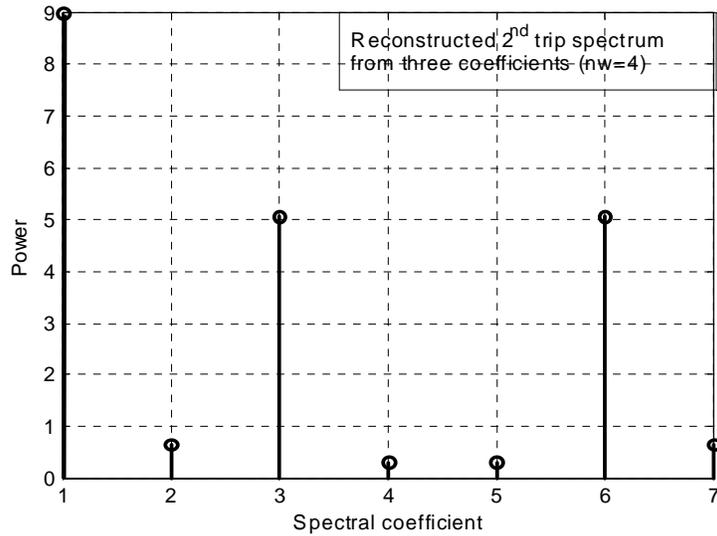
Fig. 7 Reconstructed spectral coefficients of a 2nd trip DC signal after removing four replicas and recohering the signal (code).

The main spectrum peak to maximum sideband in this case is 9/5.05 (2.5 dB) and should give sufficient margin against errors due to noise. This we conclude by observing that with similar ratios performance of the SZ(8/6) code is satisfactory.

The dependence of notch width on trip number parallels the SZ(8/64) case whereby for the 2nd trip two replicas suffice, for the 3rd trip the notch is 50% of the unambiguous interval because the total number of replicas is four; the total number of replicas becomes eight in the case of the 4th trip signal, yet the required notch width is 50% to mitigate the effect of the large sidebands which are far from the coherent peak.

6. Conclusions

Systematic phase codes with periods L=7 (or 5) can be applied to sequences of length mL hence can match well the typical range of dwell times ($M = 30$ to 70) needed fore accurate estimation of spectral moments.

The codes have the same type of modulation for all L-1 trip echoes but require different notch widths for filtering the strong trip echoes. This is because the sidebands have the same powers but are distributed differently depending on which trip with respect to the 1st is cohered. The worst error would occur if the largest side band is furthest away from the main spectral peak.

It is possible to tailor the code so that the best performance (larger recovery area in the parameter space of 1st to 2nd trip power ratios and spectrum widths) is for the 2nd to 1st and 3rd to 1st trip echoes. This is important because overlaying storms at these close ranges are most frequent and more detrimental to signal recovery than at furthest range.

7. References

Cho, J. Y. N., 2005: Multi-PRI Signal Processing for the Terminal Doppler Weather Radar. Part II: Range–Velocity Ambiguity Mitigation, *J. Atmos. Oceanic Technol.,* **22,** 1507–1519.

Chu, D. C., 1972: Polyphase codes with good periodic correlation properties. *IEEE Trans. on Information Theory*, vol. IT-18, 531-532.

Doviak, R.J., and D.S. Zrnić, 1993: Doppler radar and weather observations. Second edition, Academic Press San Diego, CA.

Frush, C., R.J. Doviak, M. Sachidananda, and D.S. Zrnić, 2002: Application of the SZ phase code to mitigate range-velocity ambiguities in weather radars. *J. Atmos. Oceanic Technol.,* **19,** 413-430.

Laird, B.G., 1981: On ambiguity resolution by random phase processing. *20th Conference on Radar Meteorology., AMS*, 327-331.

Sachidananda, M., and D.S. Zrnić, 1986: Recovery of spectral moments from overlaid echoes in a Doppler weather radar. *IEEE Trans. on Geoscience and Remote Sensing*, vol. GE-24, No.5, 751-764.

Sachidananda, M., and D.S. Zrnić, 1999: Systematic phase codes for resolving range overlaid signals in a Doppler weather radar. *J. Atmos. Oceanic Technol.*, 16, pp. 1351-1363.

Siggia, A., 1983: Processing phase coded radar signals with adaptive digital filters. *21st Conference on Radar Meteorology., AMS*, 167-172.

Zrnić, D.S., 1975: Simulation of weather like Doppler spectra and signals., *Journal of Applied Meteorology*., vol.14, No.4, 619-620.

Zrnić, D.S., 1979: Random phase radar. , *NSSL internal memorandum,* April 1979.

Zrnić, D.S., and P. Mahapatra, 1985: Two methods of ambiguity resolution in pulsed Doppler weather radars. *IEEE Trans. on Aerospace and Electronic Systems*, vol. AES-21, No.4, 470-483.